NORTHWESTERN UNIVERSITY

Adhesion in Hydrogels and Model Glassy Polymers

A DISSERTATION

SUBMITTED TO THE GRADUATE SCHOOL
IN PARTIAL FULLFILMENT OF THE REQUIREMENTS

for the degree

DOCTOR OF PHILOSOPHY

Field of Materials Science and Engineering

By

Murat Guvendiren

EVANSTON, ILLINOIS

December 2007

ABSTRACT

Adhesion in Hydrogels and Model Glassy Polymers

Murat Guvendiren

Two main topics are addressed in this dissertation: (1) adhesion in hydrogels; (2) interfacial interactions between model glassy polymers. A self-assembly technique for the formation of hydrogels from acrylic triblock copolymer solutions was developed, based on vapor phase solvent exchange. Structure formation in the gels was characterized by small angle X-ray scattering, and swelling was measured in controlled pH buffer solutions. Strong gels are formed with polymer weight fractions between 0.01 and 0.15, and with shear moduli between 0.6 kPa and 3.5 kPa. Adhesive functionality, based on 3,4-dihydroxy-L-phenylalanine (DOPA) was also incorporated into the triblock copolymers. The effect of DOPA concentration on gel formation and swelling was investigated in detail. The adhesive properties of DOPA-functionalized hydrogels on TiO_2 were investigated with an axisymmetric adhesion method. It was shown that the presence of DOPA enhances the adhesive properties of the hydrogels, but that the effect is minimized at pH values below 10, where the DOPA groups are hydrophobic. Thin film membranes were produced in order to study the specific interactions between DOPA and TiO_2 and DOPA and tissue, using a membrane inflation method. The presence of DOPA in the

membranes enhances the adhesion on TiO_2 and tissue, although adhesion to tissue requires that the DOPA groups be oxidized while in contact with the tissue of interest.

Porous hydrogel scaffolds for tissue engineering applications were formed by adding salt crystals to the triblock copolymer solution prior to solvent exchange. Salt was then leached out by immersing the gel into water. Structures of the porous hydrogels were characterized by confocal laser scanning microscopy. These hydrogels were shown to be suitable for tissue regeneration and drug delivery applications.

Diffusion-mediated adhesion between two component miscible polymer systems having very different glassy temperatures was also investigated. Axisymmetric adhesion tests were performed on thin layers of poly(tetramethyl bisphenol-A polycarbonate) (TMPC)/poly(ethylene oxide) (PEO) blends with different blend compositions. The tests were designed to investigate the effects of temperature and contact time on interfacial adhesion between two blend surfaces. Adhesion in this system is controlled by diffusive motions of the highly mobile PEO component.

ACKNOWLEDGEMENTS

I would like to begin by thanking my wonderful advisor Professor Ken Shull. He is a model academician for me having a balanced life that combines his family, his career and his students. I am also grateful to my committee members, Prof. Phil Messersmith, Prof. John Torkelson and Prof. David Dunand, for their time and thoughtful questions at both my qualifier and my defense.

I am grateful to Prof. Phil Messersmith and Dan Harrington for giving me change to collaborate with them. I would especially like to thank Chi-Yang Chao who tought me polymer synthesis and polymer chemistry. I would also like to thank Anny Flory, Michelle Seitz, David Brass, Rachel McSwain and Rebecca Webber for all of their help with my experimental work. I am also grateful to Bruce Lee, Haeshin Lee and Andrea Statz for their help. I would like to thank Prof. John Torkelson and Prof. Wes Burghardt for providing equipments in their labs.

I am thankful for all of the Shull group members, past and present, who have been both colleagues and friends. I would like to thank Nelson Nunalee, Chau-Jean Lin, Andy Schoch, Daniel Carvajal, Aleta Hagman, Michelle Seitz, David Brass, Michelle Nunalee, Rachel McSwain, Rebecca Webber, Anny Flory, Rafael Bras, Kevin Henderson, Kendra Erk, Marc Palmeri, Katie Otim, Yan Sun, and Raj Boya.

I would like to thank my family, my parents Iffet and Erdal and my sister Berna, for all of their love and support throughout my life. I would like to thank my aunt Nimet Yilmaz who came all the way from Turkey with my family for my graduation ceremony. I would also like to thank Joyce and Mike Loverde, and Aunt Joan Gadzic. Finally, I offer a special thank you to my wonderful fiancee, Sharon Loverde for being supportive and understanding.

To my parents, Iffet and Erdal

and my sister, Berna

TABLE OF CONTENTS

LIST OF TABLES

CHAPTER 2

CHAPTER 3

CHAPTER 4

LIST OF FIGURES

CHAPTER 2

CHAPTER 6

CHAPTER 1

INTRODUCTION

CHAPTER 1

INTRODUCTION

There are two main objectives of the work presented in this dissertation: (1) to study adhesion in hydrogels; (2) to investigate adhesion in model glassy polymers. The first part of my research is divided into 4 sub-categories, which correspond to chapters 2, 3, 4 and 5. The final chapter focuses on the second part of my research, which is adhesion in model glassy polymers.

In order to study the adhesion in hydrogels, I first developed a self-assembly technique for the formation of hydrogels, described in chapter 2. Hydrogels based on poly(methyl methacrylate) - poly(methacrylic acid) - poly(methyl methacrylate) (PMMA-PMAA-PMMA) triblock copolymer solutions were self-assembled by a vapor phase solvent exchange mechanism. Hydrogels were formed by exposing the solutions to saturated water vapor. As water diffuses into the solution, the hydrophobic end-blocks form aggregates that are bridged by the hydrophilic mid-blocks. Structure formation in the gels was characterized by small angle X-ray scattering, and swelling was measured in controlled pH buffer solutions. After swelling to equilibrium in water or controlled pH buffers, strong gels are formed with polymer weight fractions between 0.01 and 0.15, and with shear moduli between 0.6 kPa and 3.5 kPa.

These hydrogels provide a unique model system to study adhesion in aqueous environments. For this purpose, in chapter 3, I incorporated 3,4-dihydroxy-L-phenylalanine (DOPA), a modified amino acid which is believed to be responsible for water resistance adhesion in marine mussels, into the PMMA-PMAA-PMMA copolymers. The effects of DOPA on the solvent exchange process and the swelling of the hydrogels were studied in detail. The adhesive properties of DOPA-functionalized PMMA-PMAA-PMMA hydrogels on TiO_2 were

investigated by using an axisymmetric adhesion method. DOPA incorporation significantly enhanced adhesion, giving critical energy release rate values as high as 2 J/m^2.

In chapter 4, I investigate the adhesive properties of DOPA-functionalized thin films by using a membrane inflation method. In this method, a membrane is attached to the end of the glass tube, which is inflated into contact with the substrate. In order to separate the surfaces, the pressure was deflated. The interaction between the surfaces was investigated by measuring the the contact area and release pressure. The results showed that the presence of DOPA enhances the adhesion of hydrogels on both TiO_2 and tissue surfaces. The swelling properties of these films were also characterized with a quartz crystal microbalance.

In chapter 5, I study the biocompatibility and drug release properties of the PMMA-PMAA-PMMA hydrogels. For tissue regeneration experiments, porous gels were produced by adding salt crystals to the polymer solution prior to solvent exchange. Salt was then leached out by immersing the gel into water. Structures of the porous hydrogels were characterized by confocal laser scanning microscopy. Human bladder smooth muscle cells and urothelium cells were seeded onto scaffolds. I demonstrated cell penetration into the porous structure and biocompatibility *in vitro* for short-term cultures. I also showed that these hydrogels are potential candidates for drug delivery purposes.

Finally in chapter 6, I use a model system to study the diffusion-mediated adhesion of two component, miscible polymer blends at elevated temperatures. Axisymmetric adhesion tests were performed on thin layers of poly(tetramethyl bisphenol-A polycarbonate) (TMPC)/poly(ethylene oxide) (PEO) blends with different blend compositions. The tests were designed to investigate the effects of temperature and contact time on interfacial adhesion

between two blend surfaces. A contact mechanics approach was used to determine the critical energy release rate for crack propagation within the interfacial region. The dynamics of the blends were also characterized by DSC and dynamic secondary ion mass spectrometry.

CHAPTER 2

SELF-ASSEMBLY OF ACRYLIC TRIBLOCK HYDROGELS BY VAPOR-PHASE SOLVENT EXCHANGE

CHAPTER 2

SELF-ASSEMBLY OF ACRYLIC TRIBLOCK HYDROGELS BY VAPOR-PHASE SOLVENT EXCHANGE

2.1 INTRODUCTION

There is a growing interest in polymer systems that can self-assemble to form ordered structures such as micelles, vesicles and physically cross-linked gels. These materials are useful in a wide variety of applications that include drug delivery and bio-adhesives.[1] Self-assembling hydrogels are a particularly important sub-class of these materials. Temperature[2-5], pH[6-8] and ion concentration[9,10] are some of the most widely studied external stimuli for inducing self-assembly in gels. Solvent exchange is an additional mechanism for inducing gelation, as illustrated in the recent work of Tae, *et al.*[11] In the solvent exchange process, a polymer is initially dissolved in a good solvent that is also miscible with water. Injectable solvents that are approved for human use, such as *N*-methyl pyrrolidone (NMP) and dimethyl sulfoxide (DMSO), are of particular interest for biomedical applications.[12-14] When injected into an aqueous environment, the water-miscible solvent is replaced by water, and the polymer system self-organizes to form a hydrogel. In applications as tissue scaffolds it is often useful to obtain porous gels in order to promote cell growth within the gel.[15-18]

The general requirements for the *in situ* formation of injectable hydrogels via this solvent exchange mechanism can be summarized as follows:

- The polymer molecules must have at least two hydrophobic groups attached to a water soluble segment.

- The hydrophobic and hydrophilic portions of the molecule must both dissolve in the injecting solvent, in order to minimize the viscosity of the injectable solution.
- The injecting solvent must be miscible with water.
- Self assembly of the hydrophobic groups must give aggregates with relaxation times that are adequate for the desired purpose. High-strength gels, for example, require that the aggregates be either glassy or semi-crystalline.

At a conceptual level, the simplest candidate systems meeting each of these criteria are ABA-type triblock copolymers with a water soluble mid-block (B block) and hydrophobic end-blocks (A blocks). In this study, the water soluble block is poly(methacrylic acid) (PMAA) and the hydrophobic blocks are poly(methyl methacrylate) (PMMA). The PMMA-PMAA-PMMA triblock copolymers can be fully dissolved in N-methyl pyrrolidone (NMP) and dimethyl sulfoxide (DMSO), which are both FDA-approved solvents for injection into the human body. When the solvent is gradually replaced with water, the triblock copolymer self-organizes so that hydrophobic end-blocks (PMMA) form spherical domains that act as physical crosslinks, with the hydrophilic mid-blocks (PMAA) forming bridges between these domains. This self-organized structure is examined by small angle X-ray scattering (SAXS), and the equilibrium swelling properties of the hydrogels are investigated in detail. We also study the elastic properties of the gels at low and high strains by a combination of shear rheometry and indentation. We also show that porous gels suitable for use as tissue scaffolds can be produced by incorporating salt crystals into the polymer solution prior to solvent exchange.

2.2 EXPERIMENTAL DETAILS

2.2.1 Materials

Methyl methacrylate (MMA, Aldrich) and *tert*-butyl methacrylate (*t*BMA, Aldrich) were purified by addition of trioctylaluminum solution in hexane (Aldrich) until a persistent yellowish color was observed. After degassing by freezing in liquid nitrogen (-196 ^{o}C), *t*BMA was distilled under reduced pressure and stored in a freezer, whereas MMA was distilled directly into the reaction chamber prior to polymerization. Diphenylethylene (DPE, Aldrich) was purified by addition of *sec*-butyllithium (*s*-BuLi, Aldrich) until a persistent red color was observed. The solution was stirred under nitrogen overnight, and distilled under reduced atmosphere after degassing, and stored in the freezer. Difunctional initiator was prepared by the reaction of lithium (Li) and naphthalene (both used as received) in freshly distilled tetrahydrofuran (THF) at room temperature for 24 h under a nitrogen atmosphere.[19,20] As Li reacted with naphthalene, the color of the solution became dark green. Lithium chloride (LiCl, Aldrich) was dried in the reaction chamber at 130^{o}C under vacuum for 16 h. Sodium (dispersion in paraffin) and benzophenone were added to the THF, and refluxed until a persistent purple color was observed. NMP, DMSO and dimethylformamide (DMF) were used as received.

2.2.2 Synthesis and Modification of Acrylic Triblock Copolymer

Anionic polymerization of *t*BMA and MMA was carried out under a nitrogen atmosphere by using a difunctional initiator, according to the scheme outlined in Figure 2.1. THF was distilled into the reaction chamber and stirred for 30 minutes to dissolve the LiCl. The concentration of the initiator was determined by titration of the green initiator solution with a

known amount of acetanilide in distilled THF. The chamber was then cooled with a MeOH/dry ice bath (-78^{o}C), and the THF solution was titrated by adding a few drops of initiator until a faint green color was observed. The required volume of initiator was then added, and a dark green color was observed immediately. After addition of the distilled DPE, the green color immediately changed to deep red. The molar ratio of *s*-BuLi/DPE/LiCl was 1 : 3 : 5 in all experiments.[19,21] The purified *t*BMA monomer was introduced drop wise into the reaction flask, and the deep red color disappeared. Polymerization was allowed to proceed at -78^{o}C for 6 hours. A small sample was taken by using a steel needle just before MMA transfer in order to determine the molecular weight of the *t*BMA block. MMA was then distilled into the reaction chamber, and the solution was stirred for 1 h before termination with anhydrous methanol. The final solution was concentrated and precipitated into methanol-water mixture (90 : 10) with stirring. The copolymer was then dried under vacuum overnight.

PMMA – P*t*BMA – PMMA triblock copolymer was dissolved in dioxane, and hydrolyzed with hydrochloric acid (HCl) at 80^{o}C for 6 h.[22] The colorless solution became yellowish with time. The solution was precipitated in hexane, and the polymer was washed with hexane and water several times before it was dried under vacuum at 80^{0}C overnight.

2.2.3 Characterization of Acrylic Triblock Copolymers

The molecular weights of the PMMA-P*t*BMA-PMMA polymers were determined by using gel permeation chromatography (GPC) (Waters 717Plus Auto-sampler connected to Waters 2410 Refractive Index Detector and Waters 2487 Dual λ Absorbance Detector) in HPLC grade THF referenced to polystyrene standards. The compositions of the polymers were determined by proton nuclear magnetic resonance spectroscopy (^{1}H NMR, P-Inova 500 MHz)

using d-chloroform and d-methanol for the original triblock and the hydrolyzed triblock, respectively. The molecular weight for the midblock was obtained from GPC analysis of the P*t*BMA sample removed from the polymerization prior to the addition of MMA monomer. The midblock content was also calculated from the ratio of the *tert*-butyl signal at 1.43 ppm (from P*t*BMA) to the methoxy signal at 3.60 ppm (from PMMA). The measured molecular weights for each block were converted to degrees of polymerization, and these degrees of polymerization are used in our naming convention for the different polymers.

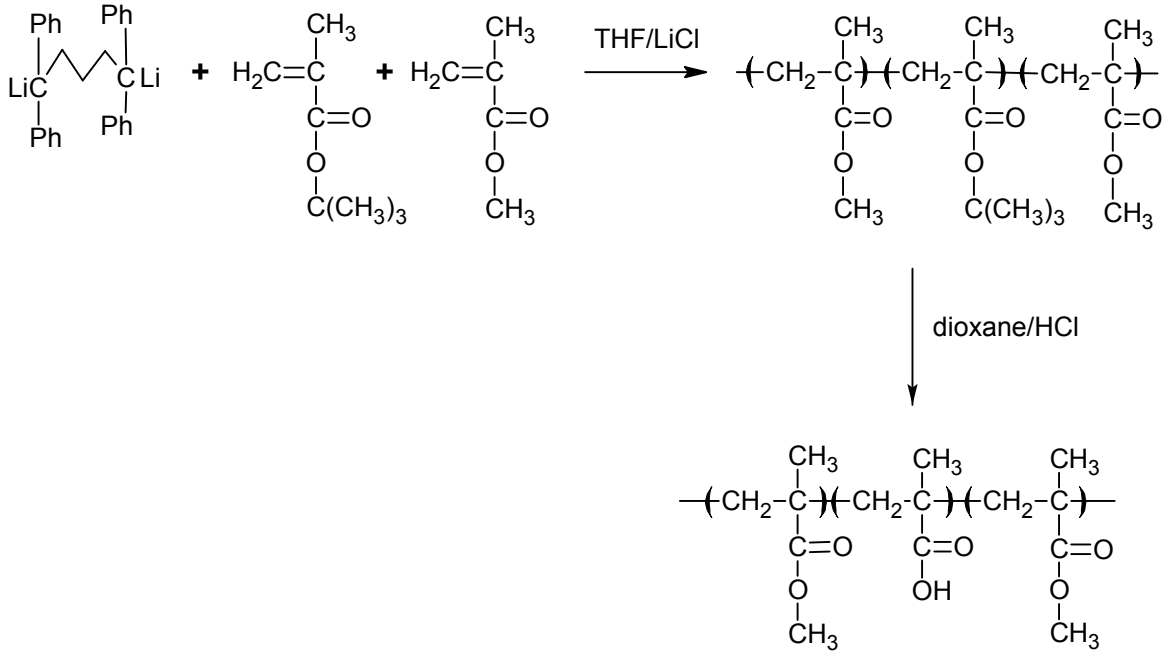

Figure 2.1. Anionic synthesis of the PMMA-PtBMA-PMMA triblock copolymer, followed by hydrolysis of the PtBMA midblock to PMAA.

2.2.4 Hydrogel Formation by Solvent Exchange

The PMMA-PMAA-PMMA triblock copolymer was dissolved in one of three solvents that is a good solvent for both mid- and end-blocks (DMF, NMP or DMSO). This solution was then exposed to a saturated water vapor about 3 h to enable water diffusion into the solution. As

water diffuses into the solution and the original solvent diffuses out, the hydrophobic end-blocks (PMMA) aggregate to form domains that are assumed to be spherical, as has been demonstrated for non-aqueous gels formed from similar triblock copolymers.[23] The hydrophilic mid-blocks (PMAA) form bridges where the two PMMA blocks from a single molecule exist in different domains, or loops where the two PMMA blocks are in the same domain. The hydrogels were then immersed in water or different buffer solutions in order to investigate the swelling characteristics of the hydrogels. The equilibrium weight fractions of polymer in the swollen hydrogels were measured at different times during the solvent exchange and swelling processes.

2.2.5 Formation of Porous Hydrogels

The PMMA-PMAA-PMMA triblock copolymer was dissolved in a good solvent, and porous hydrogels were prepared from these solutions by salt-leach method.[24] In this method, sodium chloride (NaCl) salt crystals of a defined size were added in the polymer solution. The hydrogel was formed as described above by exposing this solution to a saturated water vapor for a sufficient period of time for solvent exchange. The gel was then immersed in water for sufficient time to leach out the salt and to maintain equilibrium swelling. In order to obtain a good contrast between pores and gel, a hydrophobic dye, Hostasol Yellow 3G (Clariant), was added to the polymer solution prior to gel formation, which segregates to PMMA domains.

2.2.6 Small Angle X-Ray Scattering (SAXS)

The SAXS experiments were conducted at the 5-BM beam line at the Advanced Photon Source at Argonne National Laboratory. Hydrogels were prepared in washers as described above, and both sides of the samples were sealed with Kapton film. Scattering patterns were

recorded for scattering vectors, q ($q = 4\pi \sin\theta/\lambda$, where θ is the scattering angle), ranging from 0.1 nm^{-1} to 1 nm^{-1}, using 17 keV X-rays ($\lambda = 0.0729$ nm). The initially recorded two dimensional scattering patterns were converted to a one dimensional set of data by an azimuthal integration.

2.2.7 Shear Rheometry

A Paar Physica MCR (TEK 150PA-C) rheometer with Peltier heating system with parallel plate geometry was used to measure the frequency-dependence of the shear response of the hydrogels.

2.2.8 Confocal Laser Scanning Microscopy and Analysis

Porous hydrogels were characterized by Confocal Laser Scanning Microscopy (Zeiss ConfoCor3/510 Meta) in the Biological Imaging Facility at Northwestern University. The 488 nm line of Ar ion laser, with BM 500-520 IR filter was used in conjunction with EC Plan-Neofluar 10x/0.30 M0.7 objective lens. The pinhole was set to 100 μm. 2-dimensional (x-y) images along the z focal axis were continuously scanned at a scan speed of 2.6 μs. Optical slices were obtained at 50 μm intervals through z axis. Those images were then compiled to a 3-D projection.

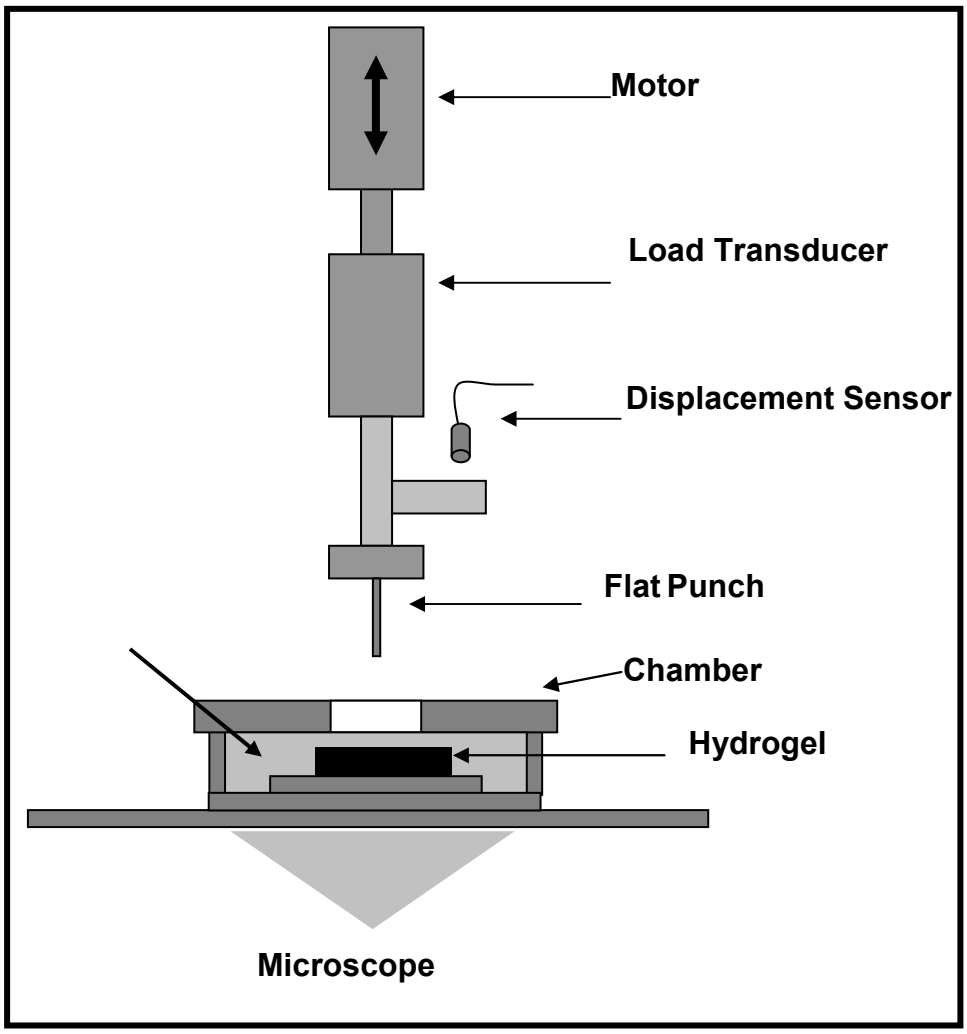

Figure 2.2. Schematic illustration of the apparatus used for the indentation experiments.

2.2.9 Indentation Method

The experimental setup used for the indentation test is shown in Figure 2.2. This characterization method is described in detail elsewhere,[25-27] and involves bringing a flat, rigid indenter into contact with a fully swollen hydrogel that is immersed in a buffer solution. A well defined-contact radius was established, corresponding to the radius of the flat-ended cylindrical

punch used as an indenter. Load and displacement data were collected through a load transducer and an optical displacement sensor.

2.3 RESULTS AND DISCUSSION

2.3.1 Characterization of Acrylic Copolymers

PMMA-P*t*BMA-PMMA triblock copolymer was synthesized via anionic polymerization, and the midblock was hydrolyzed with concentrated HCl to obtain PMMA-PMAA-PMMA triblock copolymer as described in the Experimental Section. In this chapter, we focused on two different triblock copolymers that were synthesized, which we refer to as 200-560-200 (Mn = 88,000 g/mole, PDI = 1.08) and 370-1450-370 (Mn = 200,000 g/mole, PDI = 1.09), with the numbers corresponding to the degrees of polymerization of the copolymer blocks. After the hydrolysis reaction the *tert*-butyl signal in the NMR spectrum at 1.43 ppm completely disappeared, indicating that the conversion of the midblock to methacrylic acid had been achieved.

We also attempted to convert PMMA-poly(*tert*-butyl acrylate)-PMMA triblock copolymers with similar degrees of polymerization under the same conditions. While these polymers were initially soluble, we found that they formed irreversibly crosslinked gels that were insoluble in all solvents after being stored for one day. These results were attributed to side reactions during the conversion process, leading to subsequent crosslinking of the acrylic midblocks. We note here that successful conversions of poly(*tert*-butyl acrylate) to poly(acrylic) acid reported in the literature generally involve lower molecular weights, where a very small

incidence of crosslinking will not be noticeable.[28] The relatively large molecular weights used in our experiments require the enhanced chemical stability of the methacrylic midblocks.

2.3.2 Hydrogel Formation and Characterization

The PMMA-PMAA-PMMA triblock copolymer was initially dissolved in DMF, NMP and DMSO, which are all good solvents for both mid- and end-blocks. The evolution of the self-assembled hydrogel structure is shown schematically in Figure 2.3. The solution was injected into a circular washer that was attached to a glass slide (Figure 2.3-a). It was then exposed to saturated water vapor for three hours to enable water diffusion into the solution. As water diffused into the solution and the original solvent diffused out, the hydrophobic end-blocks (PMMA) aggregated and formed spherical domains, with the hydrophilic mid-block (PMAA) forming bridges between these domains (Figure 2.3-b). The resultant hydrogel was then immersed in water to investigate the stability and swelling characteristics of these materials (Figure 2.3-c). The volume of a hydrogel formed from the 370-1450-370 copolymer expanded increased substantially after immersion in tap water, which we attribute to the pH-dependent ionization of the midblock, described in more detail below.

Small angle x-ray scattering (SAXS) was used to study the self-assembly process during solvent exchange. In Figure 2.4 the scattering intensity is shown for a 200-560-200 triblock copolymer that was originally dissolved in NMP at a concentration of 20 wt %, and exposed to saturated water vapor for either 1 h or 20 h. A scattering peak is not observed for the shorter exchange times, indicating that the formation of hydrophobic PMMA domains had not yet occurred. However, for long exposure times, when the solvent exchange reached equilibrium, we noticed a strong intensity peak at $q = q^* = 0.25\ nm^{-1}$, suggesting the formation of an ordered

hydrogel structure with an average distance between hydrophobic domains of approximately $2\pi/q^* = 25$ nm.[23]

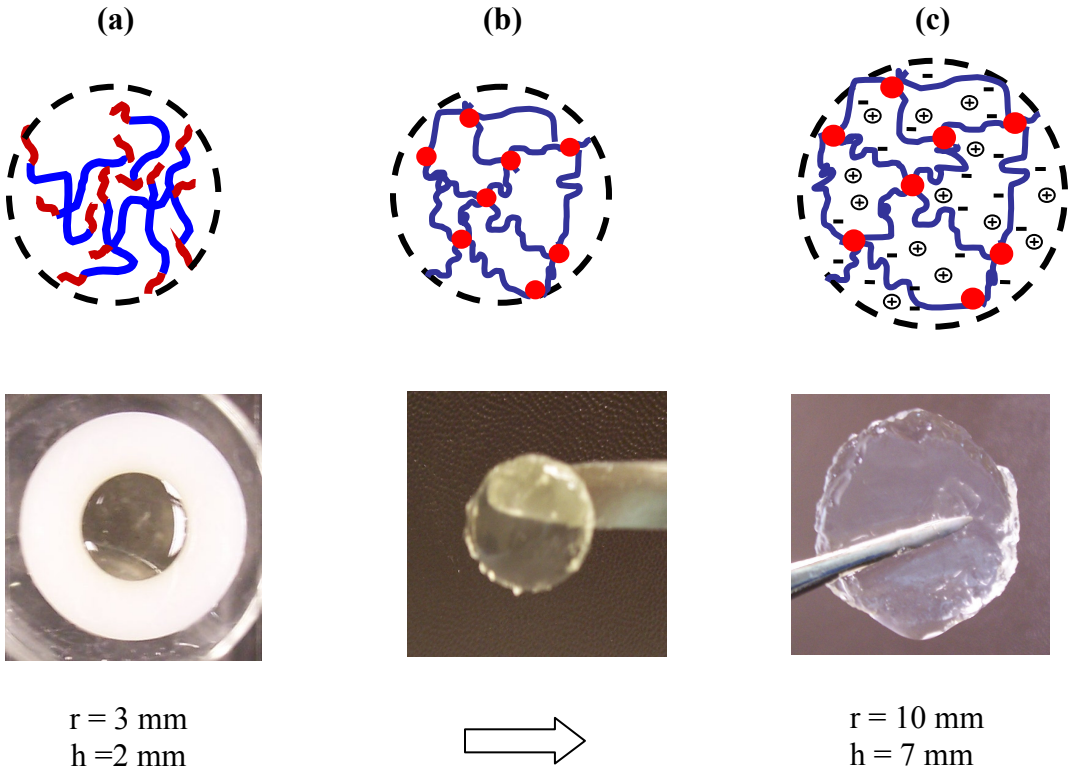

Figure 2.3. Pictures and schematic structures of the 370-1450 370 triblock copolymer: (a) 10 wt % triblock solution in NMP; (b) self-supporting gel after exposure to water vapor; (c) gel after swelling in water. The radius (*r*) and thickness (*h*) of the initial and final sample are indicated below parts (a) and (c).

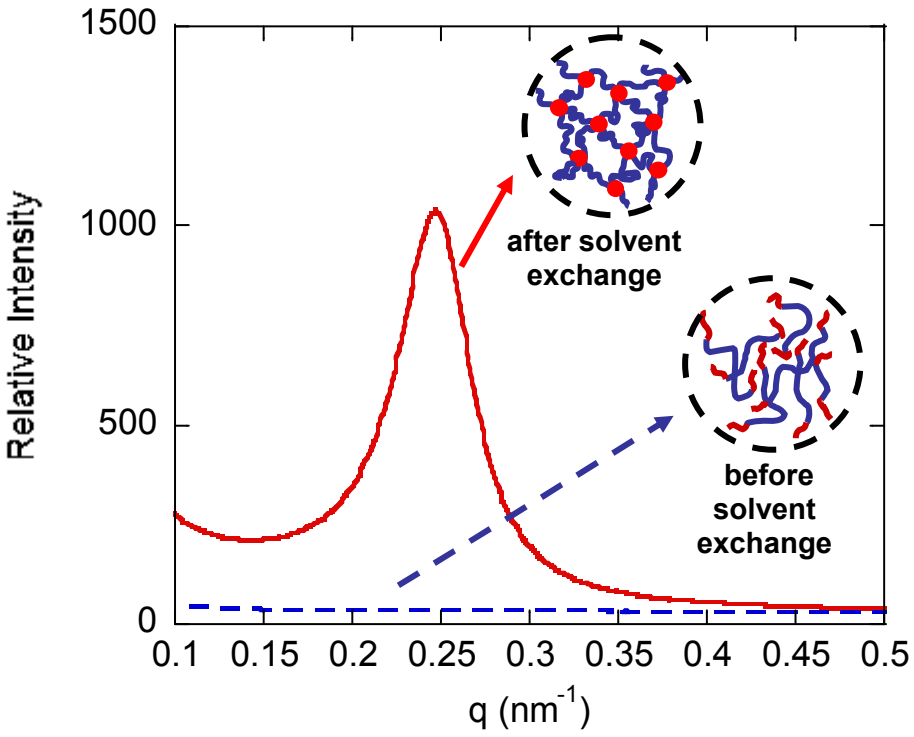

Figure 2.4. Small angle X-ray scattering patterns and corresponding schematic structures for a 20 wt % solution of 200-563-200 polymer dissolved in NMP and exposed to saturated water vapor at room room temperature: before solvent exchange and after solvent exchange.

The effect of the solvent exchange progress on the gel properties was studied by monitoring the time dependence of the weight fraction of the copolymer as a function of the exposure time to saturated water vapor. The results are summarized in Figure 2.5 for the 200-560-200 and 370-1450-370 polymers. In all cases 20 wt % triblock solutions were prepared in DMF, NMP or DMSO, and exposed to water vapor for up to 6 h. There was a large increase in the triblock fraction for the 200-560-200 hydrogels in NMP and DMF, indicating that solvent was being progressively expelled from these materials during the solvent exchange process. In addition, the gels became cloudy, indicative of a phase separation over length scales that are larger that the spacing of the PMMA domains. For the 370-1450-370 triblock polymer fraction in

the hydrogel remained around 0.2 for each of the solvents throughout the exchange process, with highly transparent gels formed in each case. For these materials, we believe that gelation occurs by the formation of spherical domain formation, according to the schematics in Figure 2.3.

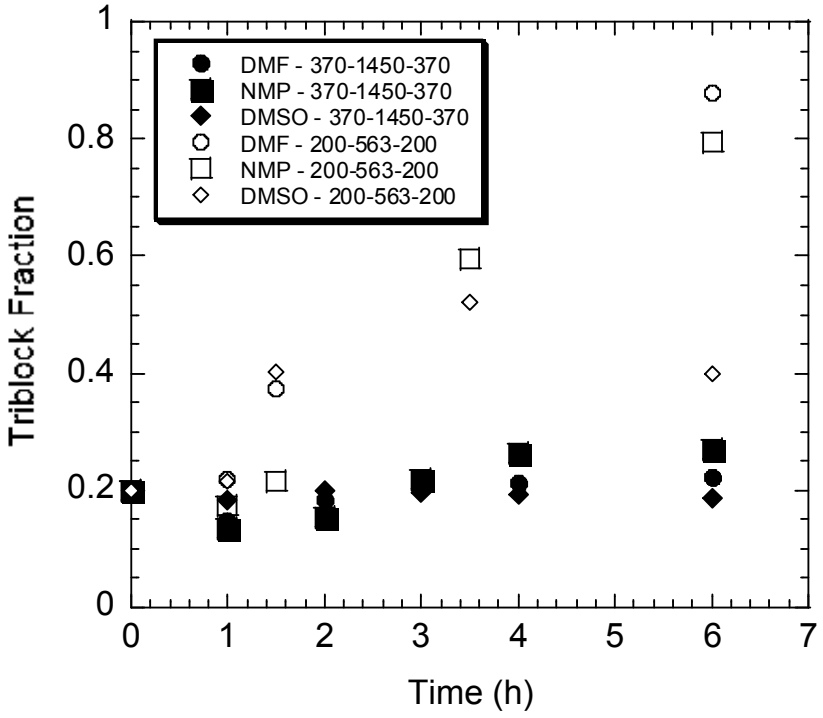

Figure 2.5. Overall weight fraction of the triblock copolymer during the solvent exchange process. Data for 200-563-200 and 370-1450-370 polymers are shown for each of the three solvents (DMF, NMP and DMSO)

The dynamics of the solvent exchange process are controlled by the collective diffusion coefficient for swollen hydrogels, which can be estimated from the following relationship for semi-dilute solutions[29]:

$$D_c = \frac{k_B T}{6\pi\eta\xi_h} \tag{2.1}$$

Here η is the solvent viscosity (1 mPa s for water at room temperature) and ξ_h is the hydrodynamic screening length. For semi-dilute solutions of a polymer in a good solvent, $\xi_h = a\phi_p^{-0.75}$ where a is a characteristic length (typically ≈ 0.5 nm) and ϕ_p is the polymer volume fraction in the solution. Using $a \approx 0.5$ nm and $\phi_p \approx 0.1$, we obtain $\xi_h = 2.8$ nm and $D_c \approx 8\text{x}10^{-7}$ $cm^2\ s^{-1}$. The corresponding diffusion distance, which must be equal to the thickness of the gels in our experiments, is given by $2(D_c t)^{1/2}$. The solvent exchange time is therefore $h^2/4D_c$. For $h = 2$ mm, we obtain a solvent exchange time of 3 h, which is consistent with the observed gelation time for the solvent exchange process.

To further illustrate the favorable characteristics of the gel formed from the 370-1450-370 triblock, we immersed the hydrogels in water after they were gelled by exposure to saturated water vapor. The equilibrium polymer fraction of the hydrogels with time is plotted in Figure 2.6. The polymer was originally dissolved in one of three solvents (DMF, NMP or DMSO), at an initial concentration of 10 or 20 wt %. After gelation by exposure to water vapor, the resultant hydrogels were immersed in tap water and allowed to re-equilibrate. The fraction of polymer in the hydrogel dropped to 1/10 of the initial fraction indicating a high degree of swelling. We attribute this swelling to the ionization of the methacrylic acid groups when the gels were immersed in water. The pH of the surrounding water was measured to be between 7.6 to 7.9 (indicating that the water used in these experiments is slightly basic), after the gels had swollen to equilibrium. These pH values are substantially higher than the *pKa* of 4.8 for the methacrylic acid groups,[30] so we expect the methacrylic acid groups to be almost completely deprotonated at the pH values corresponding to the swelling experiments.

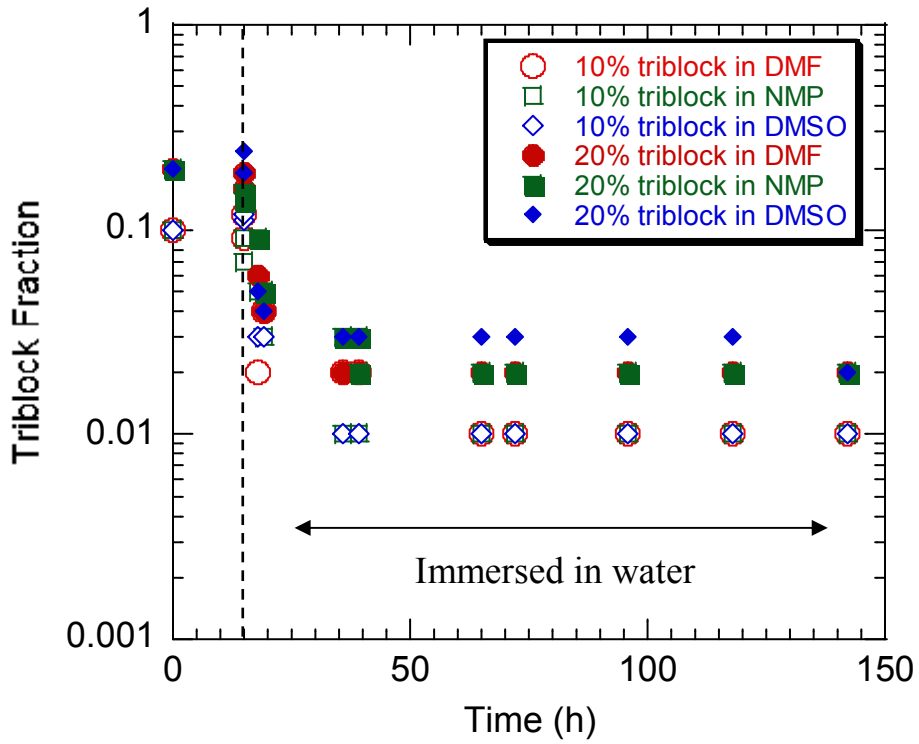

Figure 2.6. Swelling behavior for the 370-1450-370 polymer gels. The triblock was initially dissolved in DMF, NMP or DMSO at concentrations of 10 wt.% or 20 wt.%, as indicated. Dotted line represents the time of immersion.

The results of pH controlled experiments, where the gels were immersed in controlled pH buffers, are shown in Figure 2.7. Significant swelling, indicated by a decrease in the polymer volume fraction after immersion in the buffer solution, is obtained for the pH values of 5 and above. These swelling results shed some light on the success of the vapor-phase solvent exchange process. The acid-catalyzed hydrolysis of the P*t*BMA midblocks gives fully protonated PMAA midblocks, which remain in this protonated state throughout subsequent precipitation and drying steps. When the solvent exchange takes place, the pH remains low.

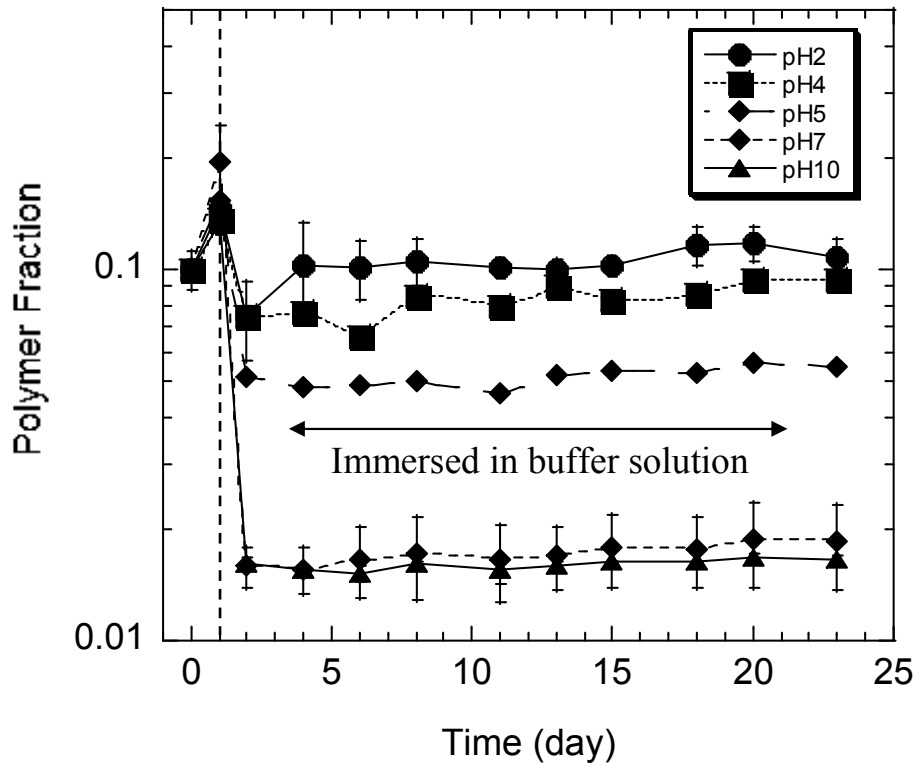

Figure 2.7. Swelling properties of the 370-1450-370 polymer gels in different buffer solutions. Hydrogels were formed from 10 wt % DMSO solutions and immersed in buffer solutions with the *pH* values indicated. Dotted vertical line represents the time of immersion.

The dissociation of the acid groups is determined by the local pH in the gel and the equilibrium constant, K_a, for the dissociation of the acid groups:

$$COOH \overset{K_a}{\Leftrightarrow} COO^- + H^+ . \tag{2.2}$$

The relative concentration of dissociated groups is determined by the difference between *pH* and *pKa*:

$$\log\frac{\left[COO^{-}\right]}{\left[COOH\right]} = pH - pK_a . \tag{2.3}$$

If there is no added salt and the internal pH is low, charge neutrality requires that $[H^+] = [COO^-]$, in which case Equation 2.3 reduces to the following:

$$pH = \frac{1}{2}\left[pK_a - \log\left[COOH\right]\right] \tag{2.4}$$

For a *pKa* = 4.8 the pH of 1 weight percent PMAA solutions in water ([*COOH*] = 0.116 M) is 3.5, in close agreement with measured values in the literature. The degree of ionization for polymethacrylic acid in water is therefore quite low and the polymers behave as neutral polymers, without strong swelling. The *pKa* is even higher in the presence of organic solvent, further limiting the possibility of ionization, and the associated enhanced swelling, during the solvent exchange process.[31]

2.3.3 Mechanical Response

The dynamic moduli of the swollen 370-1450-370 triblock hydrogels, prepared from initial solution concentrations of 10 wt.% and 20 wt.% (in DMF, NMP and DMSO) were investigated by shear rheometry. The storage and loss moduli, G' and G'', measured at room temperature, for the swollen polymer formed from a 20 wt.% of 370-1450-370 polymer are plotted in Figure 2.8. The hydrogels behave as elastic solids, with $G' >> G''$ and with very little frequency dependence of the moduli between 0.1 Hz and 100 Hz.

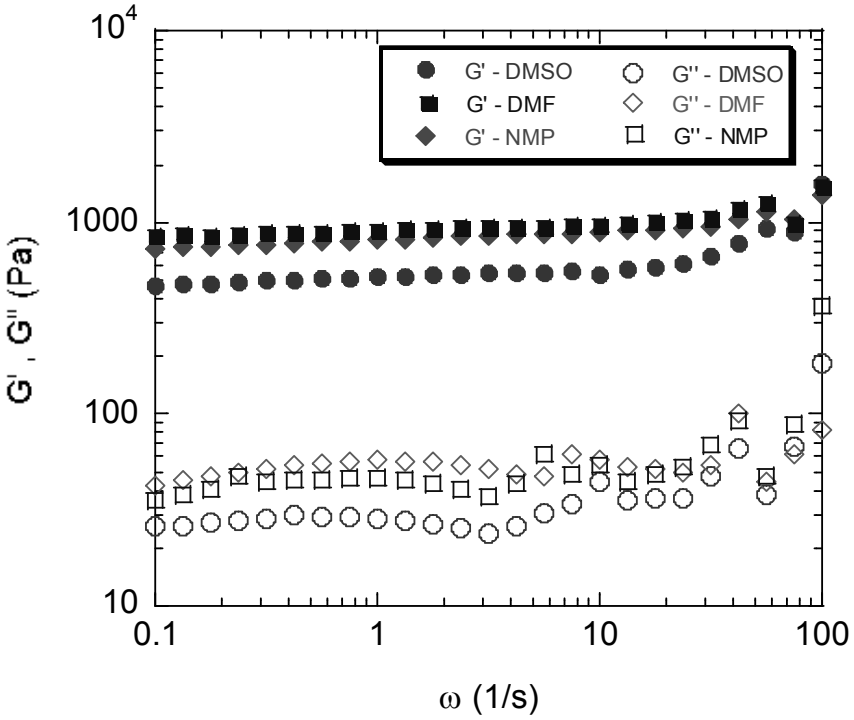

Figure 2.8. Dynamic shear moduli of swollen 370-1450-370 hydrogels that were originally dissolved in DMF, NMP and DMSO and equilibrated in tap water.

The measured moduli are in the range of 0.6 to 1.0 kPa, which is consistent with simple estimate from a Neohookean model of rubber elasticity theory, where *G* is given by the following expression[32]:

$$G = \frac{f\beta\phi_p^{1/3}\rho RT}{M}, \qquad \beta \equiv \frac{\left\langle R_{dry}^2 \right\rangle}{R_0^2}. \tag{2.5}$$

Here f is the fraction of triblock copolymer molecules in 'bridging' conformations between different PMMA domains, ρ is the density of the triblock copolymer (1.2 g cm^{-3}), R_0 is the rms end-to-end distance of the polymer in the melt state, and R_{dry} is the average value of the spacing between crosslinks in a hypothetical collapsed, dry state, with $f\beta = 1$. For a solvent-free

elastomer that was crosslinked under equilibrium conditions, $\beta = 1$. M is the number average molecular weight between crosslinks, and $f = 1$ if there are no loops or dangling ends in the network structure. In this case Equation 2.5 was used to obtain values of the quantity $f\beta$ from the measured rheological response. Values of this product are included in Table 2.1 for the 370-1450-370 gels, and for the 200-560-200 gel formed from a 10 wt % solutions in DMSO, which formed a transparent gel after the cloudy gel emerging from the solvent-exchange process was immersed in water.

Table 2.1. Properties of gels equilibrated with water (pH ≈ 7.7). Shear moduli (G) were obtained by rheometry, and values of $f\beta$ were obtained from Equation 2.5 Φin and Φp are the respective polymer concentrations of the initial solution prior to solvent exchange, and the swollen gel in the equilibrated state.

Polymer	Solvent	Φ_{in}	pH	Φ_p	G (Pa)	$f\beta$
370-1450-370	DMF	0.1	7.7	0.01	640	0.20
370-1450-370	NMP	0.1	7.7	0.01	640	0.20
370-1450-370	DMSO	0.1	7.7	0.01	560	0.17
370-1450-370	DMF	0.2	7.7	0.02	1000	0.25
370-1450-370	NMP	0.2	7.7	0.02	940	0.23
370-1450-370	DMSO	0.2	7.7	0.02	640	0.16
200-560-200	DMSO	0.2	7.7	0.15	3400	0.19
370-1450-370	DMF	0.2	4	0.07	688	0.11

The equilibrium swelling can be determined by the overall internal pressure within the gel. This pressure has two terms, an elastic pressure, Π_{el}, due to stretching of the elastic network strands, and an osmotic pressure, Π_{os}, which is due to segment/segment interactions within the

gel. The elastic pressure is determined by the volume dependence of the elastic free energy density, Δf_{el}:

$$\Pi_{el} = -V \frac{\partial}{\partial V} \Delta f_{el} \tag{2.6}$$

where V is the volume of the gel. For a Neohookean material with a low-strain shear modulus of G, the elastic free energy density is given by the following expression:

$$\Delta f_{el} = \frac{G\left(\lambda_x^2 + \lambda_y^2 + \lambda_z^2 - 3\right)}{2} \tag{2.7}$$

where λ_x, λ_y and λ_z are three principal extension ratios. For a gel that undergoes isotropic swelling $\lambda_x = \lambda_y = \lambda_z = \lambda$, and volume ratio for the swollen to unswollen gel (V/V_o), where volume of the unswollen gel is V_o, is equal to λ^3. Pure solvent has no elasticity and an osmotic pressure of zero. For a gel that is swollen to equilibrium in pure solvent, the net pressure within the gel must also reduce to zero. In this case, $\Pi_{os} = -\Pi_{el}$, and the following from the combination of Equations 2.2 and 2.7 was obtained:

$$\Pi_{os} = \frac{\partial}{\partial V}\left[\frac{3G}{2}\left(\frac{V}{V_0}\right)^{2/3}\right]_{v=v_0} = G \tag{2.8}$$

According to Equation 2.8, if a gel is immersed in pure solvent, it either expels or imbibes solvent until the osmotic pressure inside the gel is equal to its shear modulus. From the data in Table I, we have $G = \Pi_{os} = 700$ Pa, with $\phi_p = 0.07$, for the 370-1450-370 gel equilibrated in pH 4 buffer. This value is less than reported values for PMAA solutions in buffers with similar pH values and polymer concentrations by a factor of ≈ 4.[33] This difference was attributed to the

different osmotic strengths of the buffers used and to the partitioning of other species between the buffer and the gel that is not accounted for in this very simple comparison.

2.3.4 Porous Hydrogel Formation and Characterization

Porous hydrogels, useful for applications as tissue scaffolds, were produced by adding NaCl crystals with sizes between 150 and 250 μm to the mixture prior to solvent exchange. A trace amount of hydrophobic dye (Hostasol yellow 3G) was also added to the solution for imaging purposes. The solution was then exposed to a saturated water vapor for 3 h to form the gel as described above. The gel was then immersed in water overnight in order to leach out the salt crystals. The gel became clear after leaching, showing a slightly yellowish color due to fluorescent dye.

In order to characterize pore sizes and distributions, confocal laser scanning microscopy was used. A z-stack method was used where the hydrogel was optically sliced through its thickness, with 2-dimensional images were obtained for each slice. A 3-D construction of these 2-D images is given in Figure 2.9. Open pore structure was observed thought the entire gel thickness. Pore sizes of the gels were measured to be in between 600 to 860 μm which are larger than the initial particle sizes of 150-250 μm. This result is in good agreement with the swelling results which show a factor of 3 increase in linear dimensions of the gel when the exchanged material is immersed in a neutral pH buffer.

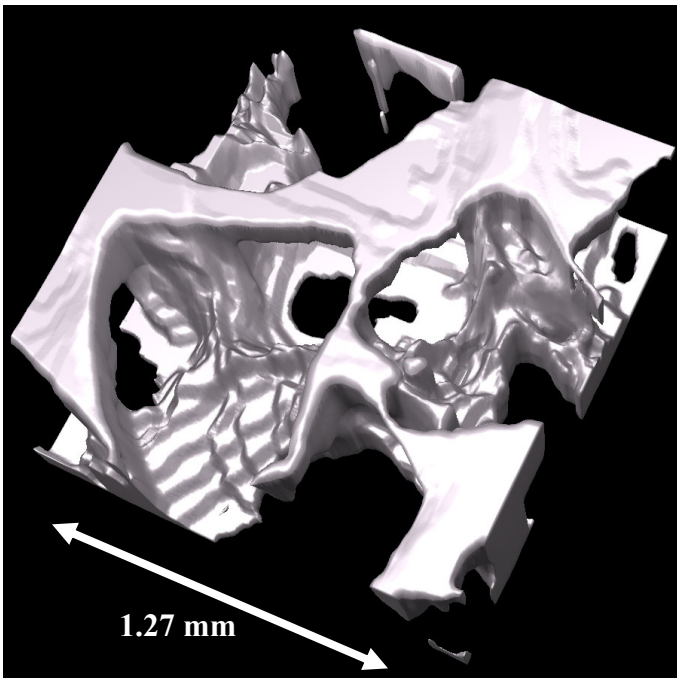

Figure 2.9. 3-D construction of a porous hydrogel obtained by confocal laser scanning microscopy.

2.3.5 Behavior at Large Deformations

In order to illustrate the behavior of those swollen gels at large deformations an indentation method, illustrated in Figure 2.10, was used. Hydrogels were prepared as described above and immersed in liquid media to equilibrate the sample. A compressive load was applied to the swollen hydrogel, after an initial contact was established by a flat-ended cylindrical steel punch with a radius a = 0.39 mm. Load (P) and displacement (δ) data were recorded during the experiment. A typical plot showing the average stress ($P/\pi a^2$) vs. the average strain (δ/a) is given in Figure 10 for 370-1450-370 polymer. The gel was formed by vapor phase solvent exchange from a 20 wt % solution in NMP, and was swollen in water to given a swollen gel with a thickness of 7 mm and a polymer weight fraction of 0.02. From Figure 2.10, it is clear that the swollen gels can withstand high strains without fracture.

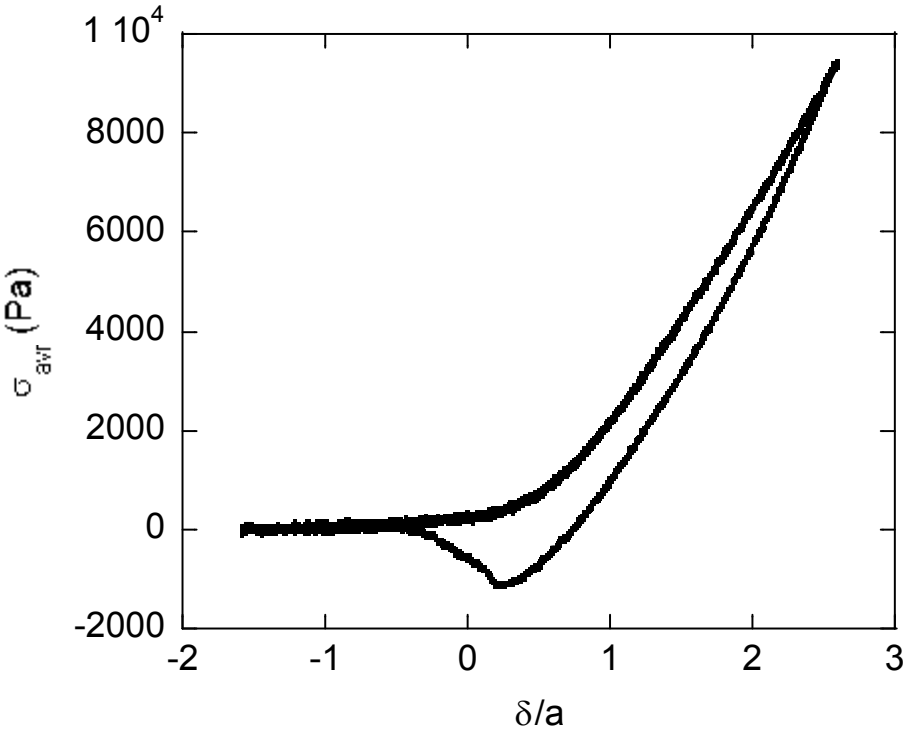

Figure 2.10. Average stress- normalized displacement curve for 370-1450-370 hydrogel originally dissolved in NMP, and equilibrated in water.

2.4 SUMMARY

A self-assembly technique has been developed for the formation of acrylic triblock hydrogels by vapor phase solvent exchange. For this purpose two PMMA-PMAA-PMMA triblock copolymers having different hydrophobic/hydrophilic block ratios were synthesized. Triblock polymers were dissolved in DMF, or in one of the injectable solvents, DMSO and NMP. Solvent exchange occurs when the solution is exposed to saturated water vapor. As water replaces the original solvent, the PMMA blocks form aggregates that are linked by the water-soluble PMAA midblocks. The equilibrium swelling and mechanical properties of the gels were

investigated, and porous hydrogels were produced by adding NaCl crystals to the polymer solution prior to solvent exchange. The results can be summarized as follows:

- Highly swollen gels are more readily obtained for the larger copolymer (370-1450-370), which also has a higher methacrylic acid content than the smaller copolymer (200-560-200).
- The methacrylic acid groups remain in the protonated state when exposed to pure water vapor. These groups become deprotonated when immersed in buffer solutions with pH > 5, resulting in a substantially decreased polymer volume faction for the 370-1450-370 gels.
- At neutral pH the gels formed from the 370-1450-370 polymer were transparent, with $G \approx 1$ kPa, and $f\beta \approx 0.2$.
- In most cases, the 200-560-200 polymer formed stiffer, opaque gels, but in one case we were able to obtain a transparent gel with $G \approx 3.5$ kPa.
- All gels are able to be deformed to several strain units prior to failure.
- Porous hydrogels are produced by adding NaCl crystals to the polymer solution prior to solvent exchange.

2.5 ACKNOWLEDGMENTS

This material is based upon work supported by the Northwestern University Materials Research Center, through the NSF MRSEC program, DMR-0520513. I gratefully acknowledge Prof. W. Burghardt and M. Seitz for assistance with the SAXS experiments. SAXS experiments were performed at the DuPont-Northwestern-Dow Collaborative Access Team (DND-CAT) Synchrotron Research Center located at Sector 5 of the Advanced Photon Source. DND-CAT is

supported by the E.I. DuPont de Nemours & Co., The Dow Chemical Company, the U.S. National Science Foundation through Grant DMR-9304725 and the State of Illinois through the Department of Commerce and the Board of Higher Education Grant IBHE HECA NWU 96. Use of the Advanced Photon Source was supported by the U. S. Department of Energy, Office of Science, Office of Basic Energy Sciences, under Contract No. W-31-10. I would like to acknowledge M. Shah for her help on 3-D construction.

This chapter appear in: “Self-assembly of acrylic hydrogels by vapor-phase solvent exchange”, Murat Guvendiren and Kenneth R. Shull; *Soft Matter*, 3, 619-626 (2007).

CHAPTER 3

SELF-ASSEMBLY AND ADHESION OF DOPA-FUNCTIONAL METHACRYLIC TRIBLOCK HYDROGELS

CHAPTER 3

SELF-ASSEMBLY AND ADHESION OF DOPA-FUNCTIONAL METHACRYLIC TRIBLOCK HYDROGELS

3.1 INTRODUCTION

There has been a growing effort to produce safe and cost effective bio-adhesives that can be applied from a low-viscosity solution, and are able to self-assemble and form strong and durable bonds in wet environments. Adhesive materials inspired by marine mussels are particularly intriguing in this respect. These organisms anchor themselves to surfaces by secreting a liquid adhesive based on mussel adhesive proteins (MAPs) that harden and form water resistant bonds within a few seconds.[34,35] The most widely studied marine mussel is the blue mussel, *Mytilus edulis*. A range of different MAPs have been isolated from the *Mytilus edulis* foot. Five of these proteins, referred to as Mefp-1 to Mefp-5, all contain an unusual amino acid, L-3,4-dihydroxyphenylalanine (DOPA).[36,37] Mefp-3 and Mefp-5 both contain large amounts of DOPA (up to 30 mol%).[36] They are found to concentrate at the interface between the adhesive surface and the substrate, and are generally supposed to play important roles in determining both the cohesive and adhesive properties of the secreted material:[38,39] As illustrated in Figure 1a, the DOPA catechol can easily oxidize to the quinone, which then undergoes crosslinking reactions that are responsible for the cohesive strength of these materials.[40-43] The adhesive role is not as well understood, although the ability of DOPA to form metal oxide

complexes is well documented.[34,35] Figure 1b shows two proposed bonding mechanisms to a titanium oxide surfaces.[44]

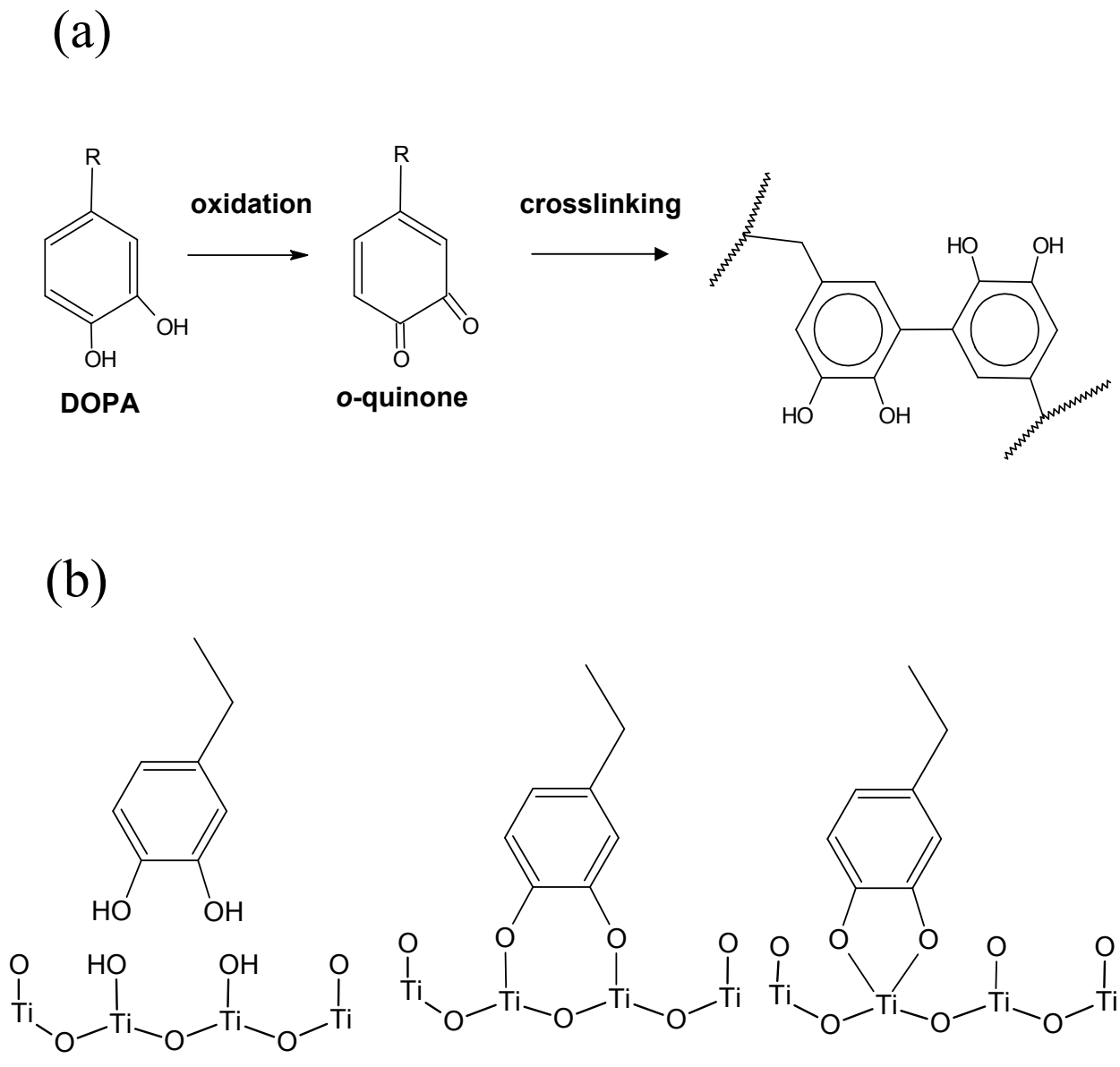

Figure 3.1. Schemes showing (a) DOPA oxidation to *o*-quinone followed by crosslinking; (b) DOPA-Ti interactions.

There have been several efforts to mimic the water resistant adhesive properties of MAPs by the incorporation of DOPA into synthetic polymers.[39,45-51] In these studies DOPA oxidation is the trigger to form a gel network via the crosslinking reactions mentioned above. However, the un-oxidized form of DOPA is believed to possess stronger adhesive properties, specifically to metallic surfaces.[38] This conjecture has been confirmed recently by the single molecule AFM experiments of Lee *et al.* [52] Furthermore, the use of DOPA oxidizing reagents (such as $NaIO_4$ and H_2O_2)[38] may complicate the future in *vivo* applications of these materials. In order to better understand the adhesive role of the DOPA, and to develop water-resistant adhesives based on DOPA chemistry, alternative gelation mechanisms that do not rely on DOPA oxidation are highly desirable.

The most widely studied stimuli for gel formation are temperature, pH, ion concentration, and UV and/or visible light. Many of these gelation mechanisms have been applied to DOPA-containing materials. For example, Huang *et al.* incorporated DOPA into a thermoreversible hydrogel,[53] and Lee *at al.* recently reported a DOPA-containing hydrogel formed by photopolymerization.[54] Neither of these systems requires any oxidizing reagents for gel formation. However, the crosslinking reactions used to form strong chemical gels can be inhibited either by oxygen, or by the DOPA itself. These issues are particularly important when one is interested in the adhesive properties, which can be severely degraded by the presence of a weak boundary layer. Self-assembled gels, which rely on physical association as opposed to chemical crosslinking, are a useful alternative to chemically crosslinked gels for this reason.

In this chapter a series of DOPA-modified triblock copolymer gels have been prepared, and their adhesive and mechanical properties have been assessed. Gelation in these

materials occurs by the formation of glassy endblock aggregates during a simple solvent exchange process. Gels were prepared by synthesizing a DOPA modified ABA type triblock copolymer, in which the hydrophobic endblocks consist of poly(methyl methacrylate) (PMMA) (A), and poly(methacrylic acid) (PMAA) is the water soluble midblock (B). DOPA is incorporated into the hydrophilic PMAA midblock. These block copolymers self-assemble to form strong hydrogels when solutions in *N*-methylpyrrolidone (NMP) or dimethyl sulfoxide (DMSO) are exposed to water vapor. The underwater adhesion of these hydrogels to TiO_2 surfaces have been studied, using an axisymmetric adhesion test, and the adhesive properties of these materials were correlated to the *pH* of the surrounding solution.

3.2 EXPERIMENTAL DETAILS

3.2.1 Materials

Methyl methacrylate (MMA) and *tert*-butyl methacrylate (*t*BMA) were degassed by freezing in liquid nitrogen after exposure to trioctylaluminum. After degassing, *t*BMA was distilled under reduced pressure and refrigerated. MMA was distilled directly into the reaction chamber prior to polymerization. Lithium (Li) and naphthalene were reacted in distilled tetrahydrofuran (THF) at room temperature for 24 h under a nitrogen atmosphere. A persistent dark green color was observed as the reaction proceeded. LiCl was baked in the reaction chamber at 130 ^{0}C under vacuum for 16 h. Diphenylethylene (DPE) was purified by distillation under reduced pressure after addition of a small amount of *sec*-butyllithium. DOPA methyl ester hydrochloride, *o*-benzotriazole-*N,N,N,N'*-tetramethyl-uronium-hexafluoro-phosphate (HBTU), *N*-hydroxybenzotriazole (HOBT), triethylamine, *N*-methyl pyrrolidone (NMP), dimethyl

sulfoxide (DMSO), dimethylformamide (DMF) and dichloromethane (DCM) were used as received from Sigma-Aldrich.

3.2.2 Synthesis and DOPA-Modification of Methacrylic Triblock Copolymer

The overall synthesis, shown schematically in Figure 3.2, includes three steps: (a) sequential living anionic polymerization of MMA and *t*BMA at -78^0 in THF with the presence of LiCl by using a difunctional initiator, (b) hydrolysis of poly(*tert*-butyl methacrylate) (P*t*BMA) midblock to poly(methacrylic acid) (PMAA), and (c) DOPA incorporation into PMAA midblock. Details of anionic synthesis of poly(methyl methacrylate) – poly(*tert*-butyl methacrylate) – poly(methyl methacrylate) (PMMA – P*t*BMA – PMMA) triblock copolymer (a), and hydrolysis reaction (b) were explained in chapter 2. In brief, lithium and naphthalene were reacted in THF at room temperature for 24 h under a nitrogen atmosphere. This initiator solution was reacted with DPE to form the difunctional initiator (red color). *t*BMA and MMA monomers were added sequentially. Before introducing MMA into the reaction chamber, an aliquot of the reaction mixture was withdrawn for analysis by gel permeation chromatography (GPC) (Waters 717plus auto-sampler with a Waters 2410 refractive index detector) in order to determine the molecular weight of the P*t*BMA midblock. The solution was then precipitated in a methanol/water mixture (90:10). The polymer was dried under vacuum overnight. The compositions of the polymers were determined by GPC and nuclear magnetic resonance spectroscopy (NMR) (^{1}H-NMR, P-Inova 500MHz) using d-chloroform. Hydrolysis of the PtBMA midblock was done in dioxane with the presence of hydrochloric acid (HCl) at 80 ^{0}C for 6 h. The solution was then precipitated into hexane. The polymer was dried under vacuum after being washed in hexane and water several times. The *tert*-butyl signal (1.43 ppm) in the NMR

spectrum completely disappeared after the hydrolysis reaction, indicating that the midblock had been successfully converted to methacrylic acid.

In order to incorporate DOPA into the PMAA midblock of the triblock copolymer, DOPA methyl ester (DOPA-ME) hydrochloride, HOBT and HBTU (1 : 2 : 2 : 1.4 mole ratio, respectively), were vacuum degassed in the reaction flask for 1 h. The flask was then flushed with nitrogen gas. DMF/DCM (50:50) was injected into the flask through the rubber septum. The system was stirred for 15 minutes, in order to fully dissolve all the ingredients and activate the methacrylic acid. In order to activate DOPA-ME, triethylamine (1 : 1 copolymer to triethylamine mole ratio) was injected into the solution. A faint yellow color was observed as the reaction proceeded. The solution was stirred for 10 h. The solution was then precipitated in hexane and washed with hexane several times before it was dried under vacuum overnight, and refrigerated. After DOPA modification significant DOPA phenyl signals at 6.6-6.8 ppm (3 H -$C_6H_3(OH_2)$) appeared in the NMR spectrum.

3.2.3 Quantification of DOPA Content

The DOPA content of the triblock copolymers was determined from a modified DOPA assay developed by White and Benedict.[55,56] The UV absorbance of the polymer solutions in DMF at the maximum absorbance wavelength of the oxidized catechol (λ_{max} = 500 nm) was recorded using a Hitachi U-2010 UV-Vis spectrophotometer. Standard curves were constructed by using solutions containing known concentrations of oxidized DOPA methyl ester.

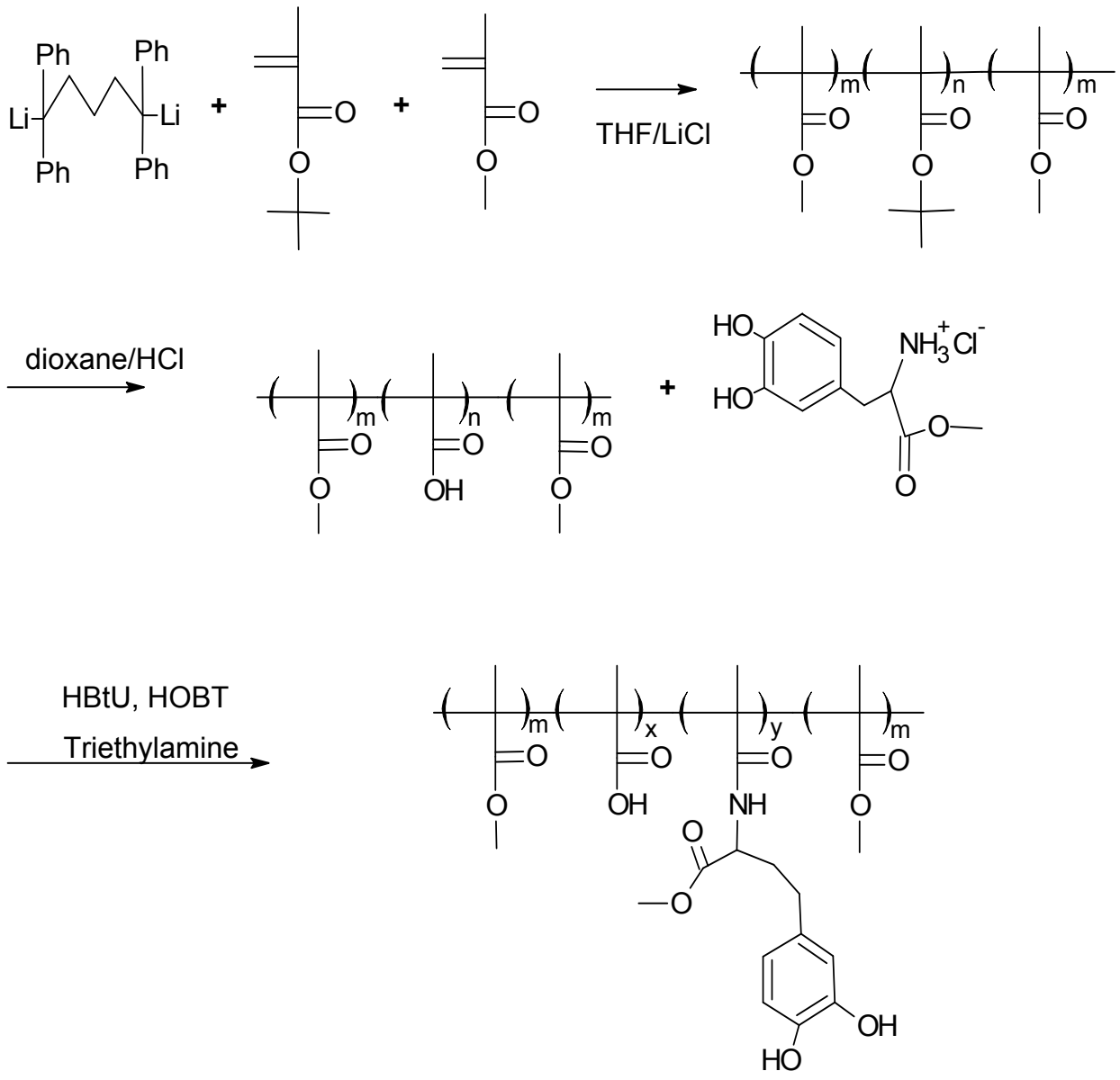

Figure 3.2. Anionic polymerization of *t*BMA and MMA in the presence of a difunctional initiator followed by hydrolysis of the P*t*BMA midblock to PMAA, and incorporation of DOPA to the PMAA midblock.

3.2.4 Self-Assembly of Hydrogels by Solvent Exchange

The DOPA-modified triblock copolymer was fully dissolved in DMSO, NMP or DMF, which are good solvents for both the PMAA and PMMA blocks. These solutions were then exposed to saturated water vapor for 3 h to enable solvent exchange with water. As water replaced the initial solvent, the hydrophobic end-blocks (PMMA) aggregated into spherical domains. The water soluble mid-blocks (PMAA) formed bridges between these domains, as was demonstrated previously for thermoreversible gels formed from similar triblock copolymers.[23] After solvent exchange the hydrogels were immersed in water or controlled pH buffers, in order to study their equilibrium swelling properties in detail. A Paar Physica MCR (TEK 150PA-C) rheometer with parallel plate geometry was used to measure the dynamic shear moduli of the hydrogels in the linear viscoelastic regime.

3.2.5 Adhesion Tests

The adhesive and mechanical properties of the DOPA-modified hydrogels in liquid media were tested using an axisymmetric indentation method.[27,57] Schematics of the adhesion test apparatus is given in Figure 3.3a. The geometry of a flat punch in contact with the hydrogel, Figure 3.3b, provides a well defined contact area having a radius, a, equal to the punch radius. TiO_2 was chosen as the substrate surface since Ti has been commonly used for medical alloys. The flat punch was coated with 50 nm of TiO_2 by electron-beam evaporation. It was cleaned with acetone and methanol sequentially, and exposed to UV-Ozone (Jelight Company Model 42 UVO-Cleaner) for 15 min prior to each adhesion experiment. The hydrogel was placed on a TiO_2 coated glass slide, which was also cleaned beforehand, and placed inside the chamber filled with liquid media. The flat punch was brought into contact with the fully swollen hydrogel in liquid

media at a constant speed of 5 μm/s. When a maximum compressive load of 5 mN was reached, the motor was reversed and the punch was retracted at the same rate. A tensile load is developed during pull-off which is an indication of adhesion between the gel and the TiO_2 coated punch. Load and displacement data were collected through a load transducer and an optical displacement sensor.

3.3 RESULTS AND DISCUSSION

3.3.1 Characterization of DOPA Modified Acrylic Polymers

The PMMA – PMAA – PMMA triblock copolymer was synthesized by sequential anionic living polymerization of tBMA and MAA, followed by the hydrolysis of the PtBMA midblock to form a water soluble PMAA midblock. The degree of polymerization of the PMMA – PMAA – PMMA triblock copolymer was 370-1450-370 (Mn=200,000 kg/mole, PDI = 1.09). DOPA was incorporated into the water soluble methacrylic acid by using carboimide chemistry, as explained above. The amount of DOPA attached to the midblock was measured by absorbance of the oxidized catechol at a wavelength of 500 nm. In this chapter, we focus on gels with three different DOPA levels, corresponding to mole fractions of DOPA incorporation into the PMAA midblock of 0, 0.2 and 0.4. These polymers are referred as DOPA00, DOPA20 and DOPA40.

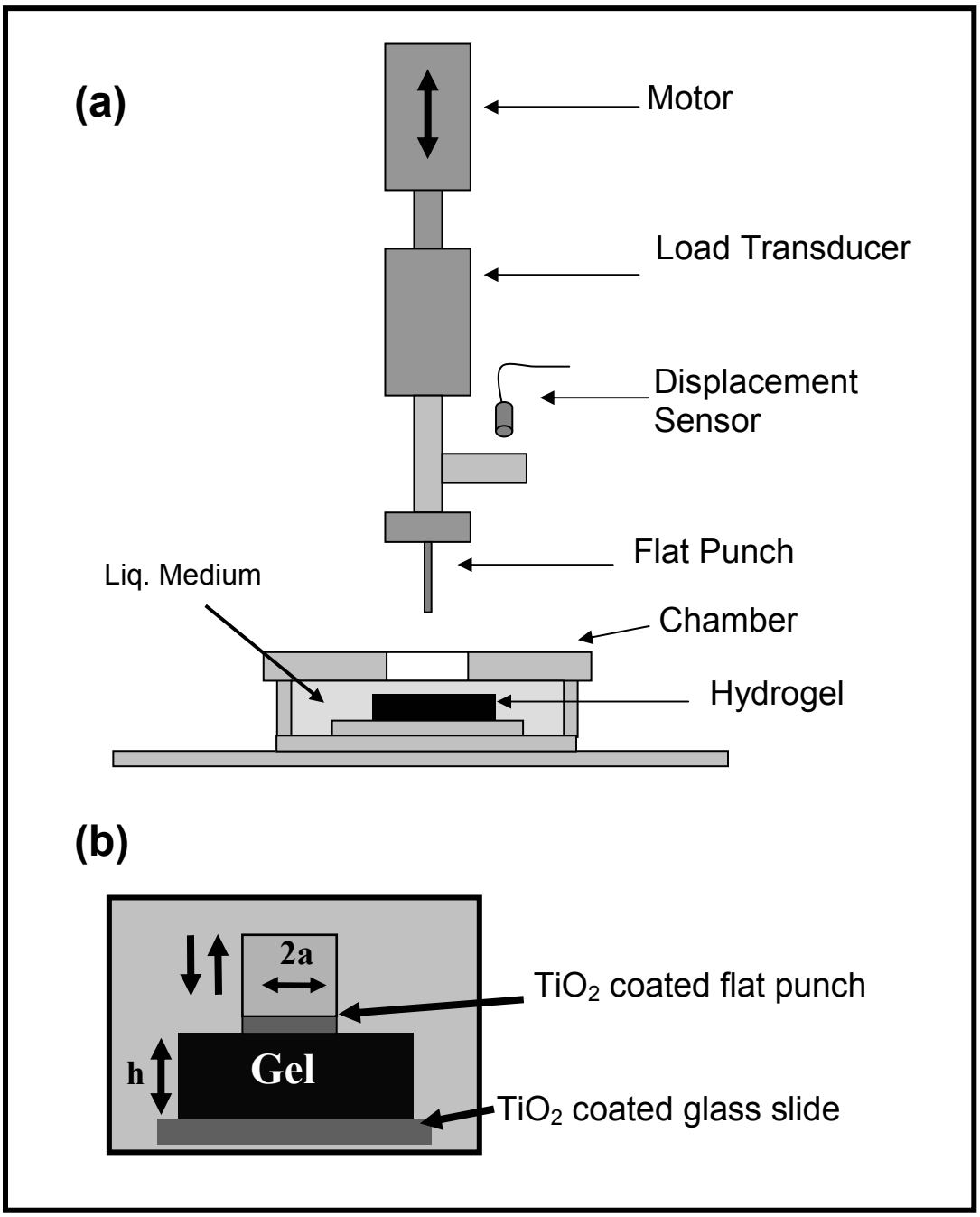

Figure 3.3. Schematic illustrations of (a) the apparatus used for the indentation experiments, and (b) the sample geometry, in which *a* and *h* denote punch radius and gel thickness, respectively.

3.3.2 Hydrogel Formation and Characterization

The four different triblock copolymers were fully dissolved in DMSO at polymer weight fraction of 0.1. These solutions were injected into circular washers, one side of which was attached to a glass slide, and exposed to saturated water vapor for 3 h (Figure 3.4a). Gelation occurs as the changing solvent quality causes the PMMA endblocks to aggregate. The gels were carefully taken out of the washers, and immersed in water (Figure 3.4b), in order to study their equilibrium swelling properties. In Figure 3.5, the time dependence of the polymer weight fraction is plotted for DOPA00 and DOPA20 gels. A decrease in the polymer fraction represents an increase in the swelling. In chapter 2, it was shown that in the absence of attached DOPA, the hydrogels swell significantly when immersed in solutions having *pH* greater than the *pKa* of methacrylic acid (≈ 4.8)[57], a result that is attributed to the ionization of the methacrylic acid groups. This general trend is preserved with the addition of the DOPA, where the polymer volume fraction is lower when immersed in solutions with a higher *pH*. However, the incorporation of DOPA into the hydrogels decreases the swelling ability of the gels at $pH = 6$ and $pH = 7.4$, a result that is illustrated schematically in Figure 3.6. This behavior is attributed to the hydrophobic nature of the fully protonated form of DOPA. For the DOPA40 material, the hydrophobic interactions are strong enough to completely deswell the polymer, resulting in nearly dry polymer, with a polymer volume fraction very close to 1.

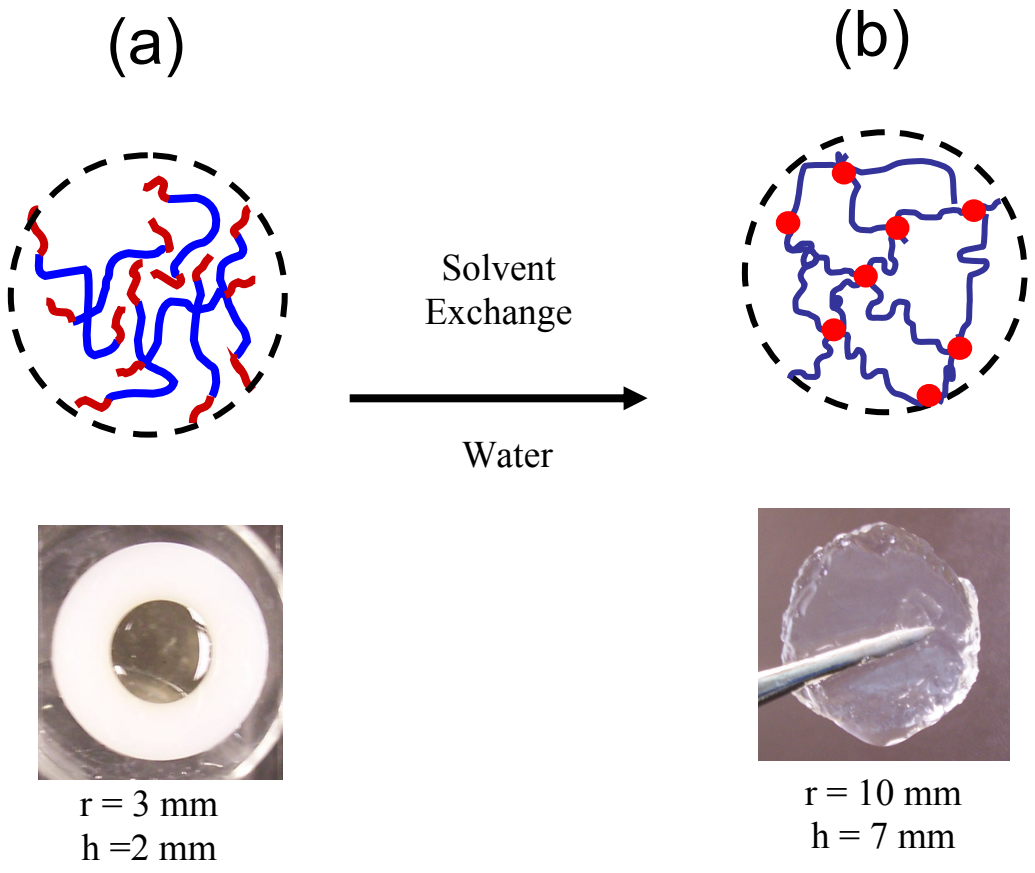

Figure 3.4. Photographs and schematic structures of the triblock copolymer: a) 10 wt % triblock solution in DMSO; b) swollen gel in water after exposure to saturated water vapor. The radius and thickness of the initial and final sample are indicated below parts (a) and (b).

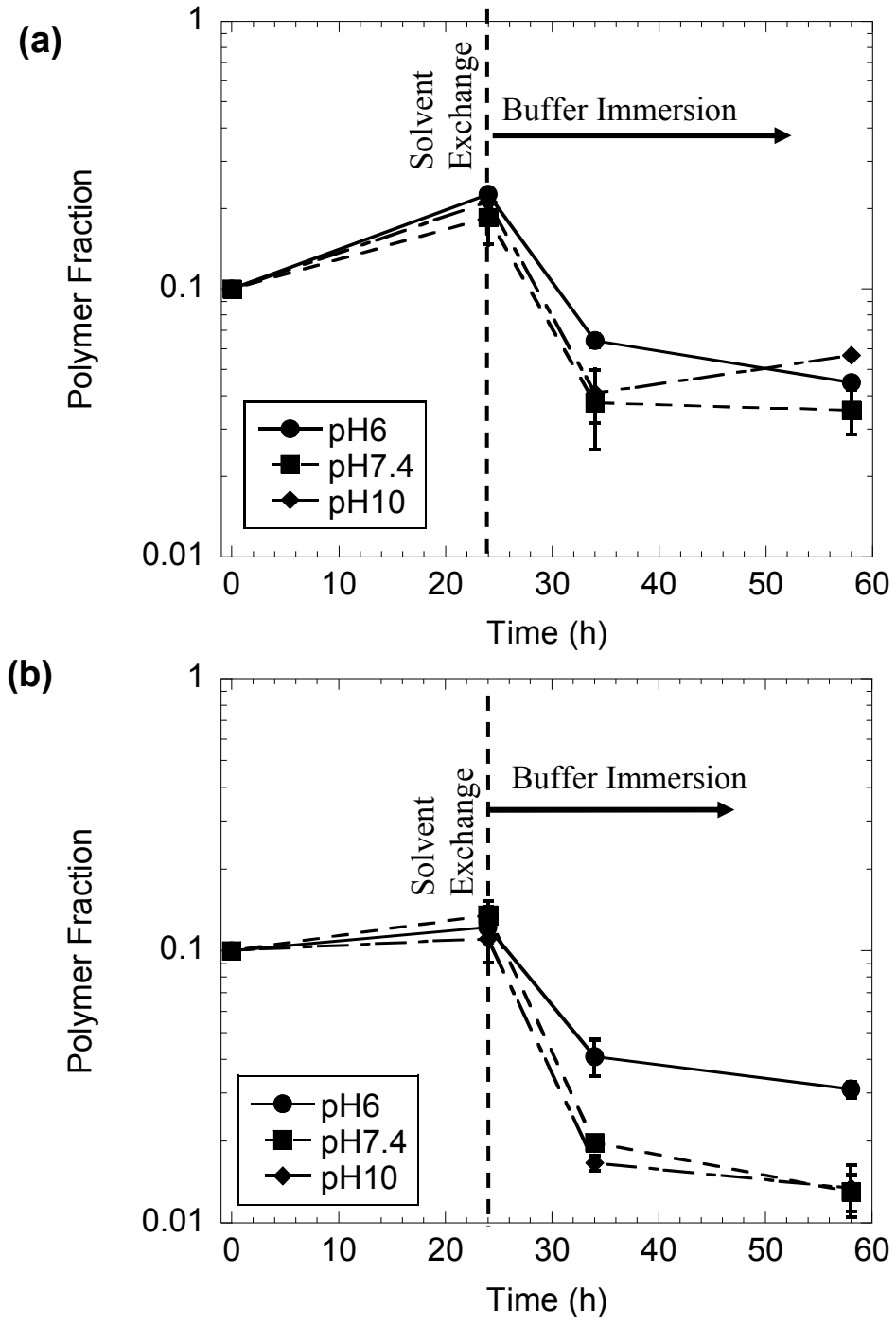

Figure 3.5. Swelling behavior of the DOPA00 (part a) and DOPA20 (part b) hydrogels. The polymer was initially dissolved in DMSO at a concentration of 10 wt %, gelled by exposure to water vapor, and immersed into different buffer solutions: pH6, pH7.4 and pH10.

Reported values for the *pKa* of DOPA are $pKa_I = 9.4$ and $pKa_{II} = 13.7$, corresponding to the removal of the first and second protons from the catechol.[58,59] If the *pH* of the swelling solution is increased above pKa_I, the DOPA groups become ionized, and they are no longer hydrophobic. This result is most clearly observed for the DOPA40 gel. The white, deswollen solid formed during the solvent exchange process, followed by immersion in neutral water, forms a highly swollen gel with a polymer volume fraction of 0.08 when immersed in a buffer with $pH = 10$. This swollen gel has a light brown color indicating the partial oxidation of DOPA, since the deprotonated form is much more prone to oxidation.

The dynamic moduli of the swollen hydrogels, prepared from initial solution concentrations of 10 wt % in DMSO, were investigated by shear rheometry at room temperature. It is previously shown in chapter 2 that equilibrated hydrogels behave as elastic solids, having moduli near 1 kPa with a specific value that is dependent on the equilibrium polymer fraction of the hydrogel. There is an increase in the modulus as the concentration of DOPA in the PMAA midblock increases, which is attributed to the decrease in swelling with an increase in the DOPA content in the midblock. The largest increase was observed in the case of DOPA40, having a $E = 5$ kPa, which was expected due to the high polymer fraction in this material. Moduli for a variety different gels obtained by shear rheometry, or from the indentation experiments described in the following section, are summarized in Table 3.1.

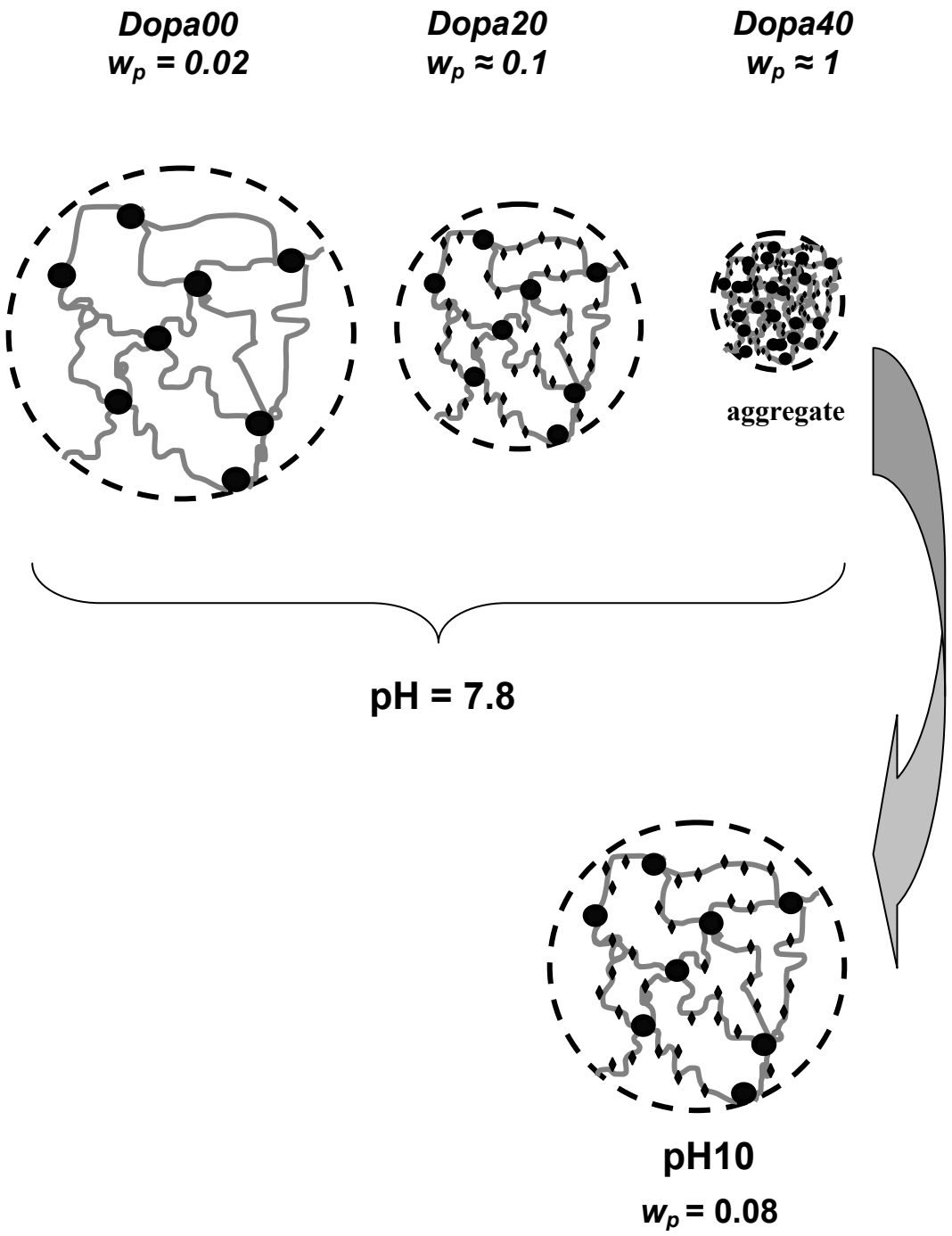

Figure 3.6. Schematics and pictures of the hydrogels equilibrated in water (top). The bottom schematics illustrate the subsequent swelling of the DOPA40 gel when immersed in a solution with $pH = 10$ buffer.

3.3.3 Adhesion Tests

The adhesion of DOPA-modified hydrogels in contact with TiO_2 was quantified with an axisymmetric indentation method. TiO_2 surfaces were cleaned prior to the experiment as described above. The TiO_2 coated flat punch was brought into contact with a hydrogel that was immersed in aqueous solution. Experiments were conducted where the surfaces were separated immediately after a compressive load of 5 mN had been attained, and after the surfaces were held in contact at this maximum load for times of 10, 20 and 30 min before they were separated. A typical plot, generally referred to as a 'tack' curve in the adhesion science community, is shown in Figure 3.7. Here the average stress ($\sigma_{avg} \equiv P/\pi a^2$) as a function of the normalized displacement (δ/a) is plotted, for experiments conducted in buffer solutions with $pH = 6$ (Figure 3.7a) and $pH = 7.4$ (Figure 3.7b). For these experiments the surfaces were kept in contact for 20 min.

The modulus of the layers is determined from the slope of the nominal stress/strain relationship. When the thickness of the elastic layer, h, is not substantially larger than the punch radius, a, the sample compliance depends on the both a and h[26]. For an incompressible elastic layer with a Poisson's ratio equal to 0.5, the relationship between σ_{avg} and δ/a for relatively small displacements is given by the following expression[27]:

$$\frac{\sigma_{avg}}{\delta / a} = \frac{8E}{3\pi}\left(1 + 1.33\left(a/h\right) + 1.33\left(a/h\right)^3\right) \tag{3.1}$$

where E is the Young's modulus of the elastic layer.

The critical energy release rate, $\mathcal{G}_c$, characterizing the adhesion of the gel to the TiO_2 surface is obtained from the maximum tensile stress, σ_p, illustrated schematically in Figure 3.7a. For our geometry, the critical enegy release rate is given by the following expression:[25,27]

$$\mathcal{G}_c = \frac{3\pi a \sigma_p^2}{32E} f_{Gp}, \qquad f_{Gp} = \left[\frac{0.56 + 1.5\left(\frac{a}{h}\right) + 3\left(\frac{a}{h}\right)^3}{\left(0.75 + \left(\frac{a}{h}\right) + \left(\frac{a}{h}\right)^3\right)^2} \right] \tag{3.2}$$

Values of *h* for the hydrogels ranged from 1 to 4 mm. Two punch sizes were employed in the experiments: *a* = 1.17 mm and 0.78 mm. The shear moduli and critical energy release rates obtained from our experimental data are listed in Table 3.1. Equation 3.2 is based on the assumption that the contact radius remains fixed at the punch radius up to the point of failure, which corresponds to the point where the applied energy release rate exceeds the critical energy release rate $\mathcal{G}_c$. In this case a linear relationship between nominal stress and strain would be obtained up to the maximum tensile stress, at which point the interface fails and the stress returns to zero, provided that *a/h* is less than 0.45[26]. This behavior is generally observed in these experiments, and the critical energy release rate is an appropriate measure of the adhesive interaction between the gel and the punch.

The dependence of the adhesion on the delay time is summarized in Figure 3.8. For a delay time of zero, the gels are actually more adhesive at a *pH* value of 10 than they are at the lower *pH* values. Our interpretation of this result is that the aggregation of the hydrophobic DOPA groups at low values of the *pH* inhibits their ability to interact with the surface. As a result longer contact times are required in order to establish contact between the DOPA groups and the titania surface at the lower values of the *pH*. For longer delay times we obtain values of

the adhesion that we feel are more representative of the equilibrated gel/titania interface. In Figure 3.9 we show values of the critical energy release rate for a delay time of 20 minutes, at *pH* values of 6, 7.4 and 10. The DOPA00 hydrogels show relatively weak adhesion to the TiO_2 surfaces, with G_c less than 250 mJ/m^2 or less in all cases. Because of the collapse of the DOPA40 gel at *pH* values of 6 and 7.4, we were only able to quantify the adhesion of this material at a *pH* of 10, where a value of G_c close to 100 mJ/m^2 is obtained. The most interesting results were obtained for the DOPA20 gels, which for long contact times adhere much more strongly at a *pH* values of 6 and 7.4 than they do at a *pH* value of 10. In fact, the DOPA/titania is strong enough so that failure occurs adhesively within the gel, but in very lose proximity to the gel/punch interface. The plateau value of $\approx$ 2 J/m^2 that is obtained for G_c at long contact times under conditions where the DOPA catechol is in its fully protonated form, corresponds to the fracture strength of the gel. The value of $\approx$ 2 J/m^2 for the gel toughness is consistent with measured values for similar physically crosslinked gels, such as gelatin.

Our results are consistent with measurements of catechol adsorption to TiO_2 surfaces, where adsorption is shown to decrease for pH values greater than 9.2, which corresponds to the *pKa* for the a deprotonation of the catechol[44]. In addition, single molecule measurements of the DOPA/TiO_2 interaction indicate that a stronger interaction is observed at low *pH* than at high pH[52]. A further complicating factor for high *pH* values is that DOPA oxidation to the quinone form occurs more readily under these conditions, producing forms that are no longer adhesive. These oxidation reactions are presumably responsible for the diminished strength of the DOPA/TiO_2 interaction observed at high *pH* values in the single molecule experiments[52], and are observed in our experiments as well. In Figure 3.9b we show the tack curve for a gel that had

been immersed in the pH = 10 buffer solution for 7 days. This gel had a brownish-red color that is indicative of oxidation of the catechol to the quinone form, which can lead to intra or intermolecular crosslinking reactions (Figure 3.1a), or to other side reactions. The adhesiveness of this gel was reduced dramatically, in comparison to the gel that had remained in the pH = 10 buffer for only three hours. The results for this oxidized gel are shown as the DOPA20-OX sample in Figure 3.9a and in Table 3.1.

Table 3.1. Swelling, mechanical and adhesive properties of hydrogels. w_i and w_p represents initial and equilibrium polymer weight fraction, E is the the Young's moduli, and G_c is the critical energy release rate for crack propagation within the hydrogel and TiO_2 interface.

sample	w_i	pH	w_p	E (kPa)	G_c (mJ/m^2)
DOPA00	0.1	6.0	0.031	1.3±0.4	225±160
DOPA00	0.1	7.4	0.013	1.2±0.4	65±50
DOPA00	0.1	10.0	0.013	0.42±0.1	200±140
DOPA20	0.1	6.0	0.045	0.9±0.4	2080±140
DOPA20	0.1	7.4	0.035	0.6±0.1	1780±90
DOPA20	0.1	10.0	0.040	0.7±0.1	200±140
Dopa20-OX	0.1	10.0	0.10	5.4±0.4	1±0.5
DOPA40	0.2	10.0	0.08	0.67	100±40

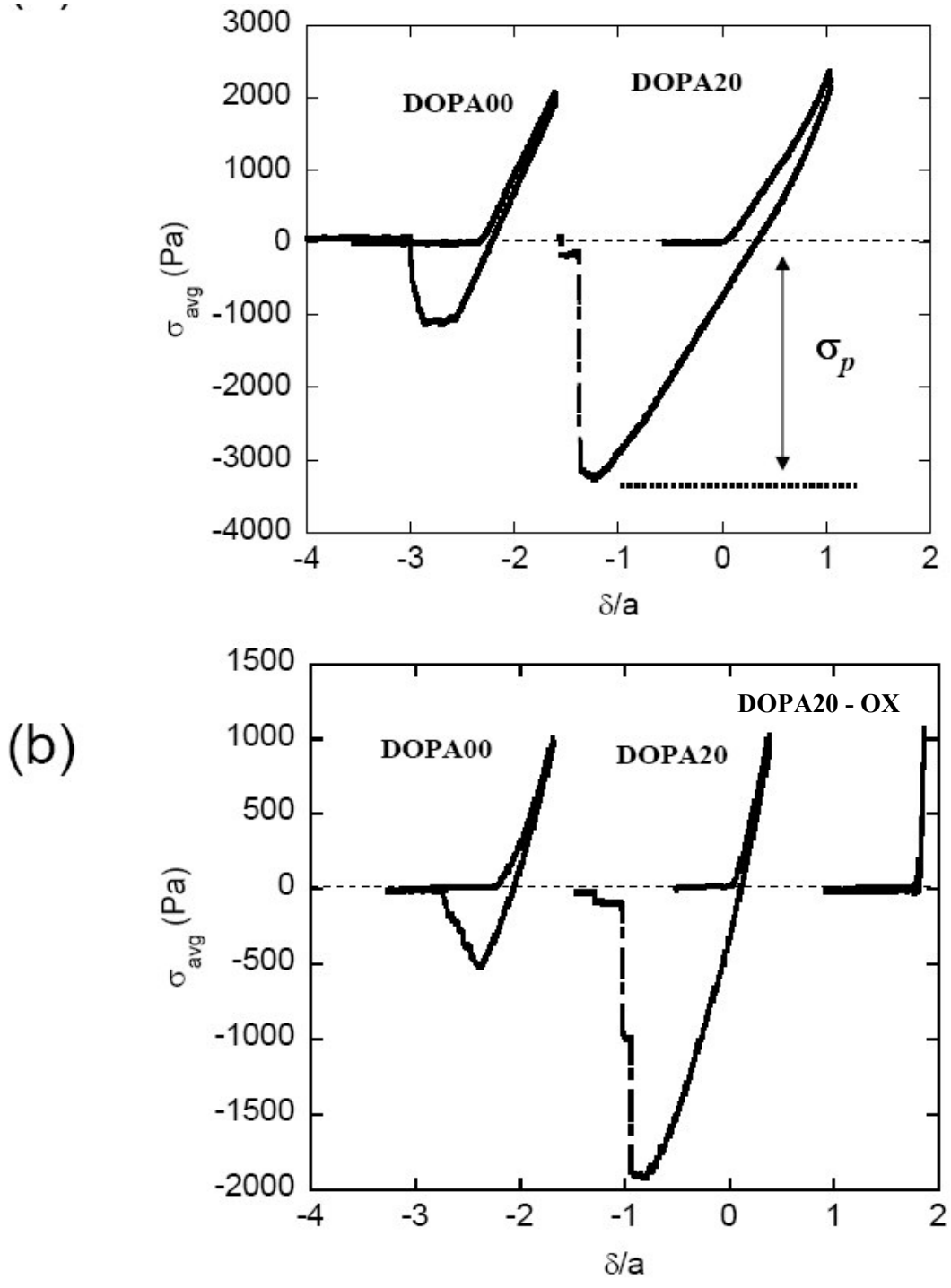

Figure 3.7. Average stress vs strain data for neat hydrogel and DOPA20 hydrogel in contact with TiO2 coated flat punch. Hydrogels were preformed by exposing 10 wt % solution in DMSO to saturated water vapor, and equilibrated in (a) *pH* = 6 and (b) *pH* = 7.4 buffer solutions.

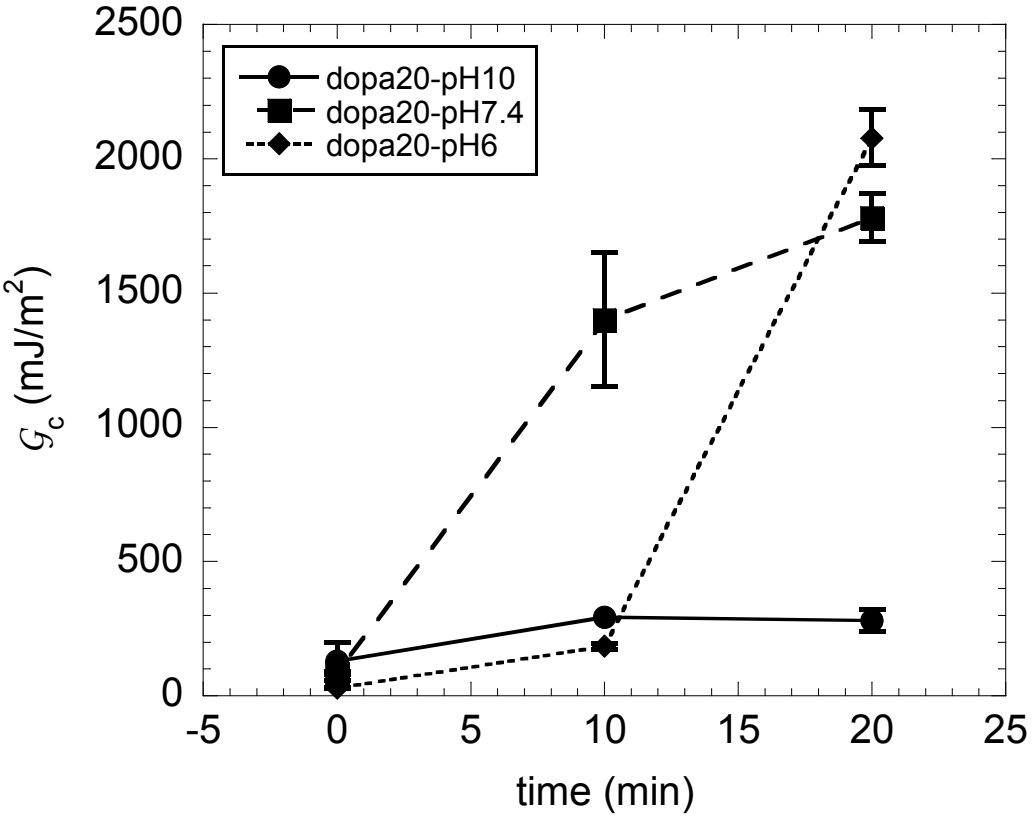

Figure 3.8. The critical energy release rate with increasing delay time for DOPA20 hydrogels in different buffer solutions.

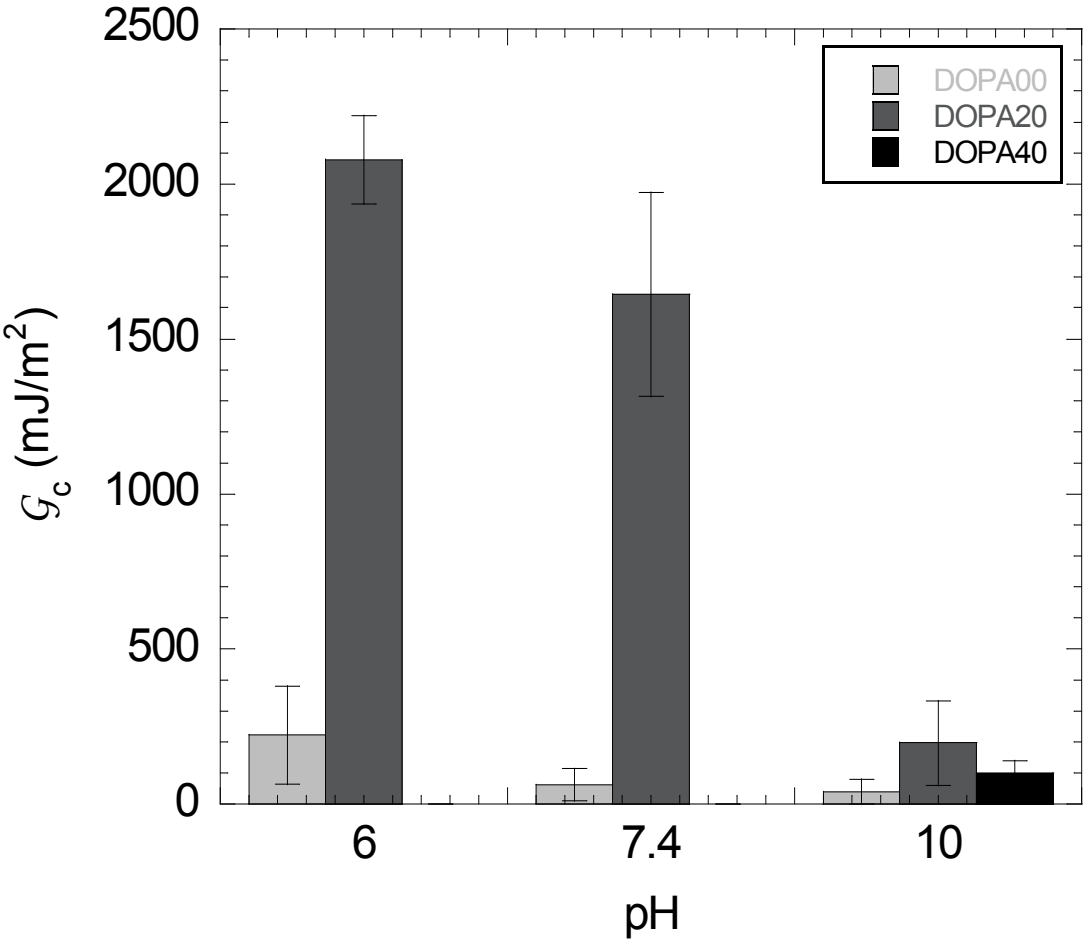

Figure 3.9. The critical energy release rate for hydrogel-TiO_2 interaction in different buffer solutions.

3.4 CONCLUSIONS

DOPA-functionalized PMMA-PMAA-PMMA triblock copolymer have been synthesized that can self-assemble and form a hydrogel *in-situ* by vapor phase solvent exchange from water miscible solvents such as DMSO and NMP. As water replaces the original solvent, the hydrophobic PMMA end-blocks form aggregates, with the water soluble PMAA mid-blocks

bridging these aggregates to form an elastic network. In order to study the effect of DOPA on the mechanical and adhesive properties of the hydrogel, the properties of three polymers with 0, 20 and 40 mole percent DOPA incorporation into the midblock have been compared. The swelling and mechanical properties of these hydrogels were investigated, as were the adhesive properties of these hydrogels in contact with a TiO_2 surface that was immersed in an aqueous medium. The results can be summarized as follows:

- Highly swollen transparent gels are easily formed by solvent exchange from triblock solutions with attached DOPA groups, giving gels with shear moduli in the kilopascal range.
- Incorporation of DOPA decreases the hydrophilicity of the midblock for *pH* values where the DOPA catechol is completely protonated (pH $< \approx 9.4$).
- At a *pH* of 10, the DOPA substituents are hydrophilic. At these high values of the pH the DOPA-modified triblock copolymers form highly swellable gels that show strong adhesion to TiO_2 surfaces, with measured critical energy release rates of ≈ 100 mJ/m^2.
- Oxidation of DOPA by prolonged exposure to high *pH* solutions reduces the adhesion significantly.

3.5 ACKNOWLEDGMENTS

This research is in collaboration with Phillip B. Messersmith from Biomedical Engineering Department at Northwestern University. This work was supported by the Northwestern University Materials Research Center through the NSF MRSEC program (DMR-0520513), and by the NIH (R01 DE14193). I would like to acknowledge Dr. Bruce Lee for a variety of helpful discussions.

CHAPTER 4

ADHESION OF DOPA-FUNCTIONALIZED METHACRYLIC TRIBLOCK MEMBRANES

CHAPTER 4

ADHESION OF DOPA-FUNCTIONALIZED METHACRYLIC TRIBLOCK MEMBRANES

4.1 INTRODUCTION

Marine mussels anchor to a variety of surfaces by secreting liquid proteins that harden and form water resistant bonds to a variety of surfaces. Studies have revealed that these mussel adhesive proteins (MAPs) contain an unusual amino acid: 3,4-dihydroxy-L-phenylalanine (DOPA)[34,60]. Although many of the details of mussel adhesion remain unknown, un-oxidized DOPA is believed to be responsible for water resistant adhesive properties, and the oxidized form of DOPA (*o*-quinone) is believed to be responsible for cohesive properties of these proteins[39]. There have been several efforts to mimic the water resistant adhesive properties of MAPs by the incorporation of DOPA into synthetic polymers[39,45-51]. DOPA-containing molecules have been found to possess good adhesion to metal, metal oxide and polymer surfaces[34,35]. In addition, these molecules have also been found to have useful mucoadhesive properties[39,53,61]. Although, the un-oxidized form of DOPA is believed to possess stronger adhesive properties, specifically to metallic surfaces[38,52], in these studies DOPA oxidation is the trigger to form a gel network via the crosslinking reactions. Furthermore, the use of DOPA oxidizing reagents (such as $NaIO_4$ and H_2O_2)[38] may complicate the future in *vivo* applications of these materials. In order to better understand the adhesive role of the DOPA and to develop water-resistant adhesives based on DOPA chemistry, alternative gelation mechanisms that do not

rely on DOPA oxidation are highly desirable[53,54]. In chapter 3, a useful alternative method to obtain crosslinked gels, self-assembly by solvent exchange, was introduced which relies on physical association as opposed to chemical crosslinking.

In this chapter, we have synthesized a DOPA-functionalized ABA type triblock copolymer in which poly(methyl methacrylate) (PMMA) is used for the hydrophobic endblocks (A), and poly(methacrylic acid) (PMAA) is the water soluble midblock (B). DOPA is incorporated into the PMMA midblock. These polymers self-assemble to form strong hydrogels when solutions in dimethyl sulfoxide (DMSO) are exposed to water vapor[57]. In order to study the adhesive properties of DOPA-functionalized PMMA-PMAA-PMMA polymers a membrane inflation method, which is a highly sensitive method for probing adhesive interactions[62] was used. The specific interactions between membrane and TiO_2, and membrane and tissue were investigated in an aqueous environment. Adhesion results show that the presence of DOPA improved the adhesion of hydrogels to a TiO_2 and tissue surface. In addition, the oxidation of DOPA in contact with the tissue significantly improves the adhesion of membrane to tissue surface.

4.2 EXPERIMENTAL DETAILS

4.2.1 Materials

PMMA-PMAA-PMMA triblock copolymer was synthesized by anionic polymerization of tert-butyl methacrylate (*t*BMA) and methyl methacrylate (MMA), followed by hydrolysis of the P*t*BMA midblock to form poly(methacrylic acid) (PMAA). The molecular weight of the resultant polymer was 200,000 kg/mole with a polydispersity of 1.09. The PMMA mid-block of

the polymer was functionalized with DOPA by using modified peptide chemistry, which gave 20 mole % conversion of the PMAA mid-block. In this chapter, two polymers were used that are referred to as DOPA00 and DOPA20, with the numbers indicating the mole % of DOPA in the midblock. The hydrophobic PMMA-PnBA-PMMA polymer (166,000 kg/mole) was obtained from Kuraray Co. LTD.

4.2.2 Sample Preparation

The membranes were prepared by spin coating each polymer solution onto a salt crystal. The membranes were then floated on water and manually transferred to the end of the cylindrical expansion chamber. A schematic representation of the membrane geometry is given in Figure 4.1a. Two bilayer membranes (Figure 4.1b) each having a hydrophobic PMMA-PnBA-PMMA membrane (spun cast from 10 wt% solution of toluene) were prepared. This supporting membrane was either covered with a PMMA-PMAA-PMMA layer (spun cast from 10 wt% solution of DMSO), or covered with a DOPA-functionalized PMMA-PMAA-PMMA layer (spun cast from 5 wt% solution of DMSO, floated onto water and then transferred to the supporting membrane). The thickness of each layer was approximately 1 μm.

4.2.3 Membrane Expansion Experiments

A schematic diagram of the apparatus used in the membrane experiments is given in Figure 4.2a. The details of the membrane expansion experiments and the apparatus have been explained by Brass and Shull[62]. In brief, the membrane is transferred to the end of a cylindrical expansion chamber and immersed in a liquid medium. The chamber was then connected to a syringe pump (NE-1000) to control the inflation rate. The membrane was inflated at an inflation

rate of typically 2 mL/h. The pressure of the membrane during inflation was measured by a differential pressure transducer (0.1-10 MPa, MKS Baratron) and recorded with time through a LABVIEW programming interface. Circular contact areas were observed when the inflated membrane came into contact with the substrate, with contact radii that were quantified by an image analysis program (ImageJ, National Institutes of Health). Typical contact images from top and side views are given in Figure 4.2b. After expansion of the contact radius to a maximum value that was determined from the images, the pump was stopped. An increase in the contact area was observed as an indication of adhesive interactions at the interface between the membrane and the substrate. After maintaining the surfaces in contact for 20 min, the air in the chamber was withdrawn in order to pull the membrane away from the substrate surface. The release pressure at which the membrane was completely separated from the substrate was used as an indication of adhesiveness. Negative pressures were needed to separate the membrane from the substrate surface, which is an indication of the adhesive interactions between membrane and the substrate. Two sets of experiments were conducted in this study. In the first set, we studied the specific interactions between DOPA and TiO_2, where the substrate was a TiO_2 coated silicone wafer. In order to investigate the adhesive properties of DOPA on tissue, pig skin was used as the substrate material in the second set of experiments.

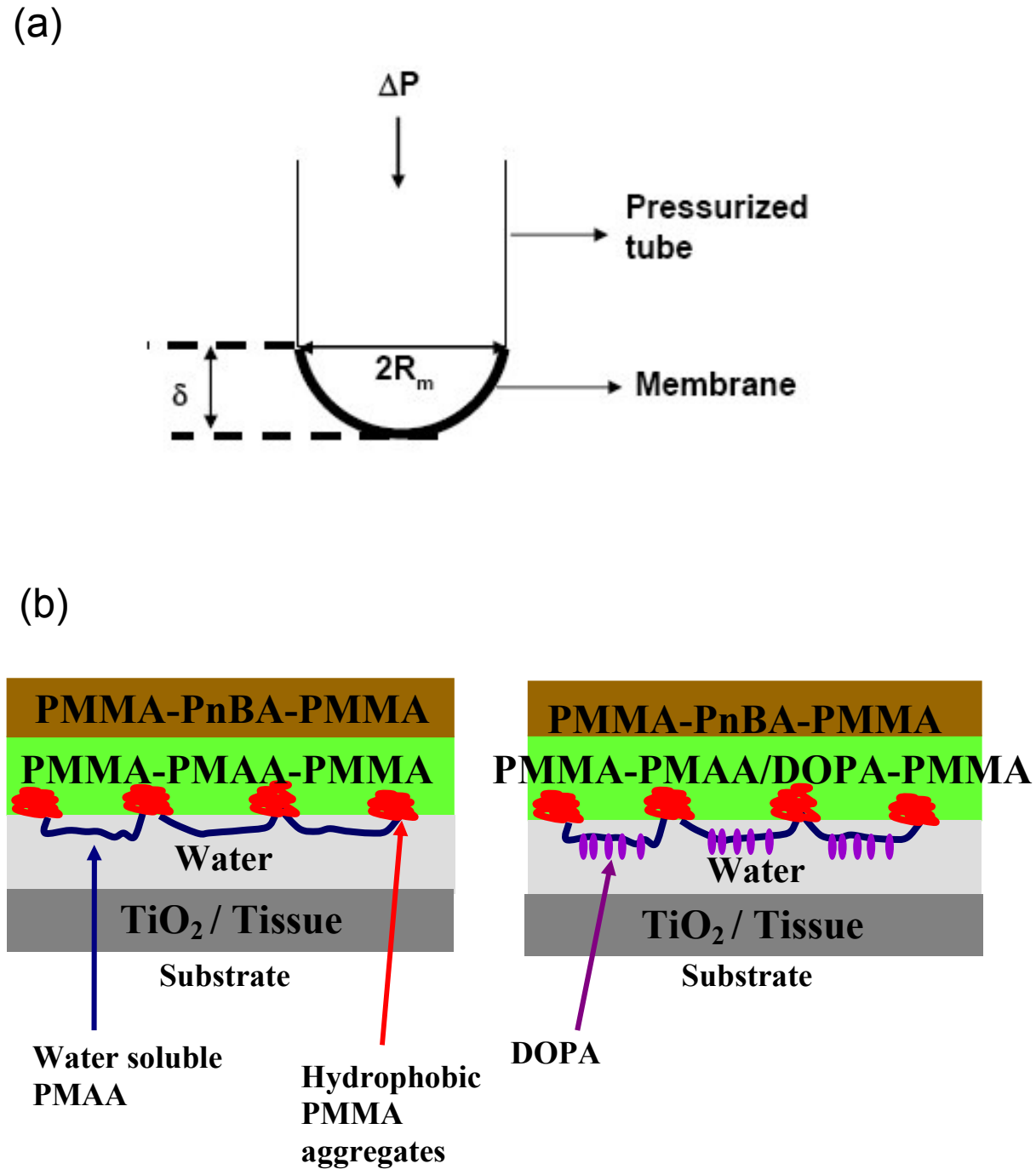

Figure 4.1. (a) Schematic representation of the membrane geometry; (b) schematic representations of model membranes.

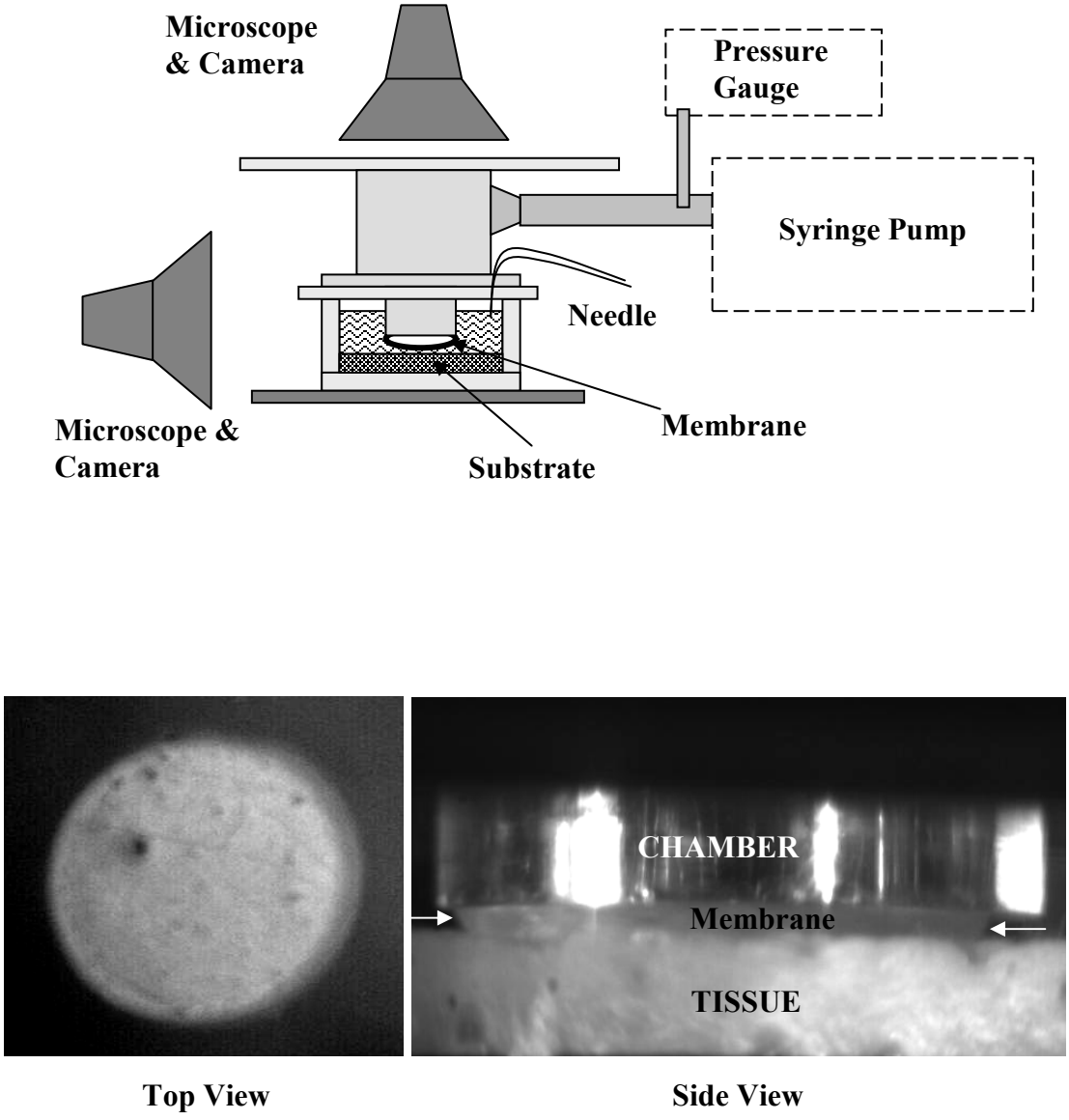

Figure 4.2. (a) Experimental apparatus for the membrane contact experiment; (b) contact images from top and side views.

4.2.4 Quartz Crystal Microbalance (QCM) Swelling Measurements

Swelling properties of the thin films were characterized by QCM under a controlled humidity environment. The experimental setup is shown schematically in Figure 4.3. AT-cut quartz crystals with circular gold electrodes (Maxtek, Inc.) designed to fit into a special holder (CHC-100, Maxtek, Inc.) were used in the experiments. The holder was placed inside the humidity chamber, and the humidity was controlled with an automatic humidity controller (ETS Inc. Model 514) connected to an ultrasonic humidifier (ETS Inc. Model 5612) and a dehumidifier system (Model 400-1904) attached to a desiccant. A humidity sensor (ETS Inc. Model 514HS) was placed inside the chamber, which was also connected to the humidity controller. The quartz crystals were exposed to UV/Ozone for 15 min using a Jelight Company Model 42 UVO-Cleaner. A thin layer of polymer film was spun cast onto the crystal from solutions in DMSO after the resonant frequency of the clean crystal was measured. The system was closed and the relative humidity was decreased down to 1-2 %, where it was maintained for 5 min to equilibrate the film. Two sets of swelling experiments were conducted. In the first set, the relative humidity of the system was set to ~95 %, resulting in a fast decrease in the frequency during the swelling of the film. In the second set experiments, the humidity was increased stepwise by allowing equilibrium swelling in each step. In each case the resonant frequency of the quartz crystal circuit was monitored by a network analyzer. The change in frequency, Δf, was used to calculate the change in thickness, Δt, by using the well-known Sauerbrey equation[63]:

$$\Delta f = \frac{2nf_0^{\,2}}{Z_q}\rho\Delta t\,, \tag{4.1}$$

where Z_q is the acoustic impedance of quartz (8.84 x 10^6 kg $m^{-2}s^{-1}$), f_0 is the fundamental resonant frequency of the resonator (5 MHz), ρ is the density of the polymer and n is the number

that represents the vibrational harmonic of the oscillator (we used the first three harmonics n = 1, 3 and 5 corresponding to f = 5 MHz, 15 MHz and 25 MHz). The swelling curves were obtained from the measurements of frequency change with humidity according to the following equation[64]:

$$\phi_w = \frac{\Delta f - \Delta f_{dry}}{\Delta f}, \tag{4.2}$$

where ϕ_w weight fraction, Δf is the measured frequency change and Δf_{dry} is the frequency change measured at zero humidity. The thickness of the films were also calculated by measuring the change in the resonant frequency of the clean crystal after the polymer was deposited onto the resonator. These thicknesses were compared with values obtained from ellipsometry before the crystal was placed into the holder.

4.3 RESULTS AND DISCUSSION

4.3.1 Swelling Results

Swelling properties of the polymer thin films were characterized by the QCM technique as described in experimental section. Thin layers of polymer films were spun cast onto the resonators from diluted DMSO solutions. The measured film thicknesses after spin coating are given in Table 4.1. The thickness of the films were measured by both QCM and ellipsometry. In order to measure the film thickness by QCM, the frequency of the bare crystal was recorded each time before spin coating. After the polymer was spun cast the thickness of the film was calculated by measuring the change in the frequency by using Equation 4.1. Ellipsometry

measurements were performed just after spin coating. Data for a PMAA homopolymer are also included in the table.

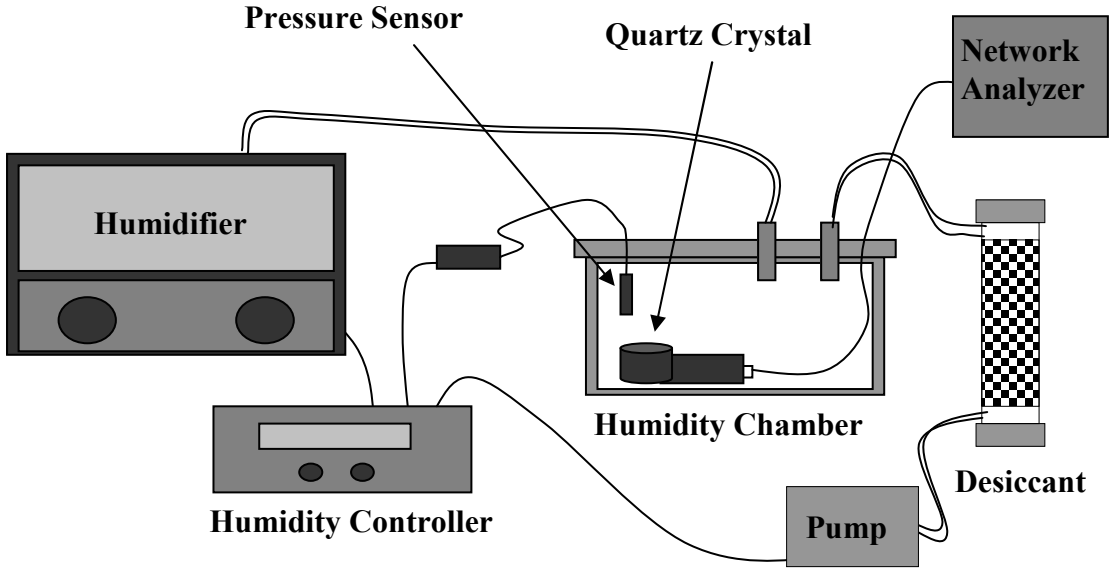

Figure 4.3. Experimental apparatus for the QCM swelling experiments under controlled humidity.

Table 4.1. The thickness of the spun cast films on quartz crystal by ellipsometry (t_E) and QCM (t_c). The calculated fractions of the solvents in the polymer layer, when exposed to solvent vapor, by using Equation 4.2 is also included. The subscripts donote the solvents.

sample	t_E (nm)	t_{QCM} (nm)	ϕ_{DMSO}	ϕ_W
DOPA00	104±20	112±11	0.63	0.57
DOPA20	20±3	18±2	0.56±0.01	0.42±0.03
PMAA	40±3	36±4	-	-

Swelling curves obtained from QCM for DOPA00, DOPA20 and PMMA homopolymer are shown in Figure 4.4. The data are plotted as ϕ_w versus change in humidity. The data for the films that were immersed in pH10 buffer were also included in the figure. For those samples, the polymer coated resonators were immersed in pH10 buffer and dried in the humidity chamber after rinsing them multiple times with distilled water. The equilibrium water fraction in DOPA00 film increases gradually with an increase in the relative humidity having a highest value of 0.4 at 95 % relative humidity. It can be seen that this result is in good agreement with the data obtained for PMAA homopolymer. In the case of DOPA20 films, water fraction is constant for relative humidities smaller than 80 %, and a significant increase is observed at 95 % humidity. The highest water fraction value in DOPA20 films was equal to 0.2. As discussed in chapter 3, we attribute this result to the hydrophobic nature of DOPA molecules at neutral *pH*.

The reported values for the *pKa* of DOPA are $pKa_I = 9.4$ and $pKa_{II} = 13.7$[59,65], corresponding to the removal of the first and second protons from the catechol. However, for methacrylic acid, $pKa = 4.8$[30]. When the films were exposed to a buffer solution having $pH > pKa_I$, the DOPA groups become ionized and are no longer hydrophobic. The PMAA groups are also ionized under these conditions because pKa_I for DOPA is greater than *pKa* for PMAA. The equilibrium water fraction in these neutralized DOPA20 films were found to be approximately 2 times larger than the original protonated films when equilibrated in 95 % relative humidity. The same result is also true for the DOPA00 films, which has a water fraction equal to 0.64 when equilibrated in 95 % relative humidity after immersion in the buffer solution with a *pH* of 10.

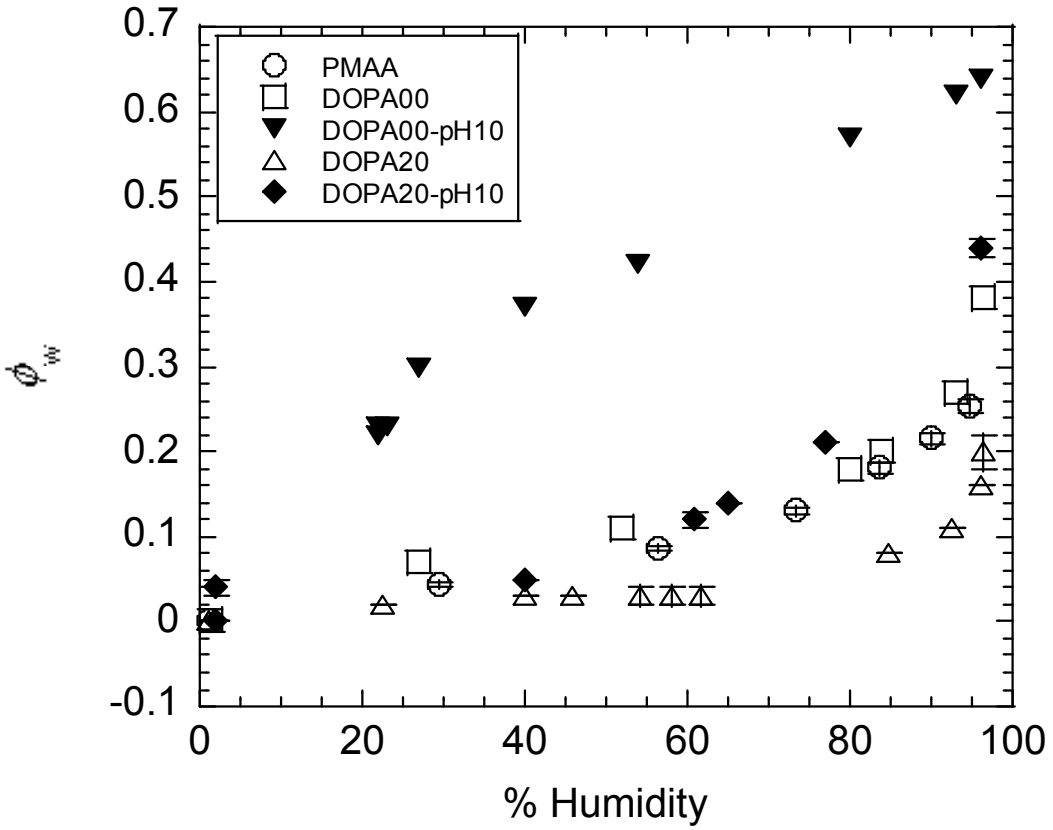

Figure 4.4. Swelling properties of the thin film DOPA00 and DOPA20 polymers measured by QCM. Equilibrium water fraction in the film was calculated from frequency response of films deposited on quartz resonators.

In order to study the solvent exchange in these films, the films were first equilibrated in DMSO vapor and then exposed to water vapor. The results are given in Table 4.1, and indicate that the films swell more in DMSO vapor than in water vapor. When the DMSO containing films were exposed to water vapor, the fraction of the solvent decreased significantly, and the films equilibrated at a water fraction lower than the initial DMSO fraction.

4.3.2 Adhesion Results: DOPA-TiO_2

Membrane expansion experiments were used to investigate the specific interactions between DOPA and the TiO_2 surface. For this purpose, bilayer membranes were prepared as described above. The membrane transferred to the end of the cylindrical expansion chamber was inflated into contact with the TiO_2 surface. Prior to the experiment, the TiO_2 surface was rinsed with acetone and methanol multiple times, and exposed to UV-Ozone for at least 15 min. The time dependence of the pressure and contact radius is given in Figure 4.5, which shows the interaction between DOPA00 and TiO_2 surfaces. When the inflated membrane came into contact with the substrate, a circular contact area was observed. After the initial contact (170 sec), the membrane was pressurized a little further, and the pump was stopped at 180 sec. The membrane was kept in contact with the substrate for about 20 min. During this period the membrane pressure did not change, however, the contact area decreased with time. This decrease in contact area indicates the poor interaction between the membrane and TiO_2 surface. When the membrane pulled away, the contact was lost at a release pressure, $P = 0$ Pa, which is indicative of a weak adhesive interaction between the DOPA00 membrane and the TiO_2 surface. This poor interaction between the methacrylic membrane and TiO_2 surface enables us us to study the DOPA-TiO_2 interaction by using DOPA20 membranes. The results given in Figure 4.6 clearly indicate two significant differences in the evolution in contact area and pressure for DOPA20 membranes when compared with DOPA00 membranes. We observe an increase in contact area when DOPA20 membrane was kept into contact with TiO_2 surface. In addition, in order to separate the two surfaces we need to apply a negative pressure of 420 Pa. These results clearly indicate that DOPA20-TiO_2 interface is much stronger than the DOPA00- TiO_2 interface.

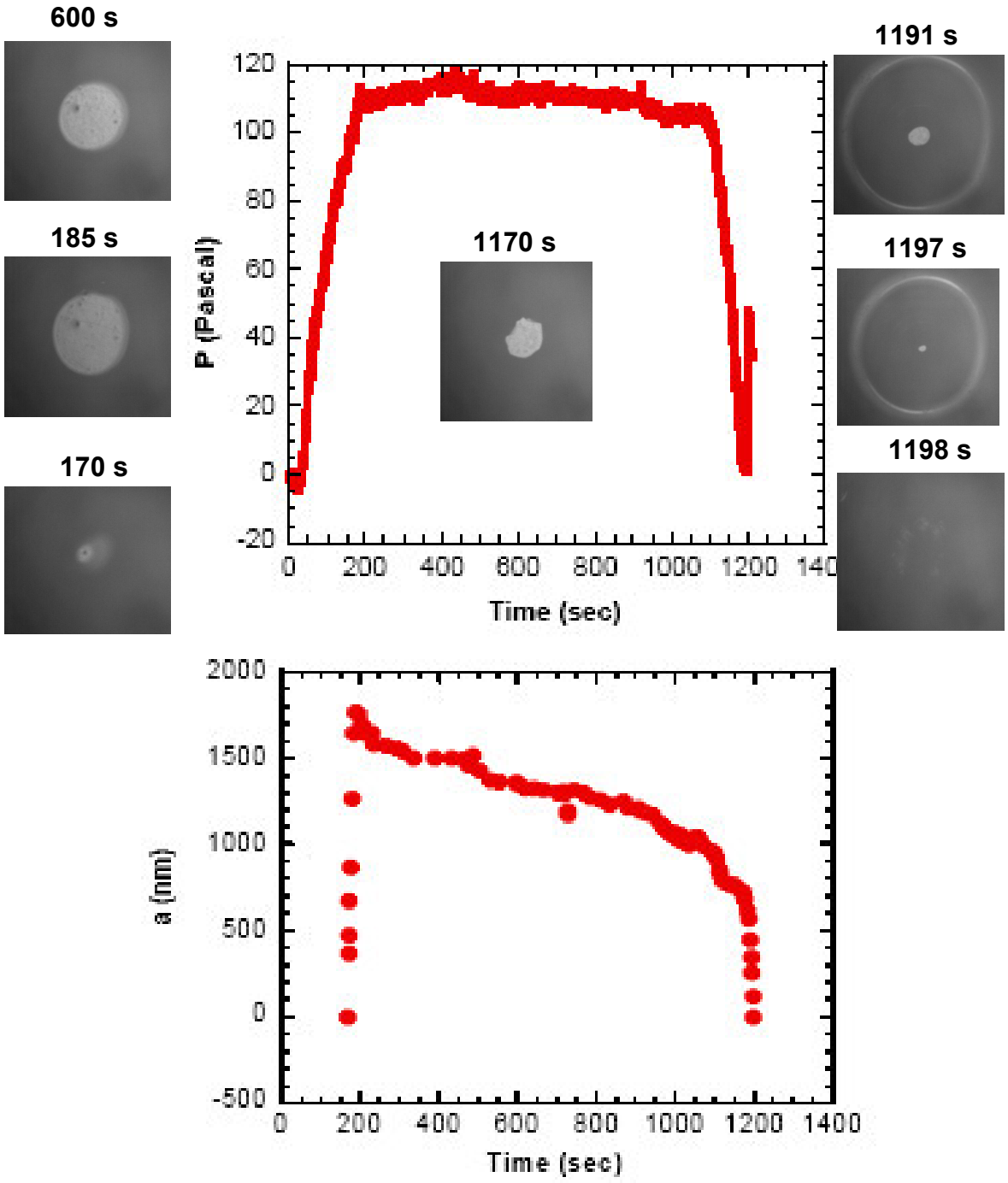

Figure 4.5. The evolution of the pressure change and contact radius during the inflation experiment.

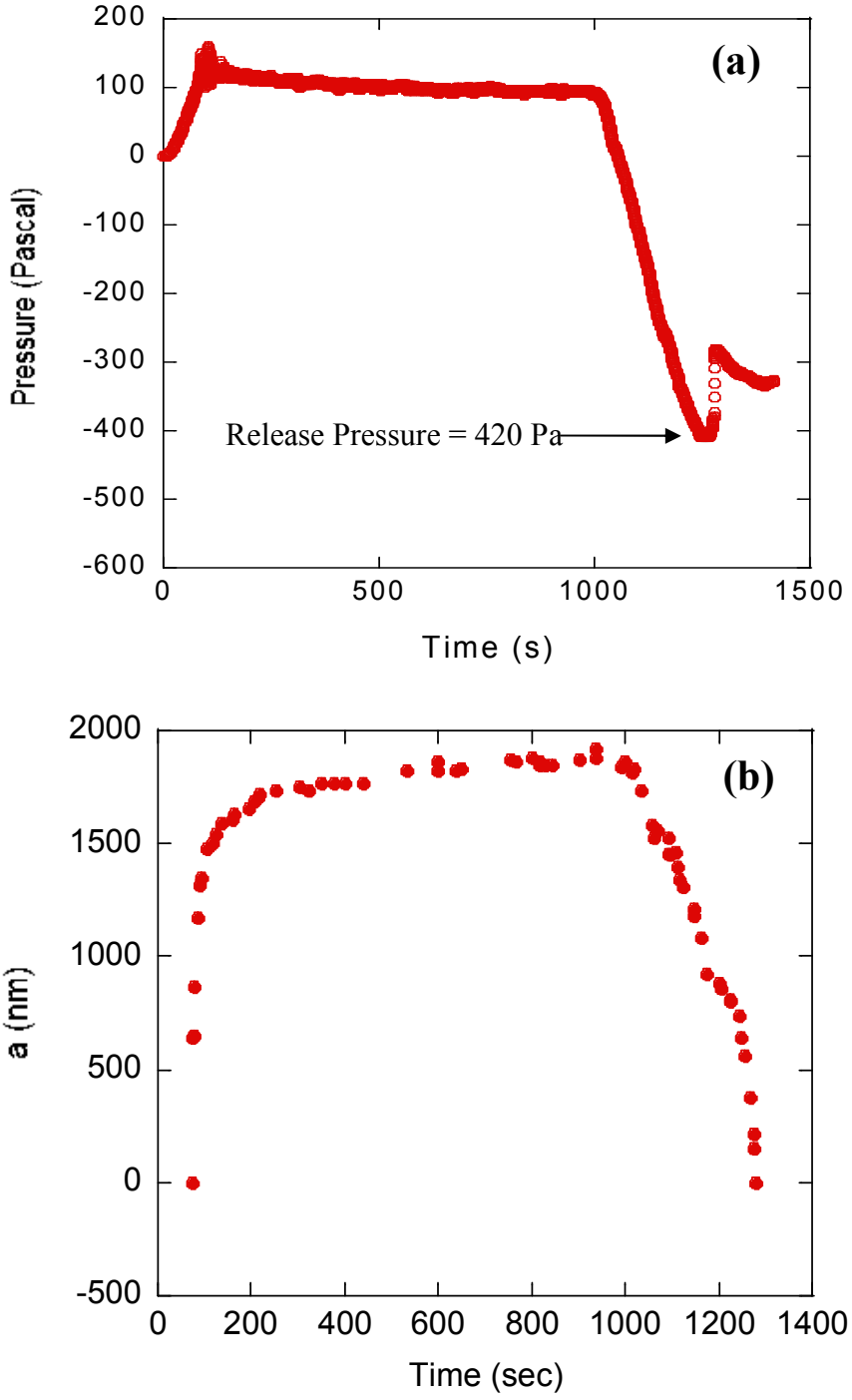

Figure 4.6. The data for DOPA20 membrane in contact with TiO_2 surface: (a) The change in membrane pressure with time; (b) the change in contact radius with time.

4.3.3 Adhesion Results: DOPA-Tissue

Membrane expansion experiments were used to investigate the specific interactions between DOPA and the tissue interface. For this purpose, we used a sample of pig skin provided by the Messersmith group. Bilayer membranes were prepared as described above. The pig skin was cut into the desired size, and attached to a glass slide using super glue. This tissue-attached glass slide was then immersed in distilled water. The membrane transferred to the end of the cylindrical expansion chamber was inflated into contact with the tissue. The evolution of the pressure and contact geometry is given in Figure 4.7. The applied pressure at the point of contact is higher for the tissue experiments than for the TiO_2 experiments because the initial distance between the un-pressurized membrane and tissue was generally three times larger than the 1 mm distance used for the TiO_2 surfaces. For these experiments we used the side view camera, due to poor contrast between the tissue and the membrane when viewed along the axis of symmetry. When the inflated membrane came into contact with the substrate, the membrane was pressurized a little further, and the pump was stopped. The membrane was maintained in contact with the substrate for 20 min. During this period we observe a drop in the membrane pressure, which can be attributed to the relaxation of the membrane. When the membrane was pulled away by withdrawing air from the membrane, the contact was lost at a release pressure equal to the pressure at which we observe the initial contact. This result clearly shows that the DOPA00 membrane is not adhesive on tissue surface. However, for DOPA20 membranes in order to separate the membrane from the tissue surface a release pressure of 500 Pa was applied **(**Figure 4.8a). This release pressure increased significantly to 2500 Pa **(**Figure 4.8b**)** when the DOPA was oxidized in contact with the membrane by injecting a concentrated sodium periodate ($NaIO_4$)

solution. The series of side images given in Figure 4.9 also revealed the adhesiveness of the membrane. When the membrane was inflated, it sticks to the tissue surface and resists detachment during subsequent depressurization.

4.4 SUMMARY

In order to study the adhesive interactions between DOPA – TiO_2 and DOPA – tissue in an aqueous environment, we used a membrane inflation method. We produced bilayer membranes having a hydrophobic membrane covered by a layer of the DOPA00 or DOPA20 triblock copolymers. The adhesive properties of membranes were investigated by using contact images and by measuring the evolution of the membrane pressure with time. The swelling of thin layers of DOPA00 and DOPA20 in controlled humidity was also characterized with the QCM. The results are summarized below.

- DOPA00 films contain 40 % water at a relative humidity of 95 %. The DOPA20 films contain only half the this water at the same humidity level.
- When exposed to $pH = 10$ buffer, both the DOPA and PMAA groups were deprotonated, doubling the swelling capacity of these films.
- For DOPA00 membranes the contact area decreases with time and the membrane was completely removed from the TiO_2 surface at a release pressure of zero. For DOPA20 membranes a release pressure of 420 Pa was needed to separate the membrane from the TiO_2 surface.
- DOPA00 membranes were completely removed from the tissue surface at $P = 0$, whereas DOPA20 membranes were removed from tissue surfaces by a negative pressure of 500

Pa. This release pressure increased to 2500 Pa when the DOPA was oxidized while the membrane was in contact with the tissue surface.

4.5 ACKNOWLEDGMENTS

This research is in collaboration with Phillip B. Messersmith from the Biomedical Engineering Department at Northwestern University. I would like acknowledge the Messersmith group for providing the tissue used in the experiments. I also would like to acknowledge Dr. Anny Flory for her help and for teaching me how to use the membrane inflation setup.

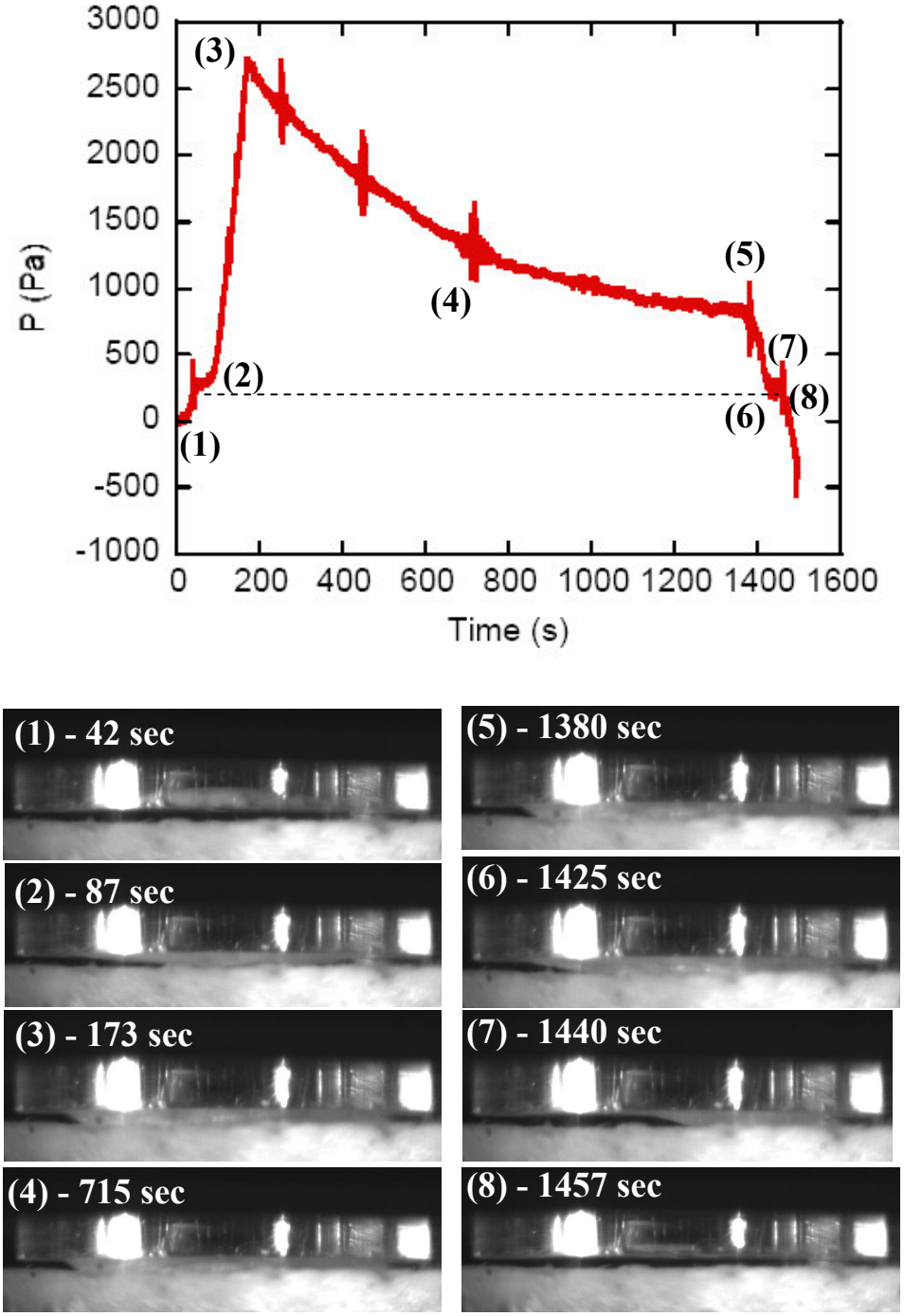

Figure 4.7. The evolution of contact in DOPA00 membrane against tissue surface.

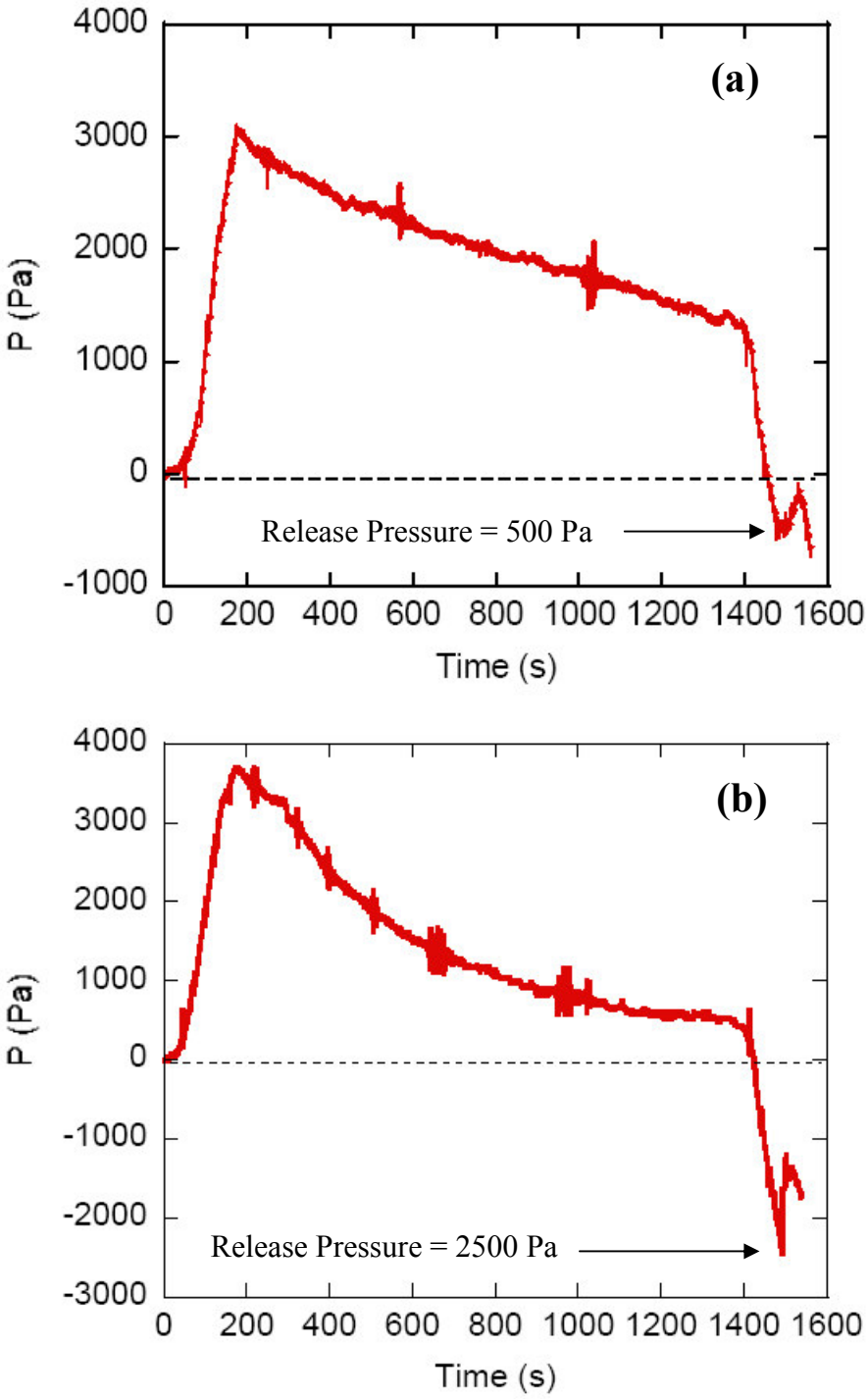

Figure 4.8. Pressure with time data for (a) DOPA20 membrane, and (b) DOPA20 membrane when DOPA was oxidized in contact with the tissue.

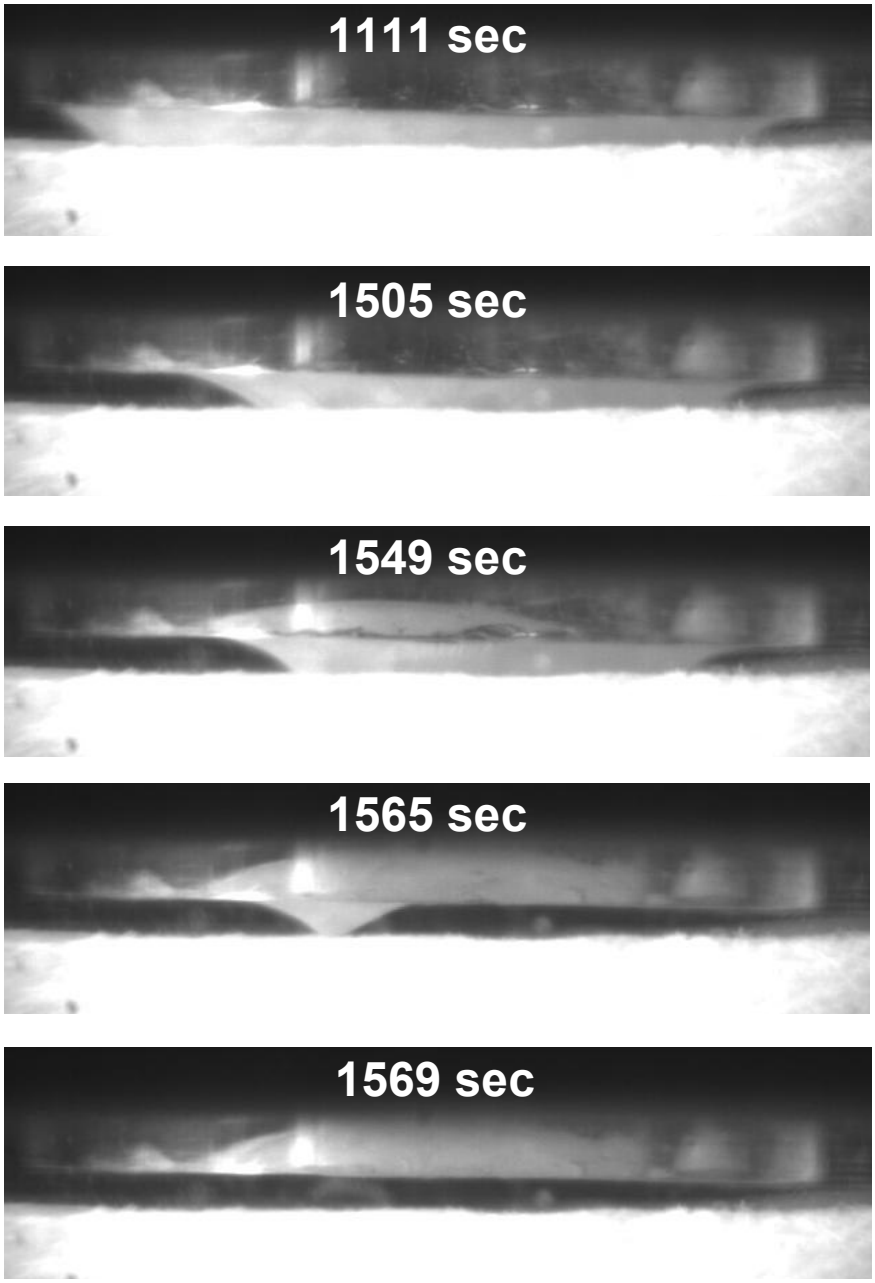

Figure 4.9. DOPA20 membrane – tissue interface during pulling the membrane away from the tissue surface by withdrawing air from the membrane. The DOPA20 membrane was oxidized with $NaIO_4$ solution while in contact with the tissue.

CHAPTER 5

HYDROGEL SCAFFOLDS FOR BLADDER TISSUE REGENERATION AND DRUG DELIVERY

CHAPTER 5

HYDROGEL SCAFFOLDS FOR BLADDER TISSUE REGENERATION AND DRUG DELIVERY

5.1 INTRODUCTION

For patients with dysfunctional or injured bladders, few options exist for restoring the functional tissue. A tissue engineering option, using autologous cells from bladder urothelium (UCs) and smooth muscle (SMCs) offers a potential solution [66-69]. However, only a small number of scaffolding materials are being extensively explored for urologic purposes, and only a small number of these are synthetically derived. Unlike biologically derived matrices, polymeric scaffolds offer reliable synthesis and characterization.

In this study, we develop an ABA type triblock copolymer gel system for potential use as a tissue engineering scaffold. The water soluble B block is poly(methacrylic acid) (PMAA) and the hydrophobic A blocks are poly(methyl methacrylate) (PMMA). The PMMA-PMAA-PMMA triblock copolymers can be fully dissolved in dimethyl sulfoxide (DMSO), which is a FDA-approved solvent for injection into the human body. When the solvent is gradually replaced with water, the triblock copolymer self-organizes so that hydrophobic end-blocks (PMMA) form spherical domains that act as physical crosslinks, with the hydrophilic mid-blocks (PMAA) forming bridges between these domains. Porous hydrogel scaffolds are formed by a porogen leach method.[24,70] Biocompatibility of these scaffolds is studied for short-term cultures *in vitro*.

The drug delivery and release properties of hydrogels are investigated by using a hydrophobic drug.

5.2 EXPERIMENTAL

5.2.1 Materials

PMMA-PMAA-PMMA triblock copolymer was synthesized by sequential anionic polymerization of tert-butyl methacrylate (*t*BMA) and methyl methacrylate (MMA) followed by hydrolysis of the P*t*BMA midblock to form poly(methacrylic acid) (PMAA). The resultant polymer has a total molecular weight of 200,000 kg/mole with a polydispersity index of 1.09. Sodium chloride (NaCl) salt crystals from Sigma were sieved to obtain salt particles < 40 μm and particles with sizes ranging from 40 to 120 μm. DMSO was used as received from Sigma.

5.2.2 Formation of Porous Hydrogels

Porous hydrogels were formed by solvent exchange method followed by a porogen leach method.[24,70] In brief, the PMMA-PMAA-PMMA triblock copolymer was dissolved at 10 wt% in DMSO, which is a good solvent for both blocks. The solution was mixed with NaCl salt crystals of defined size (4 wt%). The mixture was filled into a circular washer one side attached to a glass slide, and immersed in 18.2 MΩ cm distilled water to form gels. Hydrogels were formed immediately via solvent exchange. The hydrogel was maintained in water for three days in order to leach the salt crystals out. The water was exchanged multiple times with fresh distilled water to completely remove the salt crystals. The hydrogels were then re-equilibrated in phosphate buffer solution (PBS). In order to obtain a good contrast to image the pores, a hydrophobic

fluorophore, C.I. Solvent Yellow 98 thioxanthone dye (under trade name of Hostasol Yellow 3G by Clariant)[71], was added to the DMSO solution prior to solvent exchange.

5.2.3 Tissue Regeneration Experiments

Porous hydrogels used for tissue regeneration experiments were formed under sterile conditions. All tools used in the process, and the salt particles, were autoclaved at 120 ^{o}C for 90 min beforehand. The initial 10 wt% polymer solution in DMSO was diluted to 5 wt% in order to filter through a sterile filter. Porous hydrogels were formed as described above, and equilibrated in a PBS buffer. Two sets of scaffolds, each set containing 3 gel samples, were produced, one without the fluorophore serving as a control set. For cell studies, $3x10^5$ human bladder smooth muscle cells (SMCs) were seeded onto each scaffold for 90 min followed by $3x10^5$ human urothelium cells (UCs). Samples were incubated in culture medium for 3 days and evaluated by live/dead assay (Invitrogen)[72,73] and by DAPI staining of formalin-fixed samples.

5.2.4 Drug Delivery Experiments

PMMA-PMAA-PMMA triblock copolymer was dissolved in a good solvent in DMSO. Oxybutynin chloride, a commercially available hydrophobic drug used for urinary and bladder difficulties,[74-77] particles were mixed with the initial solution. The final DMSO mixture containing 5 wt% triblock and 2.5 wt% drug, were injected in a circular washer, one side attached to a glass slide. The mixture was exposed to water vapor overnight. The resultant hydrogel was then immersed in 4 ml of distilled water. The water was exchanged every 24 h with 4 ml of fresh distilled water. The exchanged water was collected for further analysis. During

solvent exchange a layer of DMSO was observed on the top surface of the hydrogel. This solvent was collected to investigate the amount of drug released during solvent exchange.

5.2.5 Confocal Laser Scanning Microscopy and Analysis

Porous hydrogels were characterized by Confocal Laser Scanning Microscopy (Zeiss ConfoCor3/510 Meta) in the Biological Imaging Facility at Northwestern University. The 488 nm line of Ar ion laser, with BM 500-520 IR filter was used in conjunction with an EC Plan-Neofluar 10x/0.30 M0.7 objective lens. The pinhole was set to 100 μm. 2-dimensional (x-y) images along the z focal axis were continuously scanned at 2.6 μs. Optical slices were obtained at 50 μm intervals through z axis. Those images were then compiled to a 3-D projection.

5.2.6 Quantification of Drug Content

In order to determine the amount of released drug during the swelling of the gel in distilled water, the UV absorbance of the collected water was recorded at the maximum absorbance of the drug in water using a Hitachi U-2-1- UV-vis spectrophometer. Standard curves for water and DMSO were obtained by standard solutions with known concentrations of oxybutynin chloride.

5.3 RESULTS AND DISCUSSION

5.3.1 Formation of Hydrogel Scaffolds and Characterization

The PMMA-PMAA-PMMA triblock copolymer was initially dissolved in DMSO (10 wt %), which is a good solvent for both mid- and end-blocks. The solution was then mixed with a trace of hydrophobic fluorophore, Hostasol 3G, and NaCl salt crystals with sizes between 150

and 250 μm. The evolution of the self-assembled hydrogel scaffold structure is shown schematically in Figure 5.1. The mixture was filled into a circular washer that was attached to a glass slide (Figure 5.1-a), and immersed in distilled water, which induced immediate gelation, forming gels with the structure shown schematically in Figure 5.1-b. The resultant hydrogel was kept in water to remove all salt crystals by exchanging the water multiple times. The volume of the porous hydrogel scaffolds expanded to 3 times their original size after NaCl removal (Figure 5.1-c), and then back to 2 times their original size after equilibration in PBS.

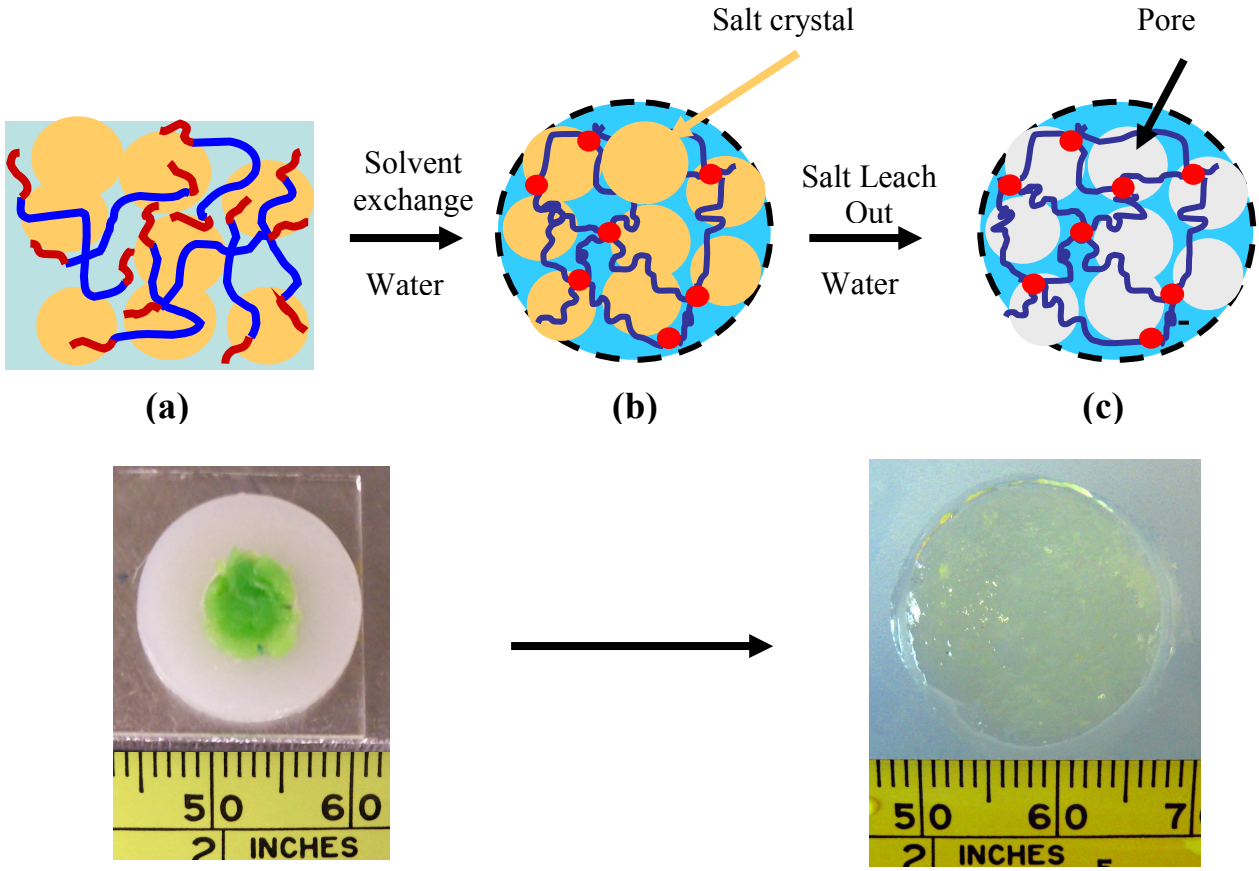

Figure 5.1. Pictures and schematic structures of the 370-1450 370 triblock copolymer: (a) 10 wt % triblock with NaCl in DMSO; (b) self-supporting gel after immersion into distilled water with trapped NaCl particles; (c) porous gel after salt was completely leached out. The green color is due to hydrophobic fluorophore, Hostasol 3G.

In order to characterize the porous structure of the hydrogels, we used Confocal Laser Scanning Microscopy. We used a z-stack method where the hydrogel was optically sliced through its thickness, with 2-dimensional (2-D) images obtained for each slice. A series of 2-D images are given in Figure 5.2. We observe open pore structure thought the entire gel thickness. The pore size of the gels were measured to be between 600 and 860 μm, which are larger than the initial particle size of 150-250 μm. This result is in good agreement with the swelling results presented in chapter 2 which show a factor of 3 increase in linear dimensions of the gel when the exchanged material is immersed in a neutral pH buffer. A 3-D construction of these 2-D images clearly showing the open pore structure is given in Figure 5.3, which was compiled from 13 slices at 50 μm intervals.

In order to form a bilayer scaffold, two mixtures of 10 wt% polymer solution in DMSO with salt particles were prepared. One of the mixtures had sieved salt < 40 μm, whereas the other mixture had 40-120 μm salts. In order to maintain the pore size integrity, sufficiently high concentrations of salt were mixed with the initial polymer solution (~60 wt%) to form a polymer-salt paste. The picture of the bilayer hydrogel and images obtained from CLSM are given in Figure 5.4. This anisotropic structure would be beneficial in cell seeding to match the cell size requirements to pore size. The UCs could be seeded in small pores whereas SMCs could be seeded in large pores. In addition, when the geometry of bladder was taken into account, an outer layer of large pores would help to offset tangential stresses in the scaffold under pressure.

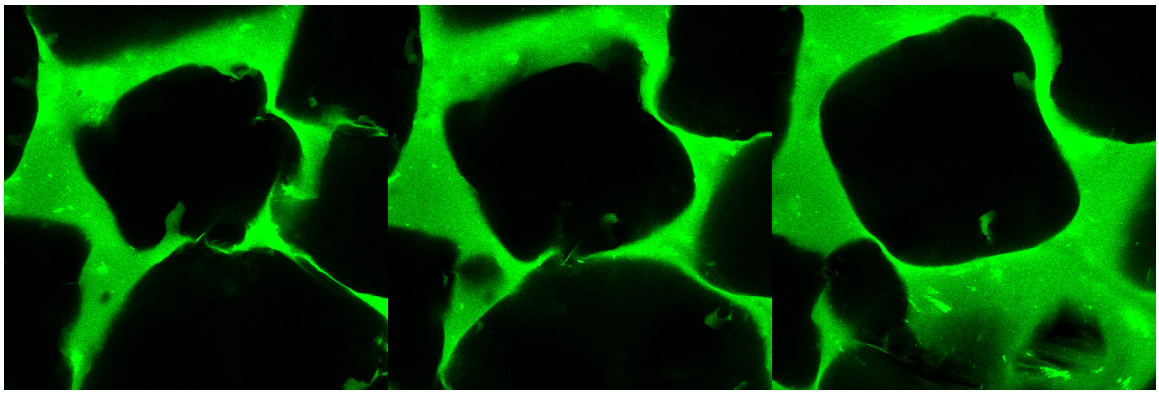

Figure 5.2. Series of 2-D images obtained from CLSM. The green and dark regions represent the gel and the pores, respectively.

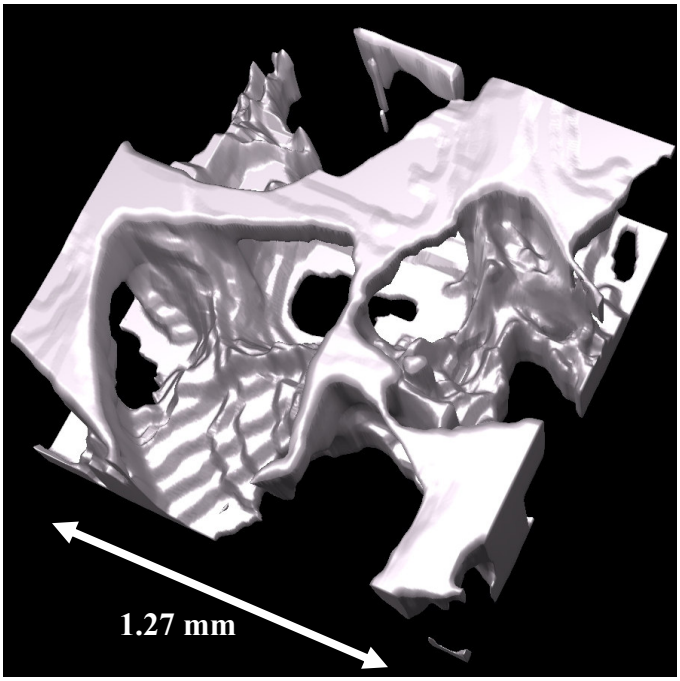

Figure 5.3. 3-D construction of a porous hydrogel obtained by confocal laser scanning microscopy.

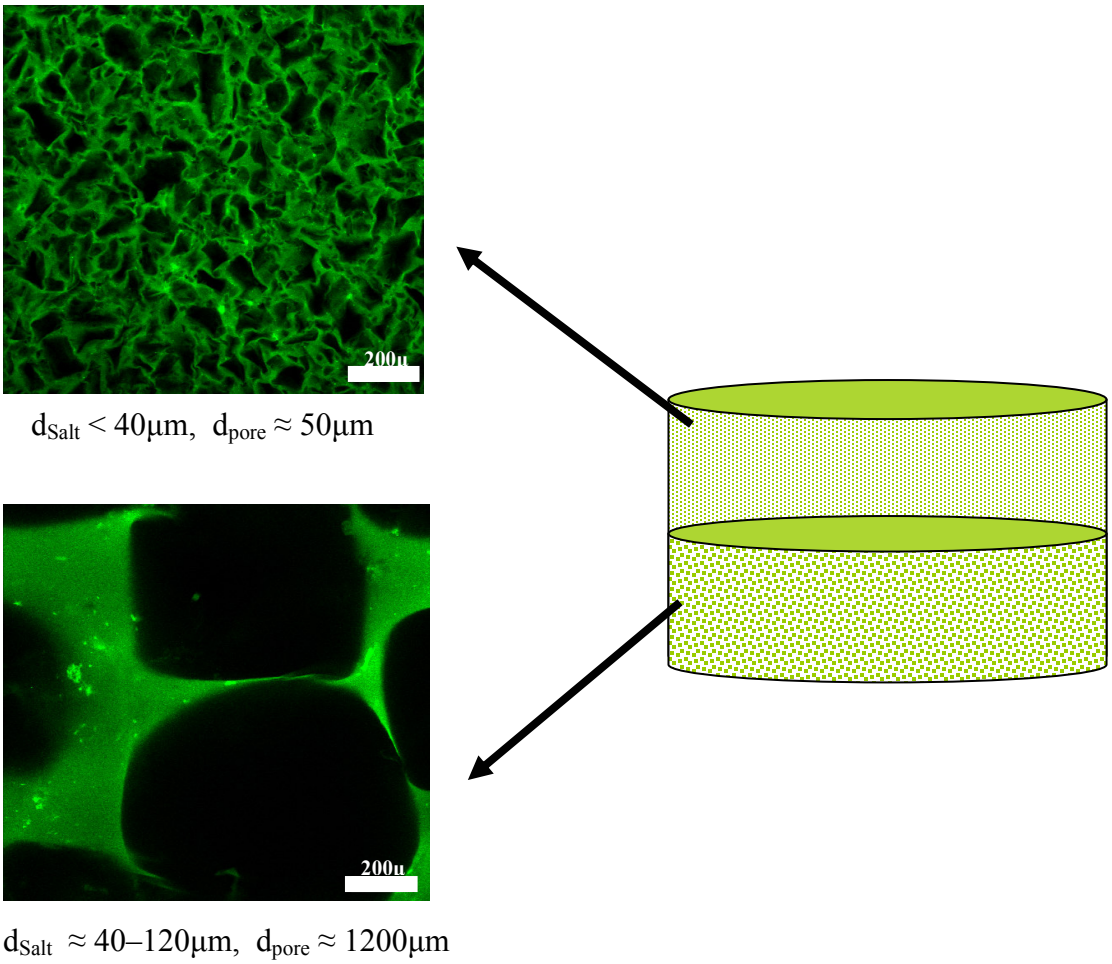

Figure 5.4. Large and small pores from a bilayer scaffold structure.

5.3.2 Biocompatibility of the Scaffolds in Vitro

For tissue regeneration experiments hydrogel scaffolds were formed under sterile conditions as described above. Control samples without hydrophobic fluorophore were also prepared to investigate the effect of fluorophore on cell seeding. Smooth muscle cells (SMCs) and urothelium cells (UCs) were seeded onto the hydrogel scaffolds in sequential order. Samples were characterized by live/dead imaging after 3 days of incubation. Figure 5.5-a. indicates that a

majority of the cells are alive showing a green color. The ethidium homodimer (EthD) stain, red, for the dead cells is retained by the polymer, but few dead cells were observed. The imaging of the formalin-fixed samples through the scaffold depth demonstrated the cell penetration into the porous structure, Figure 5.5b.

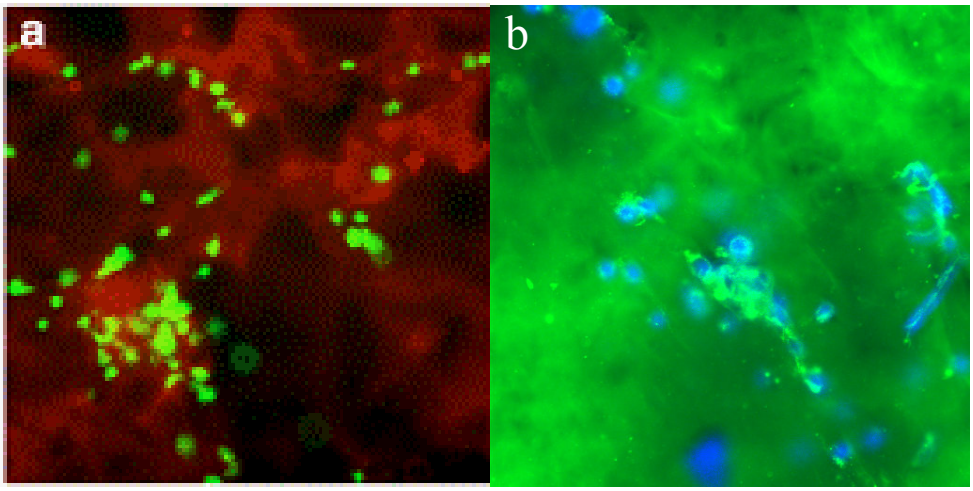

Figure 5.5. (a) Live/dead assay of the cells on the polymer gel. The majority of the cells are alive (green). (b) DAPI-stained cells (blue) on a Hostasol-loaded scaffold (green). Hydrogels for Drug Delivery and Characterization

5.3.3 Drug Rlease Experiments

The PMMA-PMAA-PMMA triblock copolymer was initially dissolved in DMSO, and the solution was mixed with the drug molecules (5 wt % and 2.5 wt %, polymer and drug molecules, respectively. The evolution of the self-assembled hydrogel loaded with oxybutynin chloride drug is shown schematically in Figure 5.6. The solution mixture was injected into a circular washer that was attached to a glass slide (Figure 5.6-a), and exposed to water vapor

overnight to form a gel (Figure 5.6-b). The exchanged DMSO was collected for absorbance analysis, in order to calculate the amount of drug released during solvent exchange. The resultant hydrogel was then immersed in water to investigate the stability, swelling characteristics, and drug release properties of these materials (Figure 5.6-c).

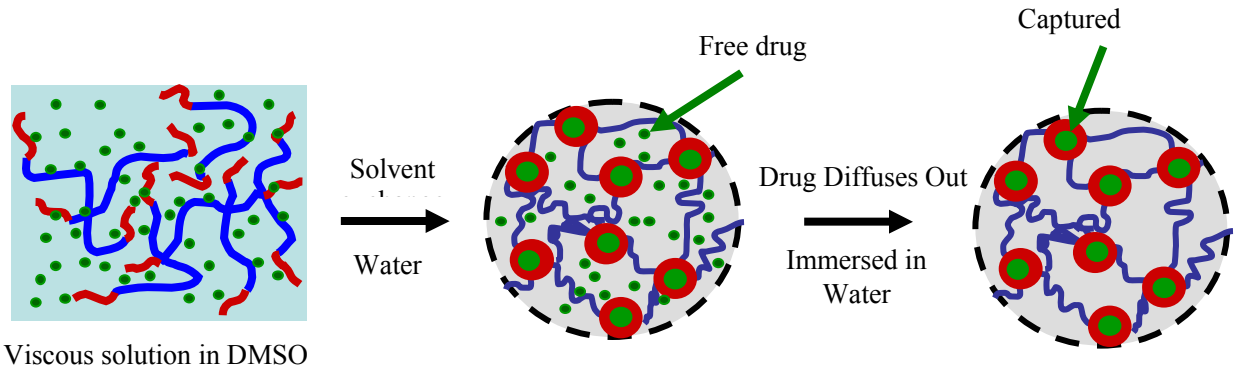

Figure 5.6. Pictures and schematic structures of the 370-1450 370 triblock copolymer: (a) 10 wt % triblock mixed with NaCl in DMSO; (b) self-supporting gel after immersion into distilled water with trapped NaCl particles; (c) porous gel after salt was completely leached out. The green color is due to hydrophobic fluorophore, Hostasol 3G.

The swelling data and drug release data are shown in Figure 5.7-a, and Figure 5.7-b, respectively. During solvent exchange, approximately half of the initially loaded drug was released with the DMSO. This result can be attributed to the hydrophobic nature of the drug, which makes DMSO a favorable solvent for oxybutynin chloride than water. The remaining drug particles were either entrapped by the PMMA aggregates during gel formation, or remained within the water inside the hydrogel. A significant decrease in the polymer fraction was observed within 4 days after they were immersed in water. The drug release results indicated that the free

drug inside the hydrogel was released within this period corresponding up to 90 mol % of initial drug. Although the drug release stopped after the fast release observed within 4 days, the gels still showed some swelling. In order to measure the amount of drug trapped in the PMMA aggregates, hydrogels were dried under vacuum, and the remaining polymer mixture was dissolved in DMSO. UV absorbance experiments performed on these solutions revealed that approximately 5 mol % of the drug molecules were incorporated in the PMMA domains, which corresponds to approximately 6 drug molecules per PMMA end-block.

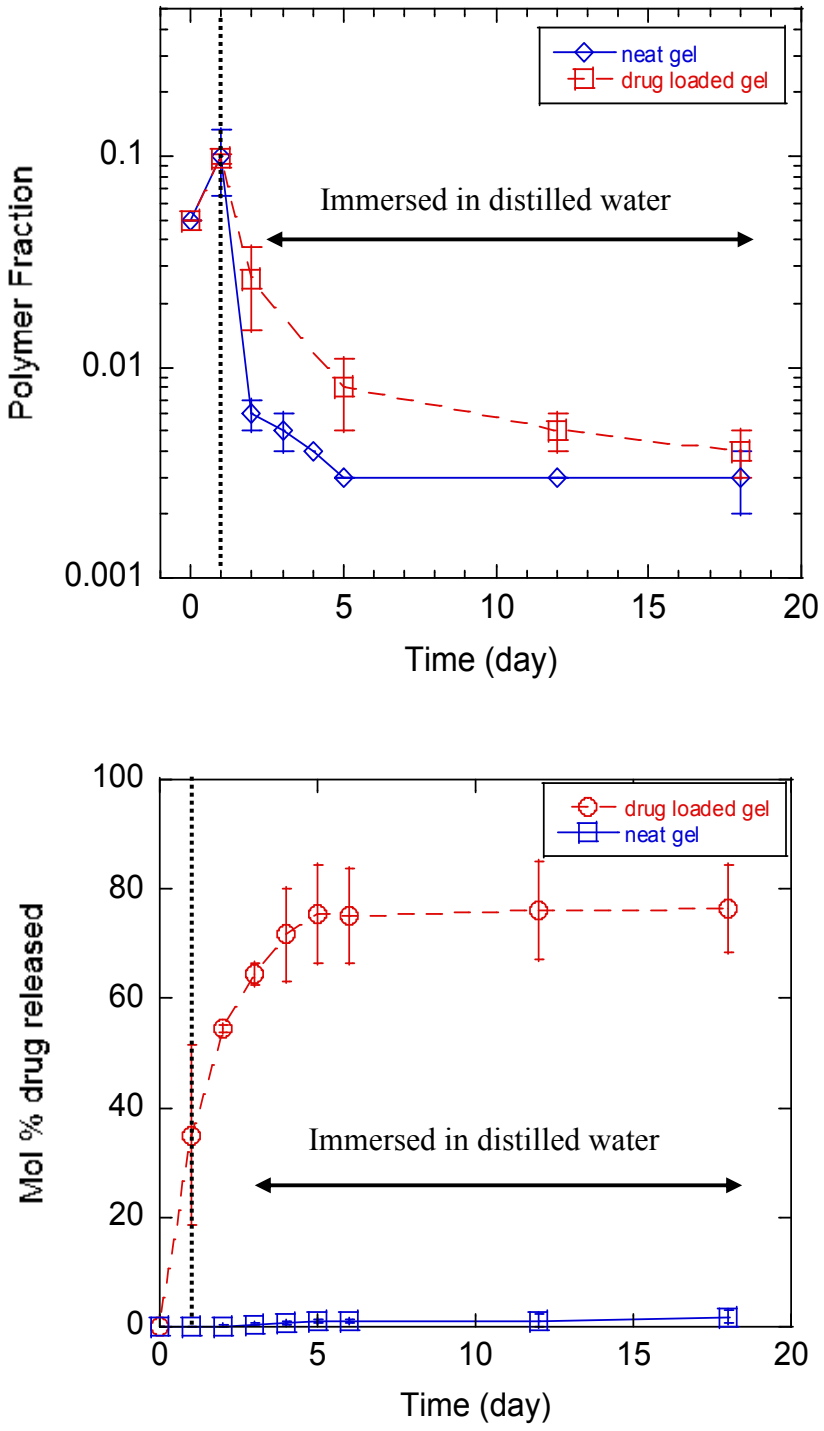

Figure 5.7. Swelling and drug release data for the drug loaded hydrogel and neat hydrogel, gel without drug.

5.4 SUMMARY AND FUTURE WORK

PMMA-PMAA-PMMA triblock copolymers were used to form porous hydrogel scaffolds. The triblock copolymer was initially dissolved in DMSO, and the solution was mixed with NaCl salt crystals of defined size. Immediate gelation was obtained by solvent exchange, by immersing these mixtures into water. The hydrogels were kept in water to leach the salt out of the gel. The swelling properties of the porous hydrogels were investigated. The porous hydrogel structure was investigated by confocal laser scanning microscopy. The biocompatibility of the scaffolds *in vitro* was studied by using human bladder SMCs and UCs. The same polymer system was used to form hydrogels for drug delivery purposes. In this case, the initial polymer solution was mixed with hydrophobic drug particles. Hydrogels were formed by solvent exchange, and then immersed in water to study the swelling and drug release properties.

The results can be summarized as follows.

- PMMA-PMAA-PMMA triblock copolymers were found to easily form stable porous hydrogel scaffolds in aqueous media by solvent exchange followed by a porogen leach method.
- The porous polymer scaffolds expanded to three times their initial size after NaCl removal and then contracted to twice the initial size after equilibration in PBS
- Uniform open pore structure was observed through the entire gel thickness.
- Bilayer scaffold systems, one layer of 50 μm pores, covered by a second layer of 1200 μm pores were produced, which would be beneficial in cell seeding, to match the cell size requirements to pore size.

- SMCs/UCs seeded onto the polymer scaffolds were found to attach and spread over time. Live/dead imaging showed that a majority of the cells were alive.
- Imaging through the scaffold depth demonstrated the cell penetration into the porous structure, and biocompatibility *in vitro* for short-term cultures.
- Hydrogels loaded with oxybutynin chloride were successfully formed by solvent exchange. During solvent exchange around 50 % of the initial drug was released with DMSO.
- Drug loaded hydrogels showed a significant drug release (90 %) with significant swelling within the first 4 days after immersion in water. The drug release stopped after this fast release; however, the gels showed some swelling.
- It is found that 5 mol % of the initial drug was remained in the gel after equilibrium, which is trapped in PMMA domains.

Some of the future directions in this part of my research can be summarized as follows:

- Studies of cell growth, morphology and phenotype as functions of seeding density and pore size.
- Controlled release of the drugs by application of an external stress.
- Extension to other commercially available hydrophobic drugs such as ipratropium bromide[78-80] and pirenzepine dihydrochloride[81-83].

5.5 ACKNOWLEDGMENTS

This research is in collaboration with Daniel A. Harrington in Earl Y. Cheng group in Urology, Feinberg School of Medicine, Northwestern University, Chicago. UV-VIS experiments were done in the Messersmith lab.

CHAPTER 6

ADHESION IN MODEL GLASSY POLYMERS

CHAPTER 6

ADHESION IN MODEL GLASSY POLYMERS

6.1 INTRODUCTION

There is widespread interest in the adhesion of polymer-polymer interfaces, as they play an important role in polymer applications[84-89] including adhesives, sealants, coatings, etc. This is also true for polymer blends, which can provide a mechanism for meeting the needs of specific applications that could not otherwise be met by a single polymer. Considerable progress has been made on immiscible polymer blends, these blends typically posses a weak interface, and their strengthening mechanisms have been studied indetail[90-98]. Although it is not common to find pairs of miscible polymers, creating blends of these is often useful as well. In these cases an understanding of interfacial interactions between miscible polymers and the mechanism by which they interact is a necessity. The interest of research has been concentrated on the molecular origins of fracture and adhesion of glassy polymers[99-101] including welding of these systems describing a state of thermally induced molecular mixing at the interface[102]. Similar studies involving semicrystalline polymers have been much more limited due to the more complex microstructure of semicrystalline polymers[103-107]. In their recent paper McSwain *et.al* show that a thin layer of a semicrystalline polymer sandwiched between two glassy polymers serves as an adhesive layer.[108] The strength of the glassy interface depends on temperature and it enhances only for temperatures above the melting temperature of the semicrystalline layer, where diffusion between two polymers is able to take place.

In order to develop a greater understanding of these diffusive interactions, adhesion tests were performed on the blends of two component with very different glass transition temperatures. In this paper, PEO, a semicrystalline polymer that serves as a model system due to its low melting temperature of 66 ^{o}C, is used as the diffusing component. This polymer has a glass transition temperature of approximately -60^{o}C in the amorphous phase[109]. The second component used in this study is a glassy polymer, TMPC, which has a glass transition temperature of approximately 190 ^{o}C[110,111] providing a wide range of contact temperature that can be used in our experiments. In fact, the high glass transition temperature of TMPC ensures that the adhesion tests probe interactions due to the presence of the PEO. The bulk characteristics of the blends were investigated by DSC, and the diffusion of PEO in TMPC was characterized by dynamic SIMS (DSIMS). A contact mechanics approach was used to determine the critical energy release rate for crack propagation within the interfacial region. In order to perform the specified adhesion tests, two layers of TMPC/PEO blends were brought into contact above melting temperature of PEO, the surfaces were kept in contact for a specified time and then separated. The effects of contact temperature and contact time were studied in detail.

6.2 EXPERIMENTAL

6.2.1 Materials and Sample Preparation

PEO was synthesized previously by anionic polymerization and had a molecular weight (M_w) of 70,000 g/mol and a polydispersity of 1.07. TMPC was a gift from Mark Hammersky of Proctor and Gamble. Crosslinked PDMS elastomer substrates were produced by using silicone

elastomer kit (*Dow Corning Sylgard*® 184). For grafting purposes, polystyrene (PS) with a trimethoxysilyl end group was anionically polymerized previously with M_w = 38,000 g/mol.

The sample geometry used in the adhesion experiments, which consists of a rigid spherical indenter making contact with a thin elastic layer, is given in Figure 6.1a, In this chapter a crosslinked PDMS was used as the elastomer substrate. PDMS substrate was oxidized by exposure to UV/ozone for 30 min, with a Jelight Company Model 42 UVO-Cleaner. A thin layer of trimethoxsily end group PS was spun cast onto the oxidized elastomer from a solution in toluene. In order to graft PS on to the oxidized PDMS surface sample was annealed for 1.5 h at 125 ^{o}C. The excess PS chains were removed by rinsing the surface in toluene. A layer of TMPC/PEO blend was spun cast on a glass slide from a solution of warm toluene (60 ^{o}C) and then floated onto water. This film was then transferred onto the PS surface and annealed for 1.5 h at 120 ^{o}C, which effectively grafted the TMPC to the surface because of the miscibility of the TMPC and PS[110]. This same process is repeated for the hemispherical glass indenter. The compositions of TMPC/PEO blends used in the adhesion experiments were as follows: 100/0, 95/5 and 80/20, TMPC/PEO weight percentages.

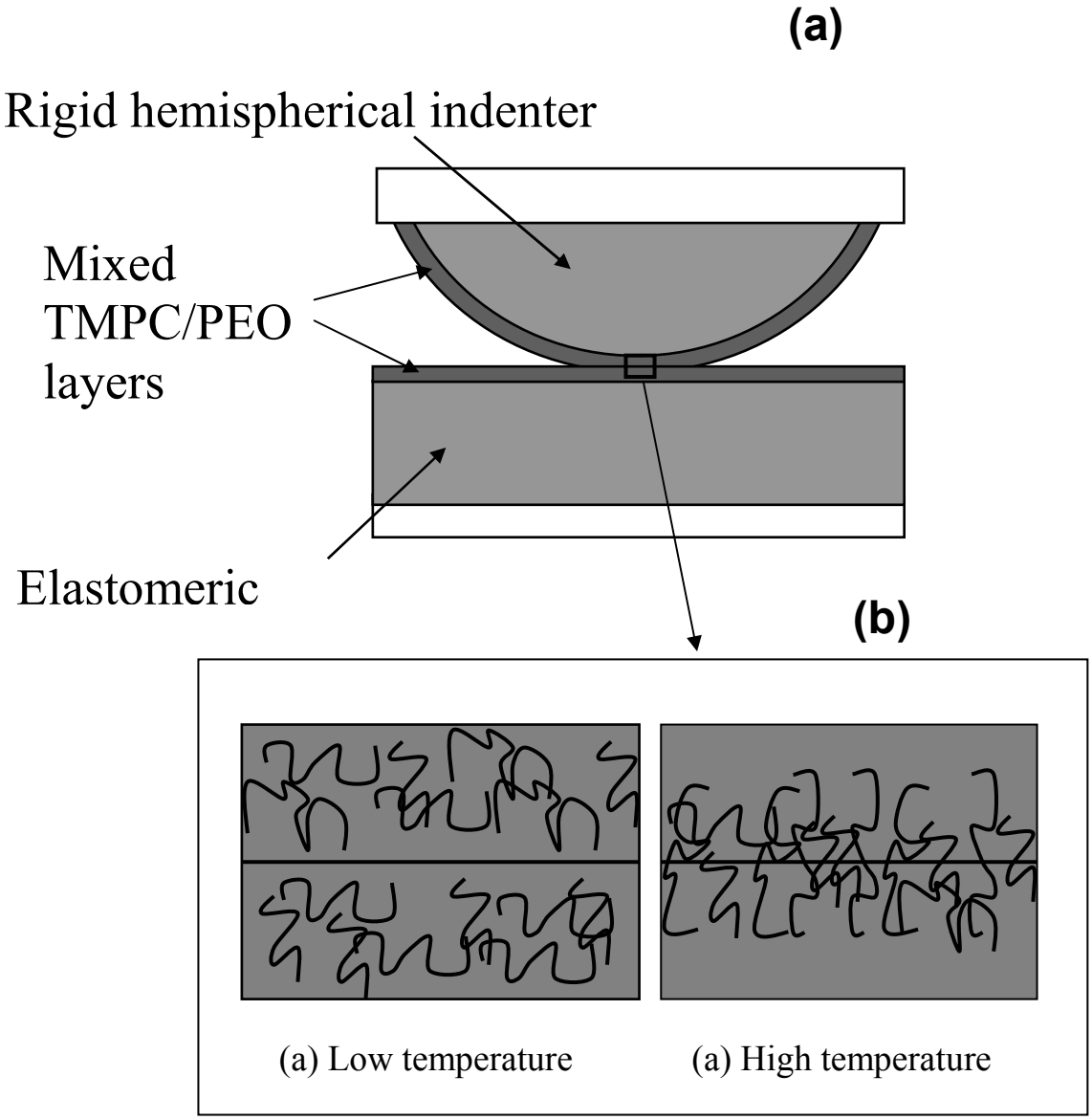

Figure 6.1. Sample set-up for mixed TMPC/PEO layers. Enlarged contact interface depicts: (a) low temperature case, where PEO chains are spread in TMPC matrix; (b) high temperature case, where PEO chains move to the interface.

6.2.2 Pull-Off Tests

Adhesion experiments were conducted with a temperature controlled axisymmetric indentation test method, which has been explained in detail previously by MAcSwain *et al.*[108] In brief, the samples were mounted in a thermally insulated copper heating chamber, which was then connected to a 50 g load cell in series with a Burleigh inchworm stepping motor. The indenter was mounted to the lid of the heating chamber and aligned with the viewing window in the lid. This window allowed us to capture contact area images during the test from the reflected light microscope and camera mounted above the chamber. These images were used to measure the radius of contact during the test. The stepping motor advanced the elastomer sample into and out of contact with the indenter. A fiber optic displacement sensor was placed below the sample holder to detect the displacement associated with the movement of the sample. A thermocouple, placed in the heating chamber in close proximity to the sample, was connected to a temperature controller so that the sample temperature can be controlled during the experiment.

In the adhesion experiments, the system was first heated to T_c and the temperature was allowed to stabilize at $T_c \pm 3^oC$. The surfaces were then brought into contact at T_c and they were kept in contact for a range of contact times, t_c, ranging from 0 to 30 min. The surfaces were then pulled apart at T_c. Load and displacement data, and contact area images, were collected throughout each experiment.

The energy release rate, $\mathcal{G}$, defined as the energy required for a crack to propagate within the interface, were calculated by using the following equation:[25,27]

$$\mathcal{G} = \frac{\left(\left(Ka^3 / R\right) + P_t\right)}{6\pi Ka^3}, \tag{6.1}$$

where P_t is the tensile load, a is the contact radius, R is the radius of the curvature of the indenter (6 mm), and K is the modulus of elasticity. For an incompressible material with Poisson's ratio = 0.5, K=16E/9 where E is the Young's modulus of the PDMS substrate. The modulus can also be obtained independently from the following displacement –load relationship:[25,27]

$$\delta = \frac{a^2}{3R} + \frac{2P_t}{3Ka}, \tag{6.2}$$

In this chapter, we use a simple model to relate the load-displacement relationship to the relationship between the energy release rate and crack velocity. In this model, the system is defined as an indenter attached to a spring, which is given in Figure 6.2. Therefore, the total displacement in the system, which is the motor displacement, δ_m, composed of two independent parts: the displacement of the spring, δ_s, and the displacement of the indenter, δ, which is the actual measured displacement by the displacement sensor. This relationship can be written as follows:[112,113]

$$\delta_m = \delta_s + \delta = \left(\frac{P}{K_s}\right) + \left(\frac{a^2}{3R} + \frac{2P}{3Ka}\right), \tag{6.3}$$

where, K_s is the spring constant of the load cell. As we mentioned above, the contact perimeter can be viewed as a crack having a velocity, v, which is equal to the rate of change of the contact radius, -(da/dt). As the contact recedes, a decreases, and the crack propagates. The velocity dependence of the $\mathcal{G}$ depends on both the surface layer and the underlying elastomer, which is a complicated function. The following empirical equation defining the velocity, v, dependence of the energy release rate is useful in presenting the results[86,89]:

$$\mathcal{G} = \mathcal{G}_0 \left[1 + \left(\frac{v}{v^*} \right)^n \right], \tag{6.4}$$

where $\mathcal{G}_0$ is the threshold adhesion energy, v^* is a characteristic crack velocity and n is the exponent that defines the shape of the relationship between $\mathcal{G}$ and v. The empirical formula was fit to the experimental data by changing the three variables, $\mathcal{G}_0$, v^* and n, in Equation 6.4.

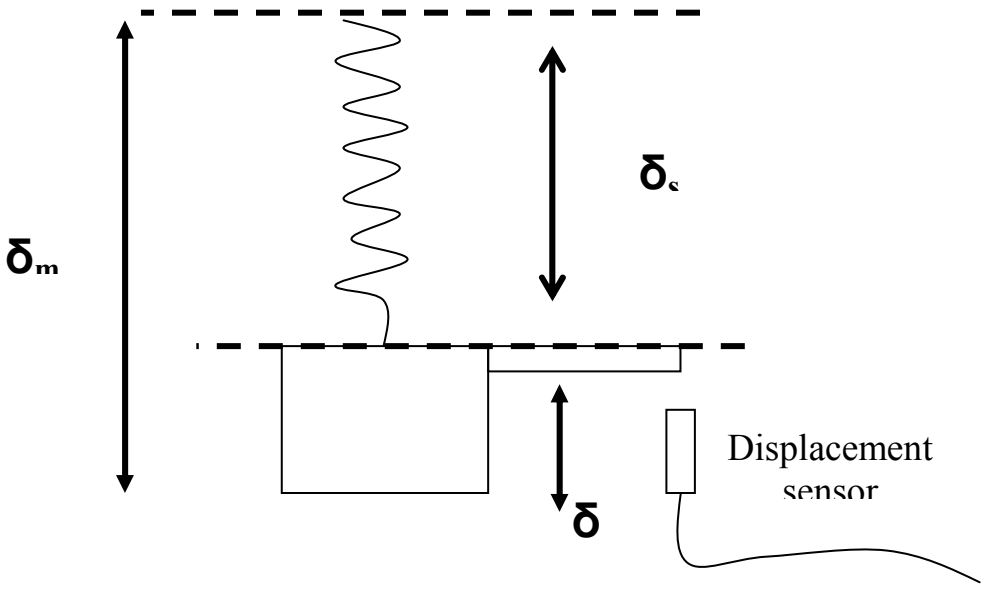

Figure 6.2. Scheme showing the simple model showing an indenter attached to a spring for displacement calculations, in which δ is the measured displacement, δm is the motor displacement and δs is the displacement due to spring effect.

.

6.2.3 Differential Scanning Calorimetry (DSC)

DSC experiments were performed on a Mettler Toledo DSC 822 under a dry nitrogen atmosphere. Concentrated solutions of TMPC/PEO blends were made in warm toluene. Concentration of these blends ranged from 90/10 to 0/100 TMPC/PEO (relative weight percents in the mixture). The aluminum DSC pans were placed on a heated surface and the solution was added drop-wise to the pan to allow evaporation of the toluene without crystallization of the PEO. Once the toluene evaporated, the pan was removed from the heat and sealed. The procedure used for the scan involved initially heating the sample from room temperature to 215 ^{o}C and holding for 10 min to remove any thermal history. A scan rate of 10 K/min was used as the sample was cooled from 215 ^{o}C down to -85 ^{o}C, held for 5 minutes, and then heated back to 215 ^{o}C.

6.2.4 Dynamic Secondary Ion Mass Spectrometry (DSIMS)

In order to obtain a depth profile of the diffusion of PEO into TMPC, dynamic SIMS experiments were performed on a Physical Electronics 6650 DSIMS instrument. In these studies, the sample surface was bombarded with a 250 nA, 4 kV O^{2+} primary ion beam, which had a profiling rate of 0.28 nm/sec and a beam diameter of approximately 40 μm. This beam interacted with and fragmented the polymer chains in the sample, results in the emission of secondary ions from the sample surface. Positively charged secondary ions were detected from the center 15% of the etched crater area by mass spectrometry. To detect the movement of the PEO chains, a deuterated form of the polymer, with a molecular weight of 90,000 g/mol, was used and tests were run on a number of samples with different annealing temperatures. In these studies, samples were made by creating a double layer with deuterated PEO (dPEO) and TMPC. dPEO was

directly spun cast onto Si substrate, forming a layer of 7 nm. A layer of TMPC (242 nm) was spun-cast onto glass and floated on top of the dPEO layer.

SIMS analysis of polymer layers spun-cast onto silicon was difficult due to charging of the sample. To correct for this issue, a 600 eV defocused electron beam was used for charge compensation. To offset any mismatch in conductivity at the interface, a layer of oxide was also grown on the surface of the silicon before spin-coating with the polymers to provide an insulating layer. This latter compensation was achieved by first rinsing the <100> silicon in a 49% HF solution to remove the native oxide from the surface. After exposure to HF, the samples were rinsed three times in deionized water, followed by isopropanol, and then dried with nitrogen gas. A layer of oxide was grown on the silicon surface by heat treatment according to the specifications of the Massoud model[114], which is based on the model for thermal oxidation of silicon proposed by Deal and Grove[115]. The silicon samples were heated to 950 ^{o}C for 2 hours, which results in an oxide growth of 52 nm. The resulting layer of oxide is thick enough to provide an insulating layer for the SIMS data acquisition.

The data for these curves were obtained in the form of counts of secondary ions collected over time. The time of the data collection is associated with the thickness of the sample, since the secondary ions are collected as the primary ion beam slowly etches the film. Therefore, the time is correlated to the thickness through independent measurements of the thicknesses of the polymer films. Conversion of the counts collected throughout the depth of the sample to the weight fraction of dPEO at these depths is obtained from the requirement that integration of the dPEO volume fraction profile must give the thickness of the originally spun-cast dPEO layer.

6.3 RESULTS AND DISCUSSION

6.3.1 Thermal Analysis

The cooling and heating curves obtained from DSC measurements for pure PEO and TMPC/PEO blends are shown in Figure 6.3. The labels for each curve represent the relative weight fractions of PEO and TMPC for the blend. The pure PEO sample (0/100) shows an endothermic melting peak at 66 ^{o}C during heating. This peak broadens as the TMPC concentration increases, and disappears when the TMPC concentration reaches 90% (90/10 blend). Similar behavior is also observed for the cooling isotherm. These results showed that PEO molecules do not have enough mobility to crystallize in the TMPC/PEO blends having PEO concentrations less than 10% and that PEO and TMPC are miscible. Similar results have been reported for miscible blends such as poly(acetoxystrene)/PEO[109]. Moreover, PEO is found to be miscible over a large range of temperatures and compositions with bisphenol-A polycarbonate (PC)[116-118], which has a similar molecular structure to TMPC. More quantitative information about the dynamics of the PEO/TMPC system is obtained from DSIMS experiments described below.

DSC results indicate the importance of temperature dependent dynamics of each component in the blend. Lodge and McLeish showed that in a miscible polymer blend, the local dynamics of the components may have different dependencies on temperature and composition, depending on the local environment of each component[119]. Therefore, an effective glass temperature, T_g^{eff}, for each component can be predicted from composition dependent bulk average glass transition temperature of the components[120]:

$$T_{gA}^{eff} = \left(\frac{\phi_{effA}}{T_{gA}} + \frac{1-\phi_{effA}}{T_{gB}} \right)^{-1}, \tag{6.5}$$

in which T_{gA} and T_{gB} are the glass transition temperatures of polymer A and B, and ϕ_{effA} is the effective local concentration of component A, which can be represented as follows:[120]

$$\phi_{effA} = \phi_{sA} + (1-\phi_{sA})\phi_A, \tag{6.6}$$

where ϕ_{sA} and ϕ_A represent self concentration and bulk concentration of polymer A, respectively. The calculated effective glass transition temperatures for PEO and TMPC as a function of PEO concentration are given in Figure 6.4, in which $T_{gPEO} = -60^oC$ and $T_{gTMPC} = 190^oC$. The self concentrations of the PEO and TMPC are taken as 0.4. We also included the T_g of the blend predicted by the Fox equation, which is equal to Equation 6.5 when $\phi_{eff} = 0$ [121]. One of the results obtained from this analysis is that the T_{gPEO}^{eff} is lower than the T_g of the TMPC/PEO blend, however, T_{gTMPC}^{eff} lies above the T_g of the blend obtained form Fox equation. These results are in consistent with the effective glass transition temperatures obtained for miscible PS/TMPC blends reported by Kim et al.[110]

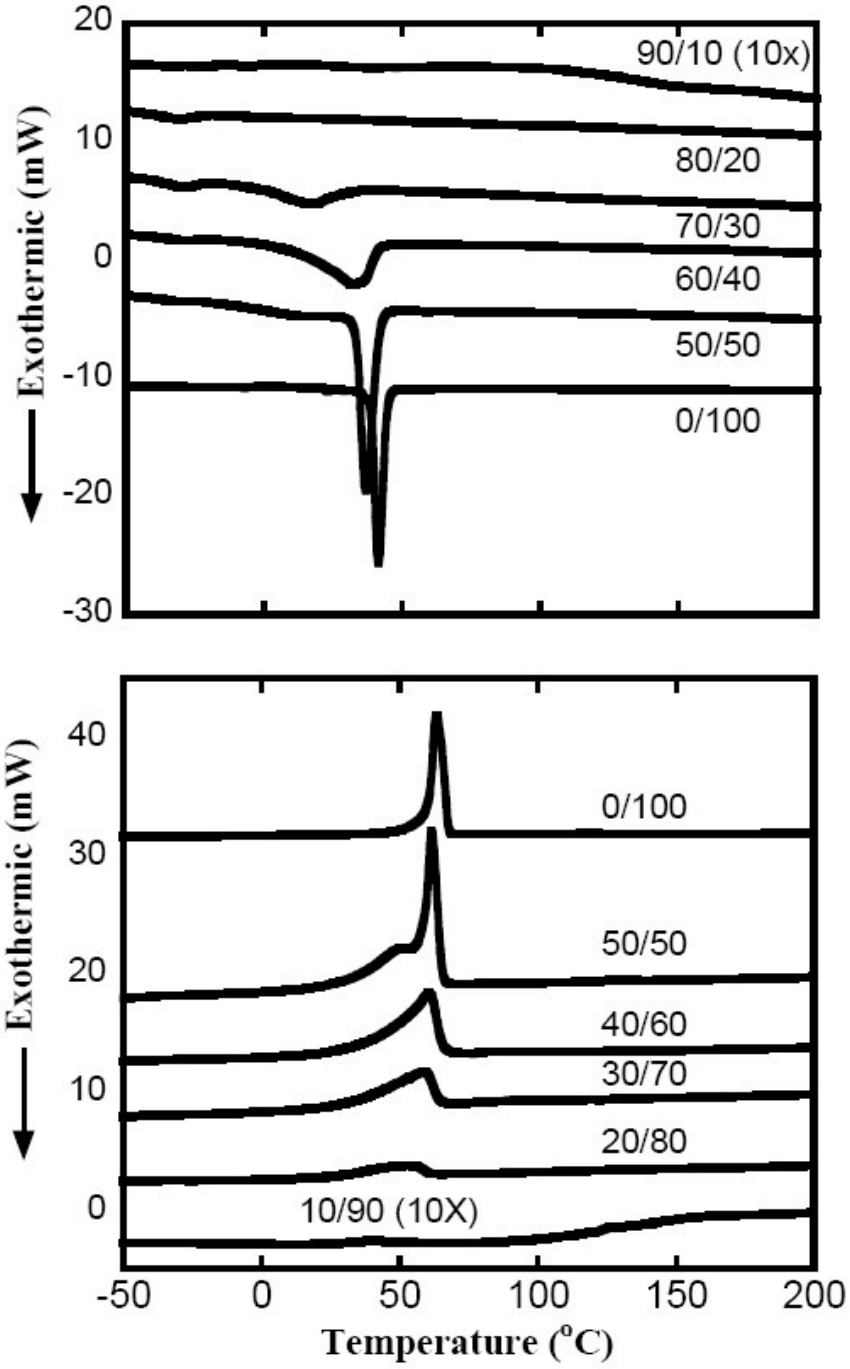

Figure 6.3. DSC cooling curves (top) and heating curves (bottom) for mixtures of TMPC and PEO.

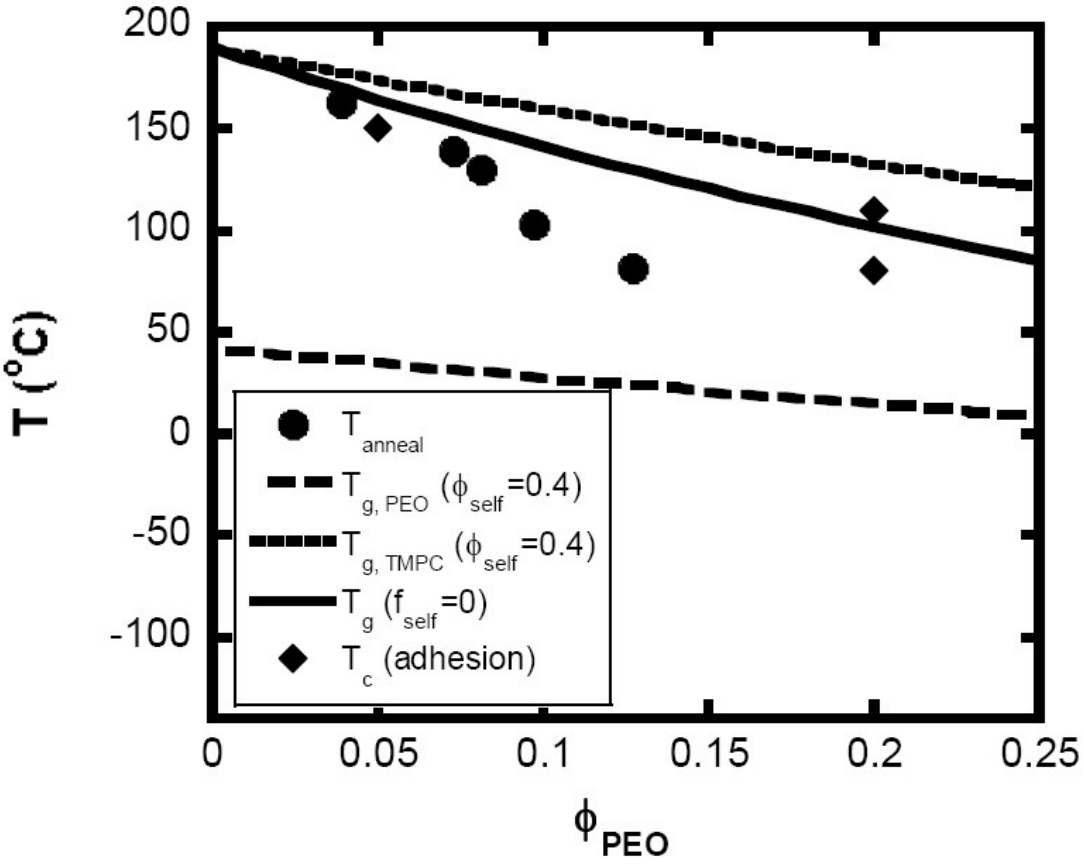

Figure 6.4. Graph of the glass transition temperature as a function of the concentration of dPEO in the sample.

.

6.3.2 Concentration Profiles via DSIMS

The depth profiles showing the diffusion of dPEO into TMPC layer were obtained by DSIMS experiments. Volume fractions of dPEO (ϕ_{dPEO}) with depth (d) for un-annealed sample and samples exposed to different annealing temperatures for 1 hour are given in Figure 6.5. Samples had a 70 Å bottom layer of dPEO and a 2420 Å top layer of TMPC. In the figure, zero depth indicates the surface of the TMPC layer, and it reaches to bottom dPEO layer at approximately 2420 Å, and reaches the Si-substrate above 2480 Å. The sample annealed at 80 ^{o}C shows a plateau corresponding to ϕ_{dPEO} = 0.125, which is a clear indication of PEO diffusion in TMPC. This plateau value of ϕ_{dPEO} decreases as the annealing temperature increases, reaching 0.03 for the sample annealed at 160 ^{o}C. The unannealed sample shows no indication of diffusion. These results show that dPEO and TMPC are miscible, and that the dPEO is able to diffuse into TMPC at temperatures ≥ 80 ^{o}C.

In order to compare the diffusion results with the effective glass temperatures of the components, the plateau values obtained from DSIMS were plotted in Figure 6.4. These plateau values represent dPEO compositions at which dPEO diffusion stops at the different annealing temperatures. As expected, all points fall inside the region defined by T_{gTMPC}^{eff} and T_{gPEO}^{eff}. The results show that the mobility of dPEO in the blends decreases and the dPEO concentration decreases.

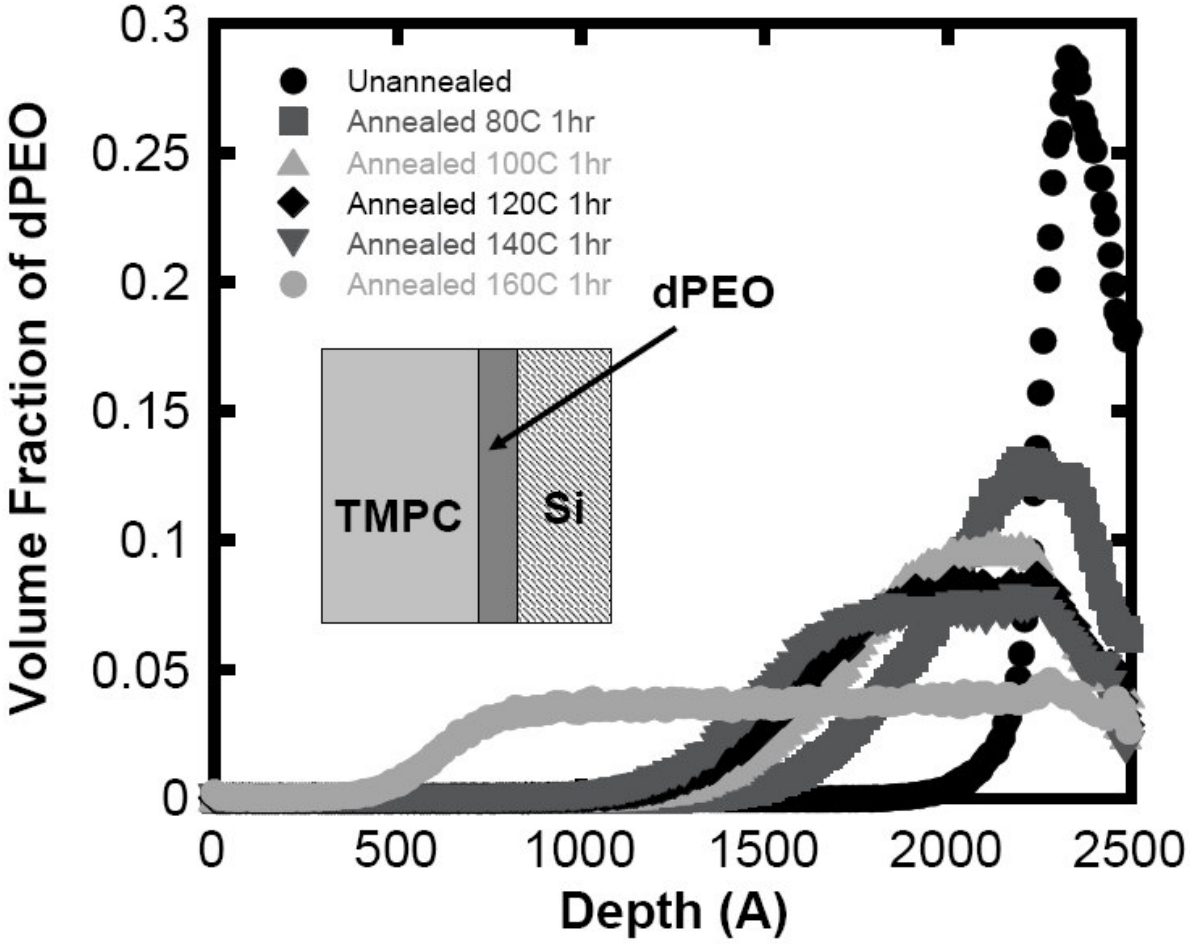

Figure 6.5. Dynamic SIMS analysis of two layer dPEO/TMPC samples annealed at different temperatures. The sketch of the sample is also included in the figure.

6.3.3 Adhesion Results

In order to study the diffusion-mediated adhesion, axisymmetric pull-off tests were performed on thin layers of TMPC/PEO blends at elevated temperatures. For this purpose, a glass indenter and an elastomer substrate, both were grafted with the thin layers of TMPC/PEO blends, were brought into contact at $T_c \pm 3\ ^oC$. The surfaces were pulled apart at the same T_c after keeping them in contact for different amounts of t_c, ranging from 0 to 30 min. A typical load vs displacement plot, is given in Figure 6.6, in which 80/20 blends were brought into contact at 100 ±3^{o}C, and pulled apart after keeping them in contact for 30 min. In Figure 6.6, the solid curve represents the experimental data, and the open circles represent the empirical fit by using Equation 6.4. For the empirical fits, the data were obtained by changing the threshold energy, $\mathcal{G}_o$, for fixed values of $v^* = 0.01$ μm/s and $n = 0.02$. $\mathcal{G}$ was plotted as a function of a by using the data obtained from these empirical predictions. As the surfaces were pulled apart, a stays constant for values of $\mathcal{G} < \mathcal{G}_o$. When $\mathcal{G}$ becomes equal to the threshold energy, the crack starts moving, indicating a decrease in the contact area. It is seen from the Figure 6.7 that, at 100 ^{o}C, the threshold energy increases with increase in contact time. This result shows that diffusion of PEO is time dependent process, and the interface becomes stronger when enough time is given for PEO diffusion to the interface.

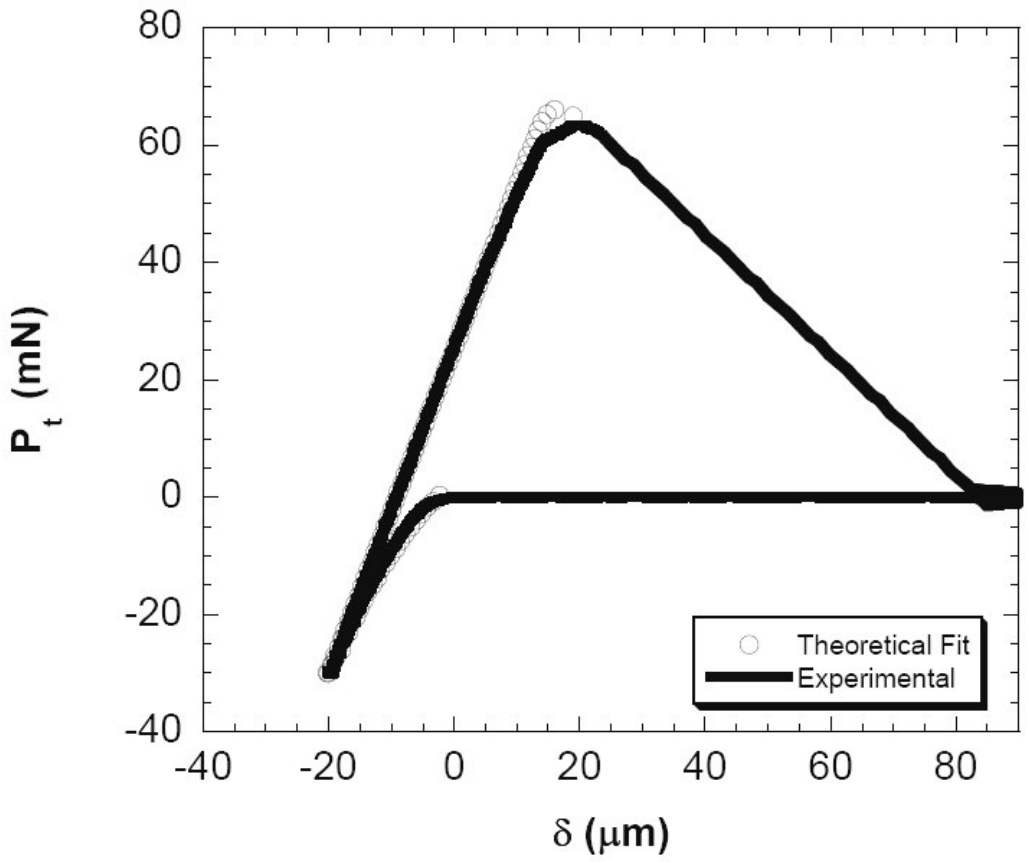

Figure 6.6. Tensile load-displacement data for 80/20 (TMPC/PEO) blend. The surfaces were brought into contact, and held for tc=30 minutes at constant compressive load (30mN) at 100±3 oC. Solid line represents experimental data, and circle represents theoretical fit.

In order to investigate the effect of contact temperature, the same experiments were done at a range of temperatures from 25 to 100 ^{o}C, for 80/20 blends. The load-displacement curves for T_c = 100 ^{o}C are given in Figure 6.8-a. The maximum pull-out load obtained from the unloading part of these curves were used to calculate the G_c by using Equation 6.1. These values are slightly higher that the G_o values obtained from empirical fits, which is plotted in Figure 6.7 by using

arrow symbols for the 80/20 sample (for T_c=100^{o}C). Figure 6.8-b clearly indicates the temperature and the contact time dependence of the critical energy release rate. For instance, at 25^{o}C, G_c is equal to 0.3 J/m^2 and does not change with the time of contact, which indicates that PEO molecules are not mobile at this condition. However, at 100^{o}C $G_c \approx$ 0.7 J/m^2 for intimate contact and increases significantly with increase in contact time reaching to ~2.2 J/m^2 for 30 min of contact time. This result clearly indicates the temperature mediated diffusion of PEO at the interface.

In order to obtain a general picture of the diffusion-mediated adhesion in TMPC/PEO blends, pull-off tests were performed at a wide range of temperature on blends having different concentrations. The results for blends 50/50, 60/40, 80/20, 95/5 and 100/0 at a range of T_c between 25 to 180^{o}C are given in Figure 6.9. In these experiments, the surfaces were maintained into contact for 10 to 20 min. For 100/0 blends representing the TMPC – TMPC interaction, the energy release rate is independent of temperature for values of T_c < 150^{o}C having a G_c=0.2 J/m^2, which shows a slight increase when T_c becomes closer to the melting temperature of TMPC. We observe a significant increase in G_c for the 95/5 blends starting from 140^{o}C, which reaches up to 3 J/m^2 at 180^{o}C. For 80/20 blends, this increase in G_c was observed around 110^{o}C, which indicates the temperature at which PEO molecules start diffusing to the interface, and the interface become stronger due to presence of PEO at the interface. However, the values of G_c stay constant for the blends having PEO concentrations greater that 20 %. In order to compare these diffusion-mediated adhesion results with the overall dynamics of the blends, the critical temperatures obtained from adhesion experiments were plotted in Figure 6.4. These temperatures indicate the temperature at which PEO molecules move to the interface, and strengthen the

interface. These results can be attributed in three folds: (1) a critical temperature is needed for diffusion-mediated adhesion of TMPC/PEO blends, which decreases with increase in PEO concentration; (3) diffusion of PEO molecules to the interface increases the strength of the interface, when the PEO mobility is lower than the pull-off rate. (2) the mobility of the PEO molecules increases as the PEO concentration increases in the blend, and for the blends containing PEO > 20 %, the diffusion rate becomes much larger than the pull-off rate showing no improvement in adhesion.

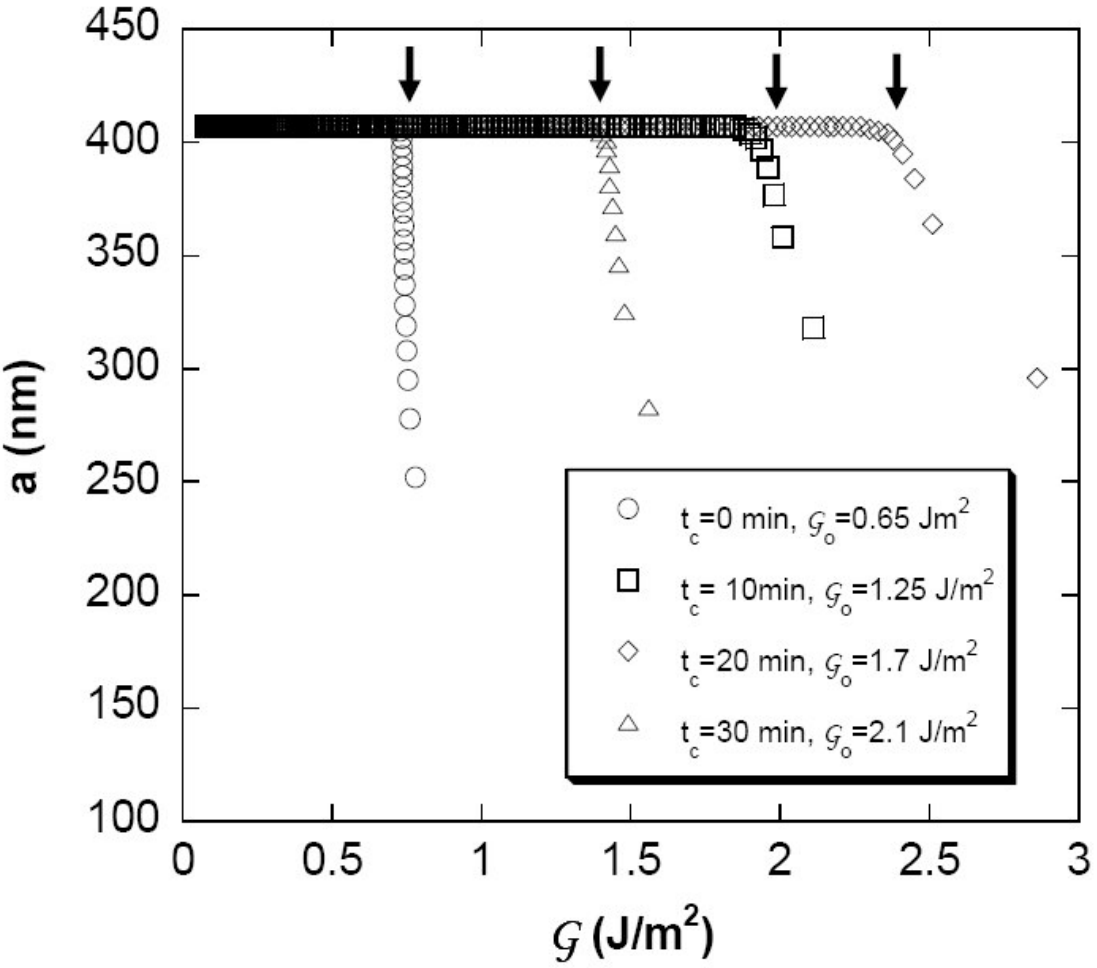

Figure 6.7. Contact radius plotted versus energy release rate for 80/20 (TMPC/PEO) blend. The surfaces were brought into contact, and heated to 100^{o}C, and held in contact for tc (0, 10, 20, 30) minutes at constant compressive load (30mN) at 100±3 ^{o}C. The arrows indicate the $\mathcal{G}_c$ calculated from Equation 6.1, by using maximum Pt.

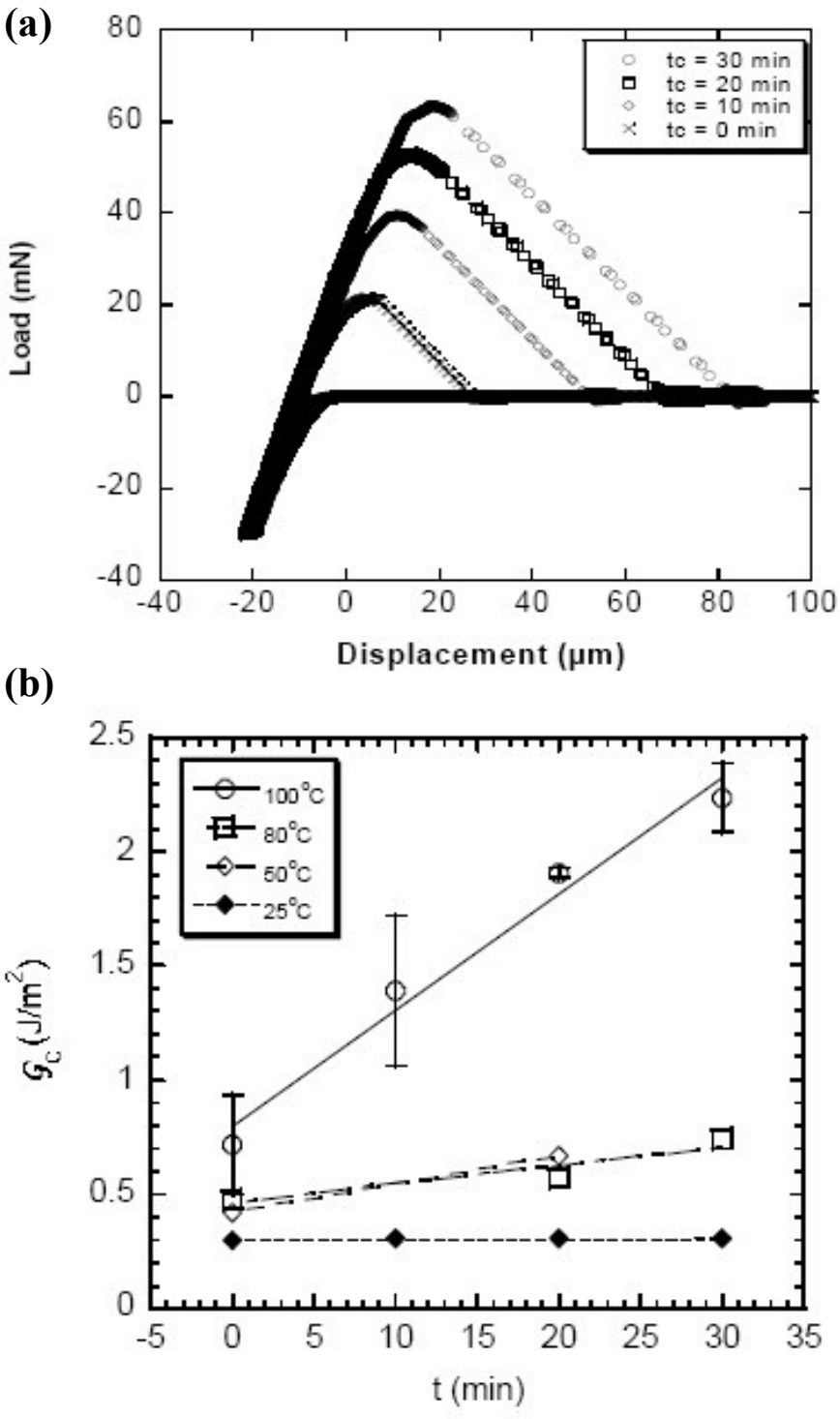

Figure 6.8. (a) Tensile load-displacement data for 80/20 (TMPC/PEO) blend for different contact times at 100±3 ^{o}C; (b) Energy release rate with contact time for different temperatures.

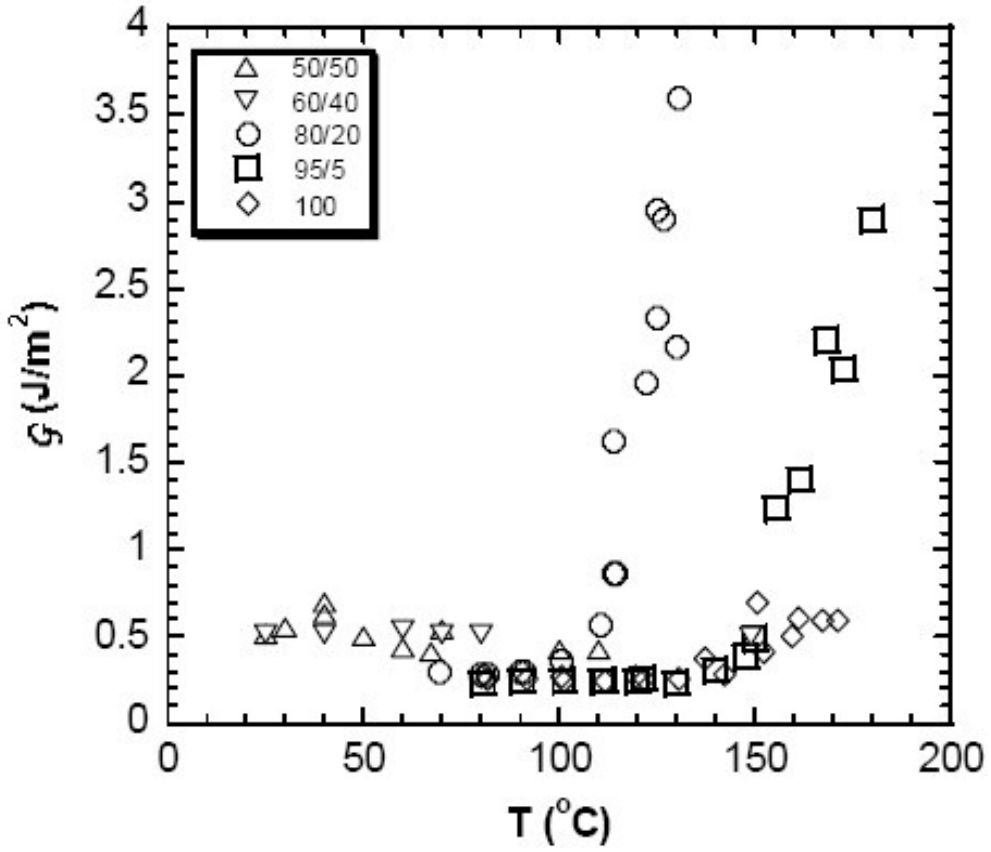

Figure 6.9. The energy release rate with respect to contact temperature. The surfaces were brought into contact, and they were kept in contact between 10 to 20 minutes.

6.4 SUMMARY

In this paper we study the diffusion-mediated adhesion between two component polymer blends having very different glass transition temperatures, which are glassy TMPC and semicrystalline PEO. The bulk properties of the blends were characterized by using DSC and dynamic SIMS. A contact mechanics approach was used to study the interfacial interaction

between two blends. The adhesion experiments were designed to characterize the effect of temperature and contact time on adhesion. The effect of PEO composition was also investigated. We also use a model to predict the relationship between energy release rate and crack velocity form relationship between load and displacement obtained experimentally. The overall results are summarized below:

- DSC studies for TMPC/PEO blends showed that the melting temperature of PEO shifts and broadens with increase in TMPC content, and it completely disappears for 90/10 blend, which is an indication of miscibility of the two components.
- The Lodge-McLeish model and Fox equation were used to demonstrate the PEO concentration dependent T_g of the blends. The T_{gPEO}^{eff} is always below the T_g of the TMPC/PEO blend, however, T_{gTMPC}^{eff} lies above the T_g of the blend obtained form the Fox equation, which is consistent with the behavior observed for miscible blends.
- Dynamic SIMS experiments revealed that dPEO and TMPC are miscible, and that the dPEO is able to diffuse into TMPC at temperatures ≥80 ^{o}C. We also observed that the mobility of the dPEO in the blends decreases as the dPEO concentration decreases.
- For 80/20 blends, the adhesion experiments showed that G_c increases significantly with increase in contact time for Tc ≥ 100, at which PEO molecules became mobile.
- The empirical relationship between G with v fitted well with the experimental data for values of v*=0.01 μm/s and n=0.02. The obtained G_o showed similar

dependency on temperature and contact time with G_c, but gave slightly higher values.

- The adhesion experiments with blends of different PEO compositions revealed that there the temperature for diffusion-mediated adhesion strongly depends on blend composition, which is in consistent with dynamic SIMS results.
- For 90/10 blends this critical temperature was found to be 140^{o}C, where as it was 110^{o}C for 80/20 blend. The highest G_c value obtained for 80/10 was 3.6 mJ/m^2 for T_c = 130^{o}C, whereas G_c reaches 3 J/m^2 at T_c=180^{o}C for 95/5 blends.
- For higher concentrations of PEO (above 20%), the mobility of the PEO molecules exceeds the rate of separation, which screens the resistance at the interface during pull-off.

6.5 ACKNOWLEDGMENTS

This research is in collaboration with previous Shull group member Rachel L. Mcswain and Thomas E. Mates from University of California.

REFERENCES

(1) Schneider, J. P.; Pochan, D. J.; (University of Delaware, USA). Application: US US, 2006; p 59 pp.

(2) Bromberg, L. *Langmuir* **1998**, *14*, 5806-5812.

(3) Jeong, B.; Bae, Y. H.; Kim, S. W. *Colloids and Surfaces, B: Biointerfaces* **1999**, *16*, 185-193.

(4) Jeong, B.; Kim, S. W.; Bae, Y. H. *Advanced Drug Delivery Reviews* **2002**, *54*, 37-51.

(5) Ruel-Gariepy, E.; Leroux, J.-C. *European Journal of Pharmaceutics and Biopharmaceutics* **2004**, *58*, 409-426.

(6) Ravi, P.; Wang, C.; Tam, K. C.; Gan, L. H. *Macromolecules* **2003**, *36*, 173-179.

(7) Dai, S.; Ravi, P.; Tam, K. C.; Mao, B. W.; Gan, L. H. *Langmuir* **2003**, *19*, 5175-5177.

(8) Ryan, A. J.; Crook, C. J.; Howse, J. R.; Topham, P.; Jones, R. A. L.; Geoghegan, M.; Parnell, A. J.; Ruiz-Perez, L.; Martin, S. J.; Cadby, A.; Menelle, A.; Webster, J. R. P.; Gleeson, A. J.; Bras, W. *Faraday Discussions* **2004**, *128*, 55-74.

(9) Rozier, A.; Mazuel, C.; Grove, J.; Plazonnet, B. *International Journal of Pharmaceutics* **1989**, *57*, 163-168.

(10) Pochan, D. J.; Deming, T. J.; Wooley, K. L.; Schneider, J. P. *Abstracts of Papers, 230th ACS National Meeting, Washington, DC, United States, Aug. 28-Sept. 1, 2005* **2005**, PMSE-117.

(11) Tae, G.; Kornfield, J. A.; Hubbell, J. A. *Biomaterials* **2005**, *26*, 5259-5266.

(12) Van Ooij, W. J.; Edwards, R. A.; Sabata, A.; Zappia, J. *Journal of Adhesion Science and Technology* **1993**, *7*, 897-917.

(13) Casali, F.; Burgat, V.; Guerre, P. *Revue de Medecine Veterinaire (Toulouse)* **1999**, *150*, 207-220.

(14) Lee, K. P.; Chromey, N. C.; Culik, R.; Barnes, J. R.; Schneider, P. W. *Fundamental and Applied Toxicology* **1987**, *9*, 222-235.

(15) Kang, J.; Beers, K. J. *Polymer Preprints (American Chemical Society, Division of Polymer Chemistry)* **2005**, *46*, 825-826.

(16) Loebsack, A.; Greene, K.; Wyatt, S.; Culberson, C.; Austin, C.; Beiler, R.; Roland, W.; Eiselt, P.; Rowley, J.; Burg, K.; Mooney, D.; Holder, W.; Halberstadt, C. *Journal of Biomedical Materials Research* **2001**, *57*, 575-581.

(17) M.P. Lutolf, G. P. R., A.H. Zisch, N. Tirelli, J.A. Hubbell,. *Advanced Materials* **2003**, *15*, 888-892.

(18) Goraltchouk, A.; Freier, T.; Shoichet, M. S. *Biomaterials* **2005**, *26*, 7555-7563.

(19) Tong, J. D.; Jerome, R. *Polymer* **1999**, *41*, 2499-2510.

(20) Varshney, S. K.; Jacobs, C.; Hautekeer, J. P.; Bayard, P.; Jerome, R.; Fayt, R.; Teyssie, P. *Macromolecules* **1991**, *24*, 4997-5000.

(21) Zune, C.; Archambeau, C.; Dubois, P.; Jerome, R. *Journal of Polymer Science, Part A: Polymer Chemistry* **2001**, *39*, 1774-1785.

(22) Schuch, H.; Klingler, J.; Rossmanith, P.; Frechen, T.; Gerst, M.; Feldthusen, J.; Mueller, A. H. E. *Macromolecules* **2000**, *33*, 1734-1740.

(23) Flanigan, C. M.; Crosby, A. J.; Shull, K. R. *Macromolecules* **1999**, *32*, 7251-7262.

(24) Mikos, A. G.; Thorsen, A. J.; Czerwonka, L. A.; Bao, Y.; Langer, R.; Winslow, D. N.; Vacanti, J. P. *Polymer* **1994**, *35*, 1068-1077.

(25) Shull, K. R.; Ahn, D.; Chen, W.-L.; Flanigan, C. M.; Crosby, A. J. *Macromolecular Chemistry and Physics* **1998**, *199*, 489-511.

(26) Webber, R. E.; Shull, K. R.; Roos, A.; Creton, C. *Physical Review E: Statistical, Nonlinear, and Soft Matter Physics* **2003**, *68*, 021805/021801-021805/021811.

(27) Shull, K. R. *Materials Science & Engineering, R: Reports* **2002**, *R36*, 1-45.

(28) Hautekeer, J. P.; Varshney, S. K.; Fayt, R.; Jacobs, C.; Jerome, R.; Teyssie, P. *Macromolecules* **1990**, *23*, 3893-3898.

(29) Adam, M.; Delsanti, M. *Macromolecules* **1977**, *10*, 1229.

(30) Yao, J.; Ravi, P.; Tam, K. C.; Gan, L. H. *Polymer* **2004**, *45*, 2781-2791.

(31) Chidambaram, S.; Gundiah, S. *Makromolekulare Chemie* **1985**, *186*, 123-129.

(32) Flory, P. J.; Rehner, J., Jr. *Journal of Chemical Physics* **1943**, *11*, 521-526.

(33) Eley, D. D.; Saunders, J.; Sparks, A. H. *Transactions of the Faraday Society* **1952**, *48*, 758-763.

(34) Waite, J. H. *International Journal of Adhesion and Adhesives* **1987**, *7*, 9-14.

(35) Waite, J. H. *Ann N Y Acad Sci FIELD Full Journal Title:Annals of the New York Academy of Sciences* **1999**, *875*, 301-309.

(36) Papov, V. V.; Diamond, T. V.; Biemann, K.; Waite, J. H. *J Biol Chem FIELD Full Journal Title:The Journal of biological chemistry* **1995**, *270*, 20183-20192.

(37) Waite, J. H. *The Journal Of Biological Chemistry* **1983**, *258*, 2911-2915.

(38) Yu, M.; Hwang, J.; Deming, T. J. *Journal of the American Chemical Society* **1999**, *121*, 5825-5826.

(39) Yu, M.; Deming, T. J. *Macromolecules* **1998**, *31*, 4739-4745.

(40) Haemers, S.; Koper, G. J. M.; Frens, G. *Biomacromolecules* **2003**, *4*, 632-640.

(41) Burzio, L. A.; Waite, J. H. *Biochemistry FIELD Full Journal Title:Biochemistry* **2000**, *39*, 11147-11153.

(42) Waite, J. H.; Qin, X. *Biochemistry FIELD Full Journal Title:Biochemistry* **2001**, *40*, 2887-2893.

(43) Monahan, J.; Wilker, J. J. *Langmuir* **2004**, *20*, 3724-3729.

(44) Rodriguez, R.; Blesa, M. A.; Regazzoni, A. E. *Journal of Colloid and Interface Science* **1996**, *177*, 122-131.

(45) Messersmith, P. B.; Friedstat, J.; Huang, K.; Lee, B. P.; Dalsin, J.; Hu, B.-h.; (Northwestern University, USA). WO, 2003; p 60 pp.

(46) Tatehata, H.; Mochizuki, A.; Ohkawa, K.; Yamada, M.; Yamamoto, H. *Journal of Adhesion Science & Technology* **2001**, *15*, 1003-1013.

(47) Yamamoto, H.; Kuno, S.; Nagai, A.; Nishida, A.; Yamauchi, S.; Ikeda, K. *International Journal of Biological Macromolecules* **1990**, *12*, 305-310.

(48) Yu, M.; Deming, T. J. *Polymeric Materials Science and Engineering* **1998**, *79*, 248-249.

(49) Deming, T. J.; Yu, M.; Hwang, J. *Polymeric Materials Science and Engineering* **1999**, *80*, 471-472.

(50) Deming, T. J. *Current Opinion in Chemical Biology* **1999**, *3*, 100-105.

(51) Dalsin, J. L.; Hu, B.-H.; Lee, B. P.; Messersmith, P. B. *Journal of the American Chemical Society* **2003**, *125*, 4253-4258.

(52) Lee, H.; Scherer, N. F.; Messersmith, P. B. *Proceedings of the National Academy of Sciences of the United States of America* **2006**, *103*, 12999-13003.

(53) Huang, K.; Lee, B. P.; Ingram, D. R.; Messersmith, P. B. *Biomacromolecules* **2002**, *3*, 397-406.

(54) Lee, B. P.; Dalsin, J. L.; Messersmith, P. B. *Biomacromolecules* **2002**, *3*, 1038-1047.

(55) Waite, J. H.; Benedict, C. V. *Methods in Enzymology* **1984**, *107*, 397-413.

(56) Lee, B. P.; Chao, C.-Y.; Nunalee, F. N.; Motan, E.; Shull, K. R.; Messersmith, P. B. *Macromolecules* **2006**, *39*, 1740-1748.

(57) Guvendiren, M.; Shull, K. R. *Soft Matter* **2007**, *DOI: 10.1039/b615412c*.

(58) Saleem, M. M. M.; Wilson, M. T. *Biochemical Journal* **1982**, *201*, 433-444.

(59) Liu, B.; Burdine, L.; Kodadek, T. *Journal of the American Chemical Society* **2006**, *128*, 15228-15235.

(60) Waite, J. H.; Tanzer, M. L. *Biochemical and Biophysical Research Communications* **1980**, *96*, 1554-1561.

(61) Schnurrer, J.; Lehr, C. M. *Proceedings of the International Symposium on Controlled Release of Bioactive Materials* **1995**, *22nd*, 306-307.

(62) Brass, D. A.; Shull, K. R. *Langmuir* **2006**, *22*, 9225-9233.

(63) Sauerbrey, G. *Zeitschrift fuer Physik* **1959**, *155*, 206-222.

(64) Chen, W.-L.; Shull, K. R.; Papatheodorou, T.; Styrkas, D. A.; Keddie, J. L. *Macromolecules* **1999**, *32*, 136-144.

(65) Moser, J.; Punchihewa, S.; Infelta, P. P.; Graetzel, M. *Langmuir* **1991**, *7*, 3012-3018.

(66) Atala, A. *Handbook of Stem Cells* **2004**, *2*, 565-570.

(67) Atala, A. *Encyclopedia of Biomaterials and Biomedical Engineering* **2004**, *2*, 1484-1490.

(68) Atala, A. *American Journal of Transplantation* **2004**, *4*, 58-73.

(69) Atala, A.; (USA). Application: US
US, 2003; pp 25 pp , which.

(70) Marshall, A. J., 2004; p 119.

(71) Buoni, D. J.; Dockus, K. A.; Wei, G.-X.; (Avery Dennison Corporation, USA). Application: US
US, 2003; p 7 pp.

(72) Bitar, M.; Salih, V.; Brown Robert, A.; Nazhat Showan, N. *J Mater Sci Mater Med FIELD Full Journal Title:Journal of materials science. Materials in medicine* **2007**, *18*, 237-244.

(73) Bitar, M.; Salih, V.; Brown, R. A.; Nazhat, S. N. *Journal of Materials Science: Materials in Medicine* **2007**, *18*, 237-244.

(74) Lu, H.; Wen, Q.; Wang, B.; Guo, R. *Shandong Daxue Xuebao, Yixueban* **2005**, *43*, 657-660.

(75) Ebert, C. D.; Sanders, S. W.; (Watson Pharmaceuticals, Inc., USA). Application: US
US, 2005; pp 31 pp , Cont -in-part of U S Ser No 286,281.

(76) Barkin, J.; Corcos, J.; Radomski, S.; Jammal, M.-P.; Miceli, P. C.; Reiz, J. L.; Harsanyi, Z.; Darke, A. C. *Clinical Therapeutics* **2004**, *26*, 1026-1036.

(77) Bennett, N.; O'Leary, M.; Patel, A. S.; Xavier, M.; Erickson, J. R.; Chancellor, M. B. *Journal of Urology (Hagerstown, MD, United States)* **2004**, *171*, 749-751.

(78) Cugell, D. W. *Am J Med FIELD Full Journal Title:The American journal of medicine* **1986**, *81*, 18-22.

(79) Lozewicz, S.; Lewisham Hospital, London, UK: ENGLAND: United Kingdom, 1989; pp 260-261.

(80) Yanaura, S.; Yamatake, Y.; Okamiya, Y. *Oyo Yakuri* **1978**, *15*, 31-39.

(81) Matsuo, Y.; Seki, A. *Arzneimittelforschung FIELD Full Journal Title:Arzneimittel-Forschung* **1979**, *29*, 1028-1035.

(82) El-Obeid, H. A.; Babhair, S. A.; Al-Badr, A. A. *Analytical Profiles of Drug Substances* **1987**, *16*, 445-506.

(83) Baehring-Kuhlmey, S. R. *Drugs of Today* **1977**, *13*, 315-318.

(84) Washiyama, J.; Kramer, E. J.; Creton, C. F.; Hui, C.-Y. *Macromolecules* **1994**, *27*, 2019-2024.

(85) Schnell, R.; Stamm, M.; Creton, C. *Macromolecules* **1999**, *32*, 3420-3425.

(86) Crosby, A. J.; Shull, K. R.; Lakrout, H.; Creton, C. *Journal of Applied Physics* **2000**, *88*, 2956-2966.

(87) Creton, C.; Brown, H. R.; Shull, K. R. *Macromolecules* **1994**, *27*, 3174-3183.

(88) Benkoski, J. J.; Fredrickson, G. H.; Kramer, E. J. *Journal of Polymer Science, Part B: Polymer Physics* **2002**, *40*, 2377-2386.

(89) Ahn, D.; Shull, K. R. *Macromolecules* **1996**, *29*, 4381-4390.

(90) Brown, H. R.; Char, K.; Deline, V. R.; Green, P. F. *Macromolecules* **1993**, *26*, 4155-4163.

(91) Char, K.; Brown, H. R.; Deline, V. R. *Macromolecules* **1993**, *26*, 4164-4171.

(92) Cho, K.; Brown, H. R.; Miller, D. C. *Journal of Polymer Science, Part B: Polymer Physics* **1990**, *28*, 1699-1718.

(93) Creton, C.; Kramer, E. J.; Hui, C. Y.; Brown, H. R. *Macromolecules* **1992**, *25*, 3075-3088.

(94) Creton, C.; Brown, H. R.; Deline, V. R. *Macromolecules* **1994**, *27*, 1774-1780.

(95) Kulasekere, R.; Kaiser, H.; Ankner, J. F.; Russell, T. P.; Brown, H. R.; Hawker, C. J.; Mayes, A. M. *Macromolecules* **1996**, *29*, 5493-5496.

(96) Shull, K. R.; Kramer, E. J.; Hadziioannou, G.; Tang, W. *Macromolecules* **1990**, *23*, 4780-4787.

(97) Washiyama, J.; Kramer, E. J.; Hui, C. Y. *Macromolecules* **1993**, *26*, 2928-2934.

(98) Willett, J. L.; Wool, R. P. *Macromolecules* **1993**, *26*, 5336-5349.

(99) Yuri M. Boiko, R. E. P. h. *Journal of Applied Polymer Science* **1999**, *74*, 825-830.

(100) Sha, Y.; Hui, C. Y.; Ruina, A.; Kramer, E. J. *Macromolecules* **1995**, *28*, 2450-2459.

(101) Schnell, R.; Stamm, M.; Creton, C. *Macromolecules* **1998**, *31*, 2284-2292.

(102) O. A. Ezekoye, C. D. L., M. T. Fahey, A. G. Hulme-Lowe,. *Polymer Engineering & Science* **1998**, *38*, 976-991.

(103) Jonza, J. M.; Porter, R. S. *Macromolecules* **1986**, *19*, 1946-1951.

(104) Cheung, Y. W.; Stein, R. S. *Macromolecules* **1994**, *27*, 2512-2519.

(105) Xue, Y.-Q.; Tervoort, T. A.; Rastogi, S.; Lemstra, P. J. *Macromolecules* **2000**, *33*, 7084-7087.

(106) Plummer, C. J. G.; Kausch, H.-H.; Creton, C.; Kalb, F.; Leger, L. *Macromolecules* **1998**, *31*, 6164-6176.

(107) Laurens, C.; Ober, R.; Creton, C.; Leger, L. *Macromolecules* **2001**, *34*, 2932-2936.

(108) McSwain, R. L.; Markowitz, A. R.; Shull, K. R. *Journal of Polymer Science, Part B: Polymer Physics* **2004**, *42*, 3809-3821.

(109) Kuo, S.-W.; Huang, W.-J.; Huang, C.-F.; Chan, S.-C.; Chang, F.-C. *Macromolecules* **2004**, *37*, 4164-4173.

(110) Kim, E.; Kramer, E. J.; Osby, J. O. *Macromolecules* **1995**, *28*, 1979-1989.

(111) Katana, G.; Kremer, F.; Fischer, E. W.; Plaetschke, R. *Macromolecules* **1993**, *26*, 3075-3080.

(112) Ahn, D.; Shull, K. R. *Langmuir* **1998**, *14*, 3637-3645.

(113) Ahn, D.; Shull, K. R. *Langmuir* **1998**, *14*, 3646-3654.

(114) Massoud, H. Z.; Plummer, J. D.; Irene, E. A. *Journal of the Electrochemical Society* **1985**, *132*, 2685-2693.

(115) Deal, B. E.; Grove, A. S. *Journal of Applied Physics* **1965**, *36*, 3770-3778.

(116) Tsuburaya, M.; Saito, H. *Polymer* **2004**, *45*, 1027-1032.

(117) Brus, J.; Dybal, J.; Schmidt, P.; Kratochvil, J.; Baldrian, J. *Macromolecules* **2000**, *33*, 6448-6459.

(118) Li, C.; Kong, Q.; Fan, Q.; Xia, Y. *Materials Letters* **2005**, *59*, 773-778.

(119) Lodge, T. P.; Wood, E. R.; Haley, J. C. *Journal of Polymer Science, Part B: Polymer Physics* **2005**, *44*, 756-763.

(120) Lodge, T. P.; McLeish, T. C. B. *Macromolecules* **2000**, *33*, 5278-5284.

(121) Fox, T. G. *Bull. Am. Phys. Soc. [2]* **1956**, *1*, 123.

Vita

Murat Guvendiren was born in Gazi District, in Ankara, in Turkiye, on May 04, 1978. His mother, Ayse Iffet Guvendiren, was also born in the capital city, Ankara, and his father, Erdal Guvendiren, was born in Mersin, located in the warm coasts of the Mediterranean Sea. He has one young sister, Berna Guvendiren. He began his education in Gazi District Primary School in 1983. He attended Private Yukselis Collage from 1988 to 1992. In June 1995, Murat graduated from Evrensel Science High School, and qualified to join Middle East Technical University, Ankara. In June 2000, Murat graduated from Middle East Technical University with a B.S. in Metallurgical and Materials Engineering after spending a year in School of Foreign Languages, major in English. Without giving a break, he began working on his M.Sc. with Professor Tayfur Ozturk on hydrogen storage. In February 2003, he got his M.Sc. degree form Middle East Technical University in Metallurgical and Materials Engineering. He has received the Best Thesis of the Year award of Dr. N Mustafa N. Parlar Research and Science Foundation, his thesis on “Effects of mechanical milling and hydrogenation of magnesium powders”. In June 2003, he began his Ph.D. working with Kenneth R. Shull at Northwestern University in Materials Science and Engineering Department, in United States. First time in abroad and living away from his family, he has had a smooth transition from metallurgy to polymer science. In his first year, he learned polymer chemistry, spending almost all of his time in the small chemistry room inside the Shull group main lab working on anionic polymerization. Following years, he learned polymer physics, adhesion and contact mechanics, which are strong expertise of Shull group. In the meantime, he was also involved in several collaborative projects, mostly on biomedical

applications of the hydrogels he developed. In fact, his collaboration with Professor Phillip B. Messersmith on “Marine mussel mimetic adhesion in hydrogels” took major part in his Ph.D. thesis. After completing his PhD, in June 2007, he continues research at postdoctoral level.